Dottorato di Ricerca in Ingegneria delle Strutture - XXIV Ciclo

Dipartimento di Ingegneria Civile, Ambientale,
Aerospaziale, dei Materiali
Università degli Studi di Palermo
Viale delle Scienze, 90128 Palermo (Italy)

Coordinatore: Prof. Giuseppe Giambanco

Masonry infilled RC frames: Experimental results and development of predictive techniques for the assessment of seismic response

Tesi di Dottorato di

Ing. Fabio Di Trapani

Relatori:

Prof. Liborio Cavaleri

Prof. Maurizio Papia

Settore Disciplinare ICAR 09

Dottorato di Ricerca in Ingegneria delle Strutture – XXIV Ciclo
Università degli Studi di Palermo, 2011-2013

TABLE OF CONTENTS

ABSTRACT

The issue of the influence of masonry infills within RC frames structures have been widely investigated in the last decades by several researchers.

The large interest addressed to this topic depends on the actual observation that when in presence of seismic events the response of framed structures is strongly conditioned by the interaction with the infills, which however are considered as non-structural elements and not included in the models.

The influence of masonry infills in structural response is so much relevant to affect not only the overall strength and the stiffness but it may radically change the possible collapse mechanisms of the structural complex under the effect of strong ground motions.

Infills panels may thus have a beneficial effect on the structural response, being able in some cases to supply the lack of resistance of structures to lateral actions, or an adverse contribution inducing unexpected and dangerous non ductile collapse mechanisms.

However the studies carried out on this topic have demonstrated that, independently from the beneficial or adverse contribution of masonry infills on structural response, their presence cannot be neglected in structural modelling both in design and verification phases.

As more deeply discussed in this thesis, several modelling approaches have been developed to represent infill-frame interaction, going from refined nonlinear FEM approaches to simplified equivalent strut models.

Especially the use of equivalent braced strut approach is pointed out in this work because of its simplicity in and the low computational effort required, which make this technique a predictive tool that is particularly attractive to perform complex nonlinear analyses of large buildings.

As base reference of the modelling techniques developed in this thesis a large experimental campaign has been carried out and is presented in Chapter 2.

The experimental investigation dealt with the cyclic behaviour of RC frame infilled with different kinds of masonry among the most employed in the worldwide building traditions.

The results of this experimental campaign have been fundamental not only to enlarge the experimental knowledge but also for the further processes of calibration and comparison of the proposed models and predictive strategies.

The research topics followed in this work regarded 3 fundamental aspects of the infill-frame interaction problem. The first is the calibration of the equivalent strut model, being able to overcome the difficulties in identification of the hysteretic parameters required by the models available in literature. The model makes use of a hysteretic "pivot" law needing few mechanical parameters for the identification and based on geometric rules rather than analytical. The study has shown that despite the simplicity of the model, it is able to provide an adequate accuracy to represent the cyclic hysteretic response of infilled frames.

A second topic investigated in this thesis regarded the issue of the local interaction between infills and RC members. The panels are in fact able to attract a large portion of the lateral actions during earthquakes that can be however supported by the frame members if the latter have an adequate transversal reinforcing. The equivalent strut approach is unable to provide information about the additional shear demand arising on beams and column ends, therefore the study was addressed to fill this predictive lack.

This was provided by means of a deep parametric study associated with the results of a detailed nonlinear FE analysis. This allowed to define a

correlation between a geometrical-mechanical parameter identifying the infilled frame system and the shear demand on the beam and column critical end sections.

The last topic was developed during a visiting period at *University of California - San Diego* and regarded the updating of the equivalent strut model able to predict simultaneously the in plane – out of plane response of an infilled frame and the reciprocal damaging in when seismic events occur.

The equivalent struts have been modelled by means of fiber elements with distributed plasticity, able to reproduce the arching mechanism developed by the masonry panels confined by the RC frames in presence of out of plane actions.

An identification procedure for the definition of an interacting in plane – out of plane model has been developed and validated on experimental basis.

1 MASONRY INFILLS AND RC FRAMES INTERACTION: GENERAL ISSUES AND LITERATURE OVERVIEW

1.1 General aspects of the infill-frame interaction

Reinforced concrete framed structures, infilled with masonry panels, are widespread and commonly employed in worldwide building traditions. The need to arrange infill walls in framed structures naturally arises by the necessity to create a separation between internal space of buildings and external environment. However, above all in the past, masonry infills ware always thought as secondary elements, and engineers did not introduced them in their models or calculations just because infills did not have to play any structural function.

It was only after significant seismic events that the observation of the damage for these buildings has shown that interaction between masonry infills and frames had a significant role in overall seismic response and capacity quite different case by case.

The topic of masonry infilled and RC frames interaction has a wide literature and is studied for 50 year and is today not definitively assessed in

all its aspects also because the role of masonry infills may or may not be beneficial when seismic occur.

Focusing the attention on the single infilled frame subjected to a lateral action (**Fig. 1.1**) it is anyway undeniable that the masonry infills contribute with a strong stiffening effect that is generally associated to a strength increasing and a reduction of lateral displacement capacity.

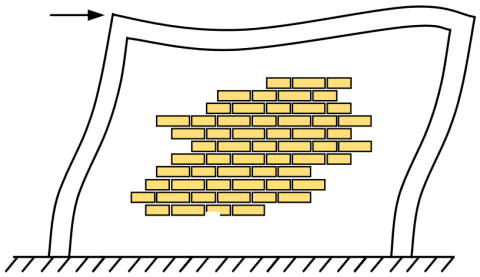

Fig. 1.1. Infilled frame subjected to lateral actions.

Even if the behaviour of a single infilled frame may be easy to predict, the contribution given at the scale of an entire building is affected by several uncertainties that cannot be assessed without performing detailed analyses.

Generally the contribution of infills on the overall capacity of structures is strongly dependant on regularity of their distribution in plan and over the height. A regular distribution of infills has a beneficial effect, especially for non-seismic designed buildings, increasing their global bearing capacity and stiffness under lateral actions. On the other hand, irregular distributions of panels may be really dangerous being the cause of a potential anticipation of the collapse when seismic events occur.

When infills are not uniformly distributed in plan and mainly concentrated in some areas, their strong stiffening capacity may cause a significant shifting of the stiffness centroid. This fact has as first effect the modification of the actual dynamical modal properties with respect to those expected during the design phases.

The participating mass ratio is spread out on higher modes not accounted and potentially dangerous. Moreover the increasing of the interaxis between the centre of mass and the centre of stiffness may generate additional torsional effects during the seismic events (**Fig. 1.2**).

When irregular distribution of infills occur over the height of buildings, it generally produces strong differences of storeys strength and stiffness being

the potential cause of soft storey collapse mechanisms where the damage is concentrated only in the storeys where infills are missing with fatal consequences (**Fig. 1.3**).

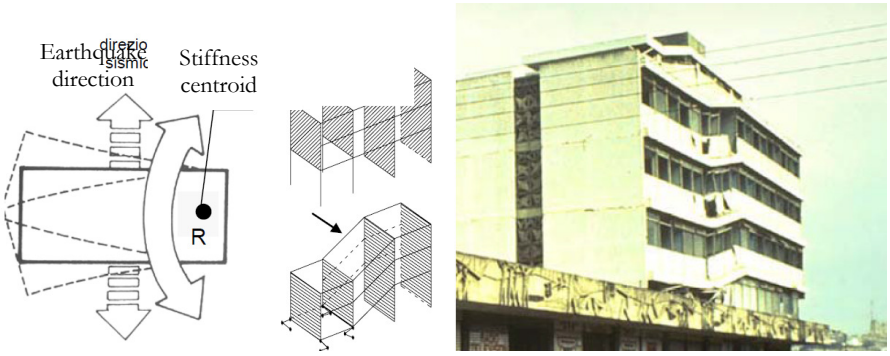

Fig. 1.2. Effects of planar irregularity in distribution of infills.

Moreover it should be also noticed that that even if the distribution of infills is regular in plan and height, the stiffness increasing causes higher restoring forces that should be carried by the infill panels. This fact has a positive contribution to the earthquake resistance until the force components that the panel transfers to the surrounding frame are compatible with the resistances of the RC members and the joints (**Fig. 1.4**). In fact the effects caused by the local interaction require the frame elements to have a bearing capacity that can exceed design values to support the efforts increase transferred by the infill. Especially in the case of low shear reinforced elements with no seismic detailing this may generate local brittle shear collapses of the columns and even of the nodes strongly compromising the overall capacity.

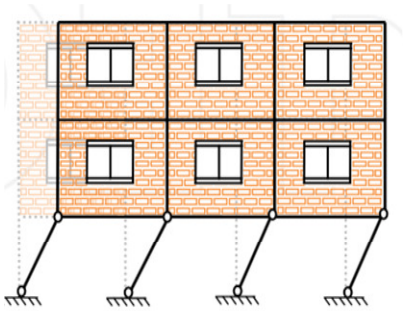

a)

b)

Fig. 1.3. Effects of irregularities in distribution of infills over the height: a) Collapse mechanism; b) Example of collapses occurred for irregular distribution of infills over the height.

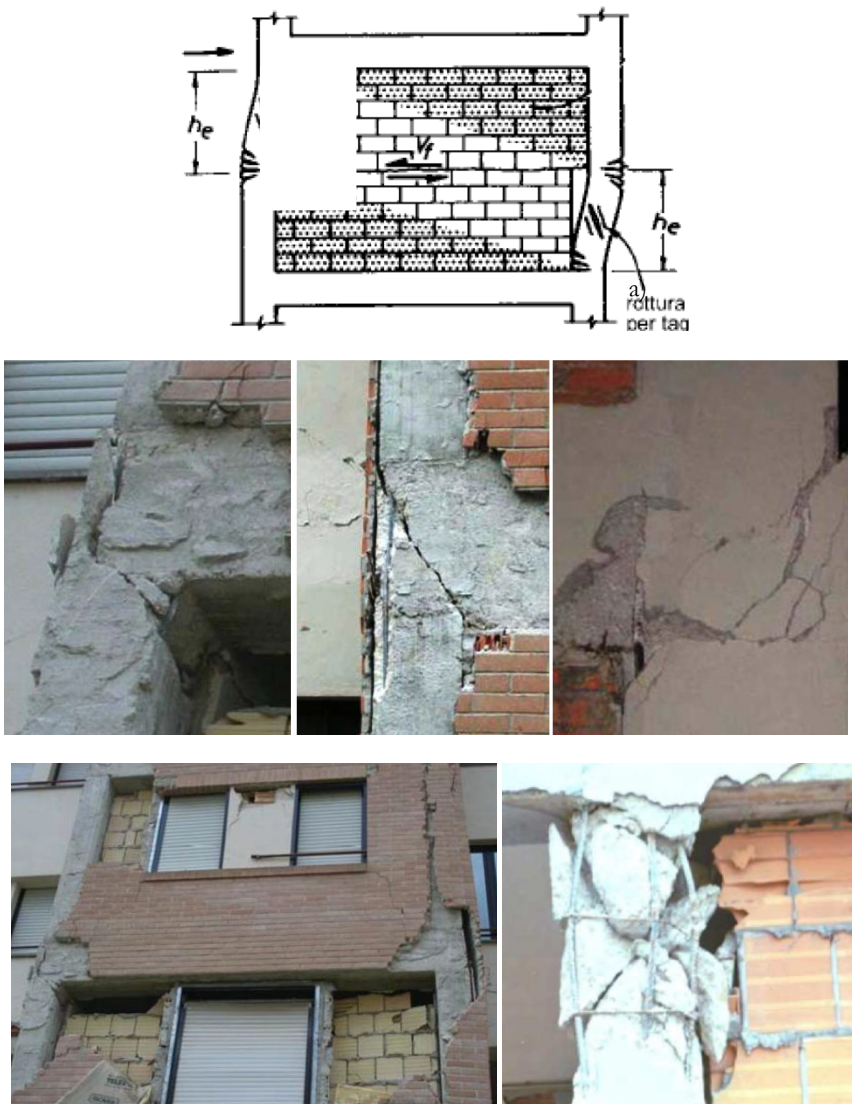

Fig. 1.4. Effects of local infill-frame interaction: a) scheme of collapse mechanism; b) sample of local shear collapse of column ends and joints due to the interaction with the infills.

Other collapse mechanisms due to the infill-frame interaction occur when infills present openings adjacent to the column in such a way the panel is shorter than the column itself. This fact modifies the design length of the column causing an unexpected increase of local shear demand. In this cases, the columns undergo an anticipated collapse that depends on the

aspect ratio and on the free length of the column. If the columns is squat shear failure occurs, otherwise the collapse is due a double plastic hinge mechanism (**Fig. 1.5**).

Fig. 1.5. Frame-infill interaction effects: local collapse due to the different infill-column height: a) scheme of collapse mechanism; b) short column double plastic hinge mechanism; c) shot column shear failure.

Despite the presence of masonry infill may produce an undesired behaviour of the structure under seismic events, in some cases their presence become fundamental for the capacity of structures to resist to earthquakes, especially when these are not seismically designed. An example is shown in **Fig. 1.6** where the plaster detachment shows that the infills contributed to increase the lateral strength and stiffness of the structure in the lower stories where the shear demand is maximum.

Fig. 1.6. Positive contribution of infills to earthquake resistance of a RC framed structure.

1.2 Behaviour of an infilled frame

The study of infill-frame interaction generally starts focusing the attention on the behaviour of a single infilled frame. When in presence of lateral actions the masonry infill detaches from the surrounding frame (**Fig. 1.7**) remaining in contact with this only in two opposite corners. This deformed configuration provides, as before mentioned, a significant stiffening effect associated to a certain increasing of strength that depends on several aspects.

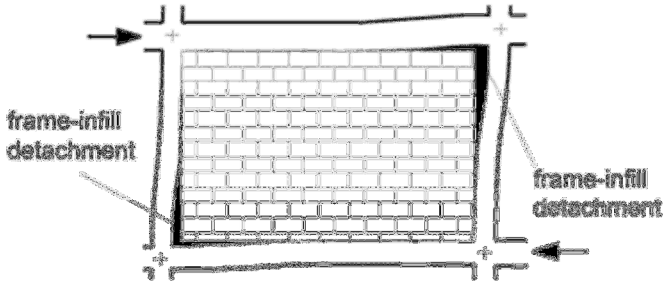

Fig. 1.7. Frame-infill detachment under lateral loads.

Frame and infill may present several coupling possibilities in terms of strength properties, elastic properties, geometrical ratios and influence of manufacturing. This aspect has as consequence that the failure modality of an infilled frame is not unique. Different collapse configurations were recognized in real cases and through experimental test. With reference to **Fig. 1.8** 6 collapse mechanisms, representing the one mainly recurring, are below summarized.

1. **Global flexural collapse:** It an uncommon collapse modality occurring only when infill is mechanically connected to the frame. The whole system behaves as a cantilever. The collapse is due to exceeding in tension and compression of masonry and concrete strength at the base sections.
2. **Horizontal sliding collapse of masonry infill:** Horizontal cracking propagate at mid-height of the panel causing the collapse for sliding. This mechanism is due to a low strength of mortar in joint beds. The collapse mechanism may also involve the frame in several ways.
3. **Diagonal shear cracking of masonry infill:** Shear cracking propagates diagonally on the infill. Cracking may involve the frame causing the shear failure of frame members or joints, or if a sliding of units occurs in proximity of the corners, a plastic hinge formation is possible at the ends of the columns.
4. **Corner crushing of masonry infill:** It occurs when local compression efforts in the contact corners with the frame exceed the strength of the corner units.
5. **Global sliding mechanism:** It is caused by the weakness of mortar or by an insufficient adherence of me mortar with the units which slides separately along horizontal and vertical joints.
6. **Central masonry crushing:** It often occurs in hollowed unit masonry infills. The panel crushes in the middle for the slenderness of vertical elements between holes.

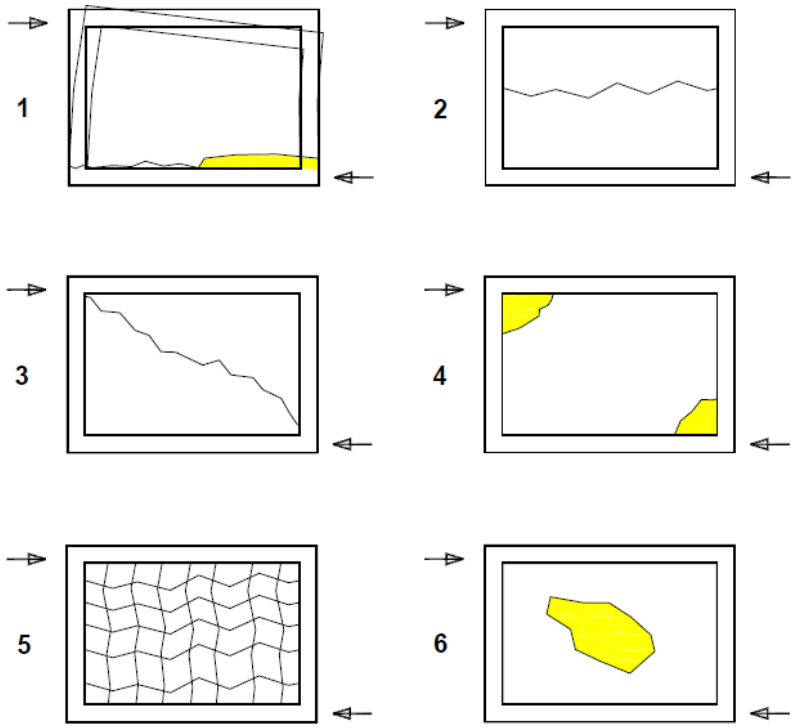

Fig. 1.8. Possible collapse mechanisms of an infilled frame.

The above described collapse mechanisms may involve the frame in different ways depending on stiffness and strength combinations between infills and frames. Mixed mode collapse modalities are also possible to develop and have been recognized. Mechanism #3 is anyway largely the mainly recognized, while mechanism #6 can be studied as a special case of #3. Mechanisms #1 and #5 have not particular interest being the first really rare and the second not particularly significant for the overall strength increasing. Therefore the study of the frame-infill interaction can be addressed to mechanisms #2, #3 and #4, covering the most of the possible cases.

1.3 Infill-frame interaction: literature mechanical approaches

The variability of the behaviour of the of infilled frame systems makes not easy to find mechanical models being computationally simple and able

to capture all the involved aspects. Several authors provided experimental and analytical studies proposing modelling strategies to predict the interaction effects. From a general point of view, two main approaches have been followed by researcher: **macromodeling** and **micromodeling**.

Moreover, depending on the typology of investigation needed, the models may account for linear or nonlinear behaviour of the materials and in the latter case it could be necessary to account for monotonic or cyclic behaviour in order to introduce the damage.

The macromodel approach (**Fig. 1.9**) is based on replacing masonry infills by means of one (or more) equivalent pin-jointed struts for each infill. This technique is the most frequently employed to perform nonlinear static or dynamic analyses because of its simplicity and a lower computational effort. Most of the technical codes also suggest the macromodelling approach for seismic assessment of infilled framed structures.

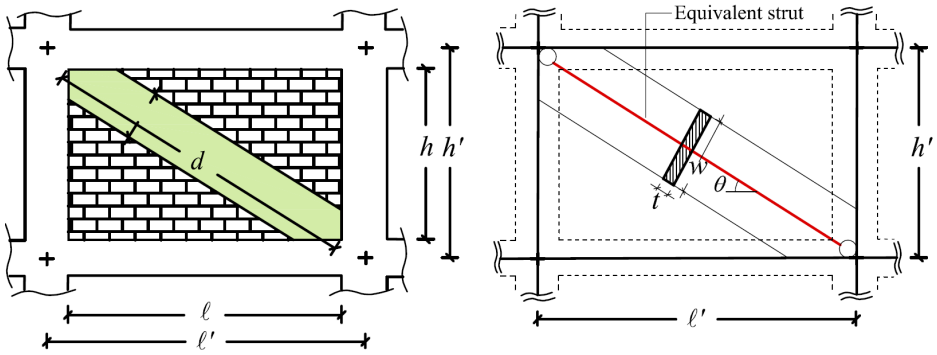

Fig. 1.9. Features of the equivalent strut in macromodel approach.

Besides the attribution of geometrical dimensions, the identification of the equivalent diagonal strut requires the assignment of specified mechanical characteristics for the strut depending on the properties of the actual system. Especially for masonries constituting infills of existing buildings, the identification of the necessary information, is affected by a large uncertainty since they depend not only on masonry properties (which present itself a significant uncertainty) but also on manufacturing and local arrangement details.

In a few words the equivalent strut should summarize all this aspects in with a single strut able to account for strength, stiffness, and damaging.

The quantity of required information depends in fact on the assessment approach (e.g. linear or nonlinear analysis) which is necessary to carry out. For a complete identification of the equivalent strut is necessary to determine at least: *a)* the initial stiffness, *b)* the peak strength, *c)* the constitutive law shape (monotonic or cyclical).

The first studies on this topic are due to Holmes (1961) who worked with brick masonry infilled steel frames. He proposed the empiric rule to replace the panel with an equivalent diagonal strut, having cross-section width w equal to 1/3 of the diagonal length d. Afterwards several other researchers followed proposed more detailed methods based on the ratio between the elastic characteristics of the infill and the surrounding frame for the identification of the equivalent strut cross-section width (e.g. Stafford Smith (1966), Stafford Smith and Carter (1969), Mainstone (1974), Dawe and Seah (1989), Durrani and Luo (1994), Saneinejad and Hobbs (1995)). More recently Papia *et al.* (2003) proposed an identification technique that introduces the dependence of the strut width not only on the stiffness ratios between frame and infill but also on the mechanical elastic properties of the infill along the diagonal direction. The definition of the elastic properties of masonry infill panels starting from the basic elastic properties was subsequently defined by Cavaleri *et al.* (2013). Other authors (Amato *et. al* (2008, 2009)) introduced the dependence of the stiffness to assign to the equivalent strut on the vertical load transmitted by the frame to the infill wall. An alternative method, based on a dynamic structural identification strategy, was also introduced by Cavaleri and Papia (2003).

Regarding to the definition of a constitutive law for the equivalent strut the study by Panagiotakos and Fardis (1996) should be mentioned.

There, the yielding force corresponding to the first cracking of the infill is determined depending on the tensile strength of the masonry evaluated by diagonal compressive tests. Bertoldi *et al.* (1993) proposed choosing the maximum strength of the strut depending on the possible failure mechanisms for the panel.

The first experimental and analytical studies on the cyclic behaviour of infilled frames structures refer to Klingner and Bertero (1978) which investigated the effect of cyclic loads by testing portions of multi-storey

buildings and also providing a first hysteretic model. Doudoumis and Mitsopoulou (1986) introduced a further hysteretic model providing for the first time an initial non-loading branch due to shrinkage of contact zones. Experimental pseudo-dynamic tests on masonry infilled RC frames were carried out by Mander *et al.* (1993, 1994) and Mehrabi *et al.* (1996) who also provided a cyclic law based on the results of tested infilled frames specimens (**Fig. 1.10**).

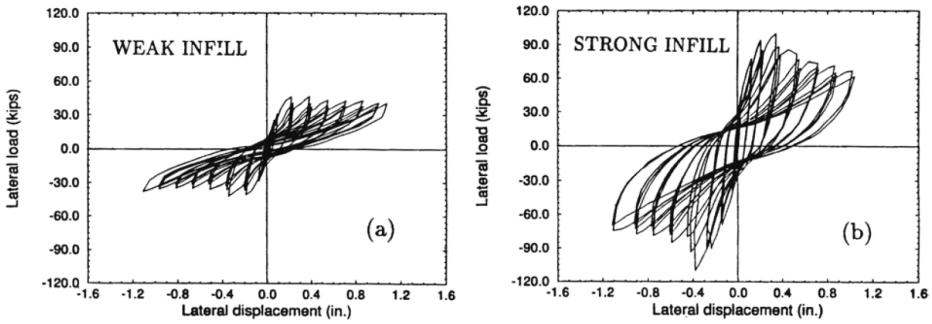

Fig. 1.10. Cyclic tests of infilled frames arranged with masonry panels having different strength (Mehrabi *et. al* (1996)) .

Other hysteretic models were further developed, each of them based on different assumptions. Madan *et al.* (1997) proposed a hysteretic single-strut model taking into account strength and stiffness decay and pinching, response, Kappos et al. (1998) presented a hysteretic model based on shear strength of infills. In the last years Cavaleri *et al.* (2005) introduced proposed a highly detailed constitutive law to account cyclic or monotonic behaviour of an equivalent single strut and provided a first calibration of the parameters involved.

After the development of several studies on single strut macromodels, some authors, recognizing the importance to account for the local shear efforts transferred by the infills to the surrounding frame, introduced the possibility to use a multiple strut configuration providing two or three struts. Among those studies Crisafulli (1997) investigated the influence of different multiple-strut configuration in structural response. In a further work Crisafulli and Carr (2007) developed a detailed multi-strut macromodel including in addition to classical truss elements, governed by axial compressive laws, a special shear frictional strut to account for the

vertical load influence on the overall strength of the panel. El-Dakhakhni *et al.* (2003) (**Fig. 1.11**) proposed a 3 strut model (having 1 concentric and 2 eccentric struts) in order to provide as much as possible a realistic distribution of moment and shear on the frame elements.

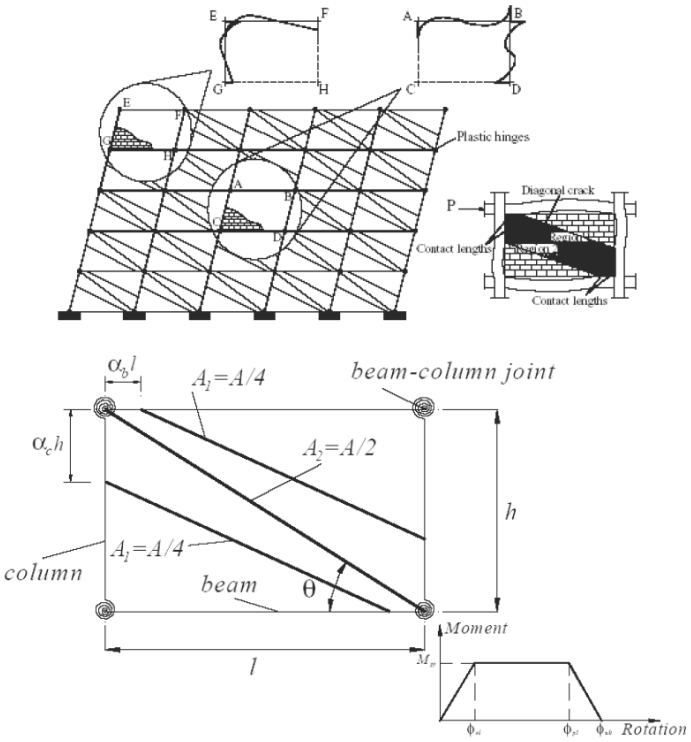

Fig. 1.11. Three-strut macromodel (El-Dakhakhni *et al.* (2003)).

Chrysostomou *et al.* (2002) aimed to obtain the response of infilled frames under earthquake loading by taking into account both stiffness and strength degradation of infills. They proposed to model each infill panel by six compression only inclined struts (**Fig. 1.12**). Three parallel struts were used in each diagonal direction, and the off-diagonal ones were positioned at critical locations along the frame members.

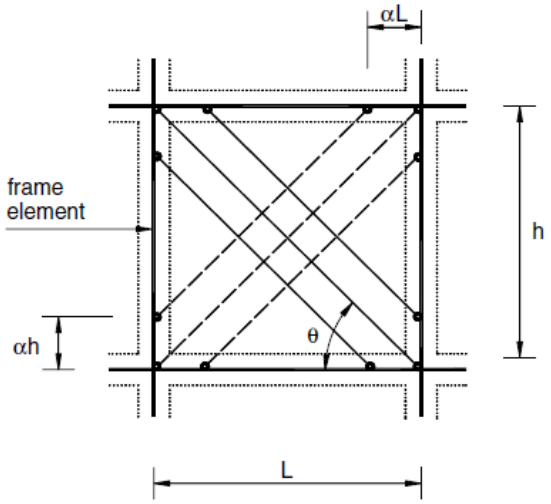

Fig. 1.12. Six-strut macromodel (Chrysostoamou *et al.* (2001)).

A substantially different approach has been instead followed by other authors which have adopted an "exact representation" of infills (micromodeling) to better reproduce frame-infill interaction. According to this modelling approach, the infill panel is modelled by means of planar shell finite elements while the frame may have modelled by shell elements or beam elements. The definition of the interface between the infill and the frame constitutes a quite sensitive question that was approached in different ways by the authors. Most of them used interface elements able to reproduce frictional effects and frame-infill detachment in contact regions. Such typology of approach, which is aimed at providing a more accurate response, is able to capture well local interaction effects and frame global internal force distribution. However the calibration is of several parameters is required to obtain a realistic results. The first studies referring to this approach are due to Mallick and Severn (1967) which adopted shell elements to model the infill and beam element for the frame (**Fig. 1.13**) in order to evaluate the stiffening effects on one storey-one bay frames.

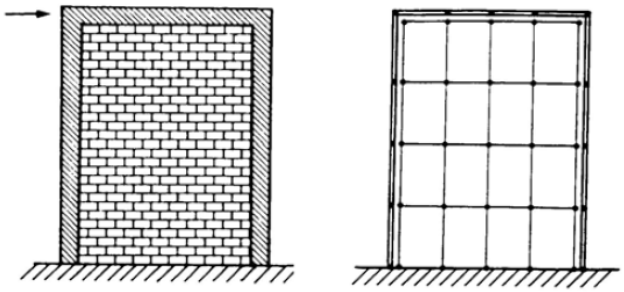

Fig. 1.13. FEM idealization proposed by Mallik and Severn (1967).

With same target Papia (1988) by means of a refined coupled FEM-BEM approach (**Fig.1.14**) investigated on the modification of the overall stiffness with the variation of the infill properties.

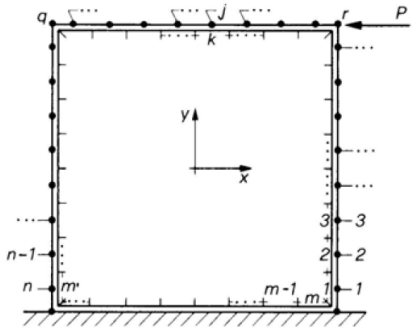

Fig. 1.14. FEM-BEM model for the infilled frame (Papia (1988)).

Also in Asteris (2003) the question of the lateral stiffness is pointed out, focusing mostly the attention of the influence of the openings in masonry panels with the variation of their extension and collocation.

More complex numerical and computationally sophisticated nonlinear micromodels were developed by Mehrabi and Shing (1997) and Shing and Mehrabi (2002) making use of smeared cracking elements (Lofti and Shing (1991)) and discrete cracking elements (Lofti and Shing (1994)) in order to capture the shear failure of reinforced concrete element and the sliding of the masonry units through dilatant interface models (**Fig. 1.15**).

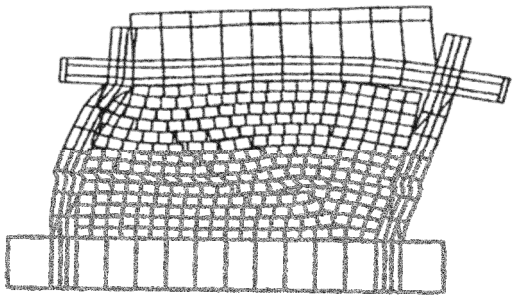

Fig. 1.15. Nonlinear numerical modelling of infilled frames (Mehrabi and Shing (1997)).

Basing on a similar but more refined finite element approach Koutromanos *et al.* (2011) provided a numerical experimental comparison of infilled frames specimens (**Fig. 1.16**) tested with a quasi-static cyclical loading and a full scale frame tested on a shake table, demonstrating a good agreement of the developed technique with the experimental results in terms of prediction of dynamic response and cracking pattern propagation on the masonry infill and the frame.

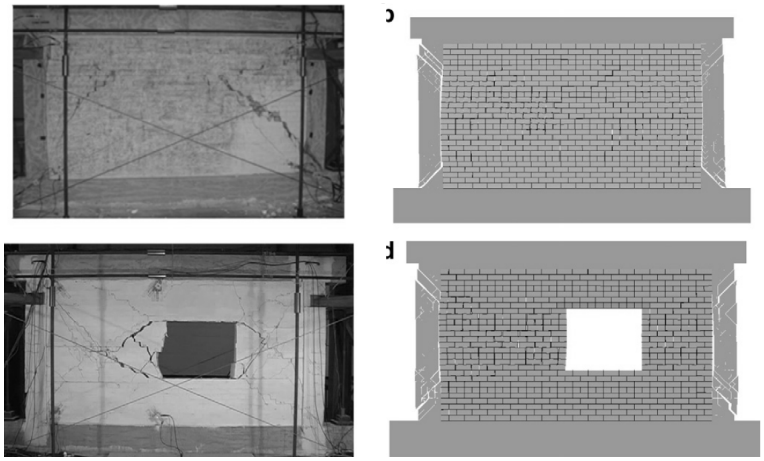

Fig. 1.16. Nonlinear numerical modelling of infilled frames (Koutromanos *et al.* (2011)).

The literature overview presented above underline that the question of the assessment of the behaviour of infilled frames have been treated a long in the past and continue nowadays to be a present issue presenting several opens aspects. The discussed models, going from the most simple to the

most complex have the limitation to be unable both computationally non heavy and accurate.

The single strut macromodels represent the easiest way to introduce the presence of the infill panels in models for current application. They are suitable for static and dynamic nonlinear analysis of complex structures and easy to identify, giving a quite good approximation despite their simplicity. Their limit lies in the geometrical disposition of the equivalent strut which makes not possible accounting for the shear transmission in critical sections. Although this question me be less relevant for buildings having a sufficient shear reinforcement of weak infills it becomes quite sensitive issue when non-seismically designed buildings are analysed. The multiple strut configurations are able to overcome this problem but are significantly affected by uncertainties arising for their calibration especially to perform nonlinear static or time history analyses.

In fact, among the above mentioned models, those including the cyclic behaviour often depend on a large number of parameters. The problem becomes more relevant in the case of multiple-strut configurations (double, triple pin jointed struts or mixed axial and shear struts) being necessary the definition of a constitutive monotonic or cyclic law for each strut.

Finally FE micromodels, represent the most accurate approach to capture the frame infill interaction being also the most similar to the real physic of the problem. Besides the stiffening effects, micromodels are able to well represent through interface elements complex issues such as the local frame infill interaction, the sliding of the units along mortar joints, the cracking propagation on infills and reinforced concrete elements.

Although this advantage they still present a double difficulty. The first one regards their proper calibration that may be really difficult to provide requiring, especially for nonlinear cases, the knowledge of several parameters and a sufficient experience to handle this kind of modelling. The second, and more relevant, is related to the necessary high computational effort. The application of micromodeling to complex structural system is in fact nowadays prohibitive for the large time required by this kind of analyses limiting for now the use of FE nonlinear micromodels to simple case study. FE models represent anyway fundamental resource in for research purposes being suitable as reference models to develop simplified

models and to study problems for which a refined representation is necessary.

In the subsequent sections some macromodels approach are described in detail with a special regard to the one involved in the research work developed.

1.4 The issue of the identification of the equivalent strut width in macromodelling approach

The first step in macromodelling approach is the definition of the equivalent strut width (w) to assign to the cross section in order to reproduce efficiently the interaction between infill and frames firs of all regarding to stiffening effects.

Many factors influence the equivalent width to attribute to the strut and is important to underline that they are not simply related to the features of masonry infill rather than on a ratio between infill properties and masonry properties. The stiffening ratio between infill and frame plays here a fundamental role since experimental tests evidence that the length of the contact region between frame and infill under lateral is strongly related to the overall stiffness. If the stiffness of the frame increases the contact length grows too increasing the stiffness of the system. Many studies therefore focused their results on the determination of this length.

In 1961 **Holmes**, observed the contact length of masonry infilled steel frames determining the first empiric rule for the equivalent strut: the replacement of the infill with a pinned strut having the same thickness of the infill and a width equal to 1/3 of the diagonal length (Eq. 1.1).

$$\frac{w}{d} = \frac{1}{3} \tag{1.1}$$

In his work Holmes proposed also a simple experimentally calibrated procedure to determine the maximum load and the ultimate displacement of the system.

A firs theoretical approach was provided by **Stafford Smith** (1966). After an experimental investigation on diagonally loaded square infilled steel frames, developed the idea of the strut suggested by Holmes, providing an

empirical curve for the evaluation of its dimensions. The experimental and analytical investigations showed a certain analogy between the frame-infill contact length α and the behaviour of a beam on an elastic foundation, so that the definition of the dimensionless parameter

$$\lambda h' = h' \sqrt[4]{\frac{E_i t}{4 E_f I_f h}} \tag{1.2}$$

was proposed in order to characterise the column-infill contact length and, consequently, the stiffness of the system.

In Eq. (1.2) t and h are the thickness and the height of the infill, respectively; h' is the height of the frame, measured between the centrelines of the beams; E_i is the Young modulus of the infill while E_f and I_f are the Young modulus of the material constituting the frame and the moment of inertia of the cross-sectional area of the frame elements (beams and columns having the same dimensions).

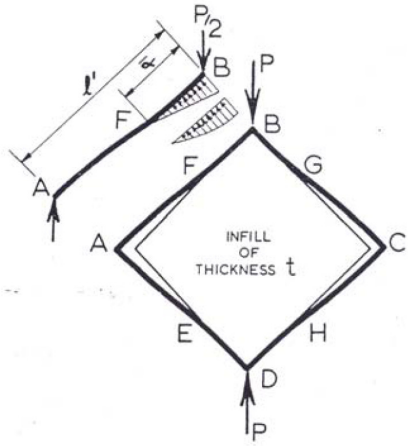

Fig. 1.17. Infill-frame interaction (Stafford-Smith (1968)).

The curve provided by Stafford Smith was based on experimental evidence and on the results of several numerical investigations carried out by means of the finite difference method. It gives the dimensionless parameter w/d for a fixed value of $\lambda h'$.

Referring to infilled frames subjected to vertical and lateral loads, Stafford Smith observed an increase in the horizontal stiffness when a vertical load was applied as a consequence of the increase of the length of

contact of the beam on the infill, but no parameters were inserted in order to take this phenomenon into account.

Later, **Stafford Smith and Carter** (1969) extended the concepts developed before to the case of rectangular frames, defining the characterising parameter

$$\lambda h' = h' \sqrt[4]{\frac{E_i t \sin(2\theta)}{4 E_f I_c h}} \tag{1.3}$$

θ being the slope of the infill diagonal, obtained by the expression $\theta = arctg(h/\ell)$, and I_c the moment of inertia of the columns.

Different curves w/d-$\lambda h'$ were defined with variation in the value of the slope θ. Further, the influence of the infill stress state along the diagonal direction was considered in the evaluation of w, due to the different secant stiffness observed with variation in the lateral load. So a set of curves was derived, for different stress levels and fixed ratio ℓ/h. Comparing these curves with the one provided by Stafford Smith (1966), it is not clear how the former are related to the latter. Moreover it should noted that no analytical form of the curves mentioned before is provided so every comparison has to be performed graphically.

Klingner and Bertero (1978), basing their work on the conclusions of Mainstone (1974), proposed calculating the width of the strut equivalent to the infill for frames having proportions 2.4 (length) against 1 (height) by means of the following expression:

$$\frac{w}{d} = 0.175 (\lambda h')^{0.4} \tag{1.4}$$

This value of w/d allows one to calculate the mean lateral stiffness of the infilled frame before the cracking of the infill. In the cases examined by Klingner and Bertero, unlike the more usual ones, the infill was connected to the frame by means of proper reinforcement passing from the infill to the surrounding reinforced concrete frame. Nevertheless, comparing the curve w/d-$\lambda h'$ expressed by Eq. (1.4) with the curves provided by Stafford Smith and Carter (1969) for an infill having the same aspect ratio, one concludes that in the first case much lower stiffness of the system is

obtained with respect to that expected in relation to the different frame-infill connection (**Fig. 1.18a**).

Durrani and Luo (1994), on the basis of the experimental work of Mainstone, proposed the following analytical relation for the evaluation of the width of the strut:

$$\frac{w}{d} = 0.32 \sin^{1.5}(2\theta) \left(\frac{E_i t h'^4}{m E_c I_c h} \right)^{0.1} \tag{1.5}$$

where

$$m = 6 \left(1 + \frac{6}{\pi} arctg \frac{I_b h'}{I_c \ell'} \right) \tag{1.6}$$

and I_b is the moment of inertia of the beam cross-section. In **Fig. 1.19b** is shown the result provided by Eq. (1.5) for square infilled frames with $I_b / I_c = 1$ and the ones given in Stafford Smith (1966) commented on above. The two formulation show a good agreement.

With reference to a further approach relating the initial lateral stiffness of the equivalent strut to the collapse condition of the system, in **Saneinejad and Hobbs** (1995) the dimensions of the strut are assumed to be constant with variation in the stress level, while the initial value of the Young modulus is assumed to be twice the secant modulus derived from the maximum resistance condition. Moreover instead using a limit analysis approach, calibrating analytical results on experimental tests on varying infill strength, the performed a calibration on the variation of the frame strength. The procedure is supported by detailed numerical FE analyses. Considering the equilibrium of the scheme reported in **Fig. 1.19** the width of the equivalent strut is still correlated to the length of the contact zones which depend on the plastic moments of the RC elements. This criterion does not allow one to compare the cross-sectional dimensions of the strut with those derived by Stafford Smith and Carter (1969) and by Mainstone (1971, 1974) varying with the level of the diagonal stress. Nevertheless, if the comparison is made in terms of initial lateral stiffness, significantly different values of *w/d* are obtained.

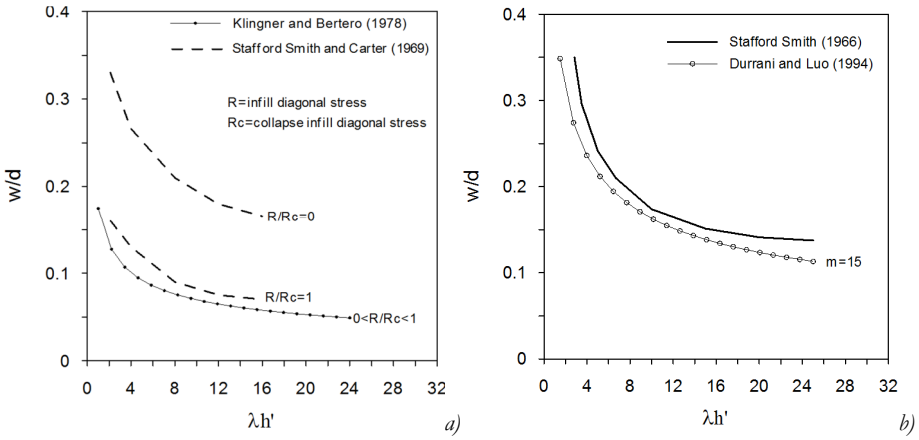

Fig. 1.18. Comparison between *w/d-λh'* curves: *a)* Stafford-Smith and Carter (1969) and Klingner and Bertero (1978); *b)* Stafford-Smith and Carter (1969) and Durrani and Luo (1994)

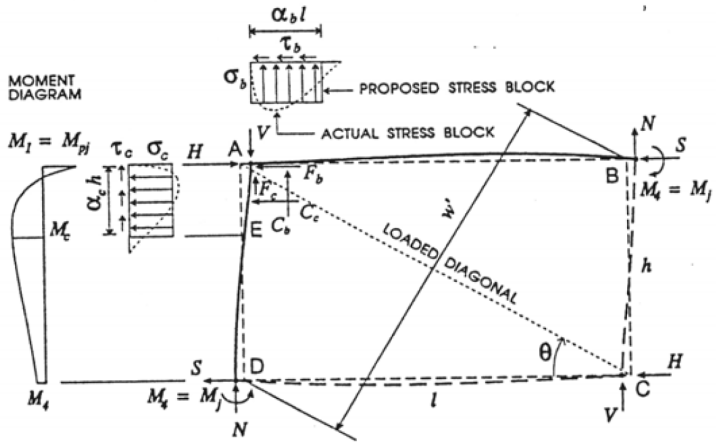

Fig. 1.19. Equilibrium of the forced acting on the infilled frame system (Saneinejad and Hobbs (1996)).

This partial review of the experimental and analytical investigations shows that the results obtained by different researchers are strongly influenced by the types of infill and test, and this conclusion is confirmed by examining and comparing results of other researches (e.g. Bertero and Brokken (1983), Valiasis and Stylianidis (1993), Panagiotakos and Fardis (1996), Mehrabi and Shing (1997), Madan et al. (1997)).

Basing on this realization **Papia** *et al.* (2003) developed a procedure for modelling the behaviour of infilled frames to be adapted to any particular

situation that is here described more in detail since it has been adopted for the research purposes of this work.

The identification of the section of the equivalent pin-jointed strut can be made by imposing the condition that the initial stiffness of the actual system (**Fig. 1.20-a**) be equal to the initial stiffness of the equivalent braced frame (**Fig. 1.20-b).**

It can be assumed that the "exact" stiffness of the system on Fig. 1.20-a can be evaluated by a micromodel approach, performed by adopting for the infill a discretization in agreement with the Boundary Element Method. This method allows an easy and reliable resolution of the contact problem in the regions in which frame and infill transmit compressive stress to each other. The shear stress in the same regions is assumed to be governed by the Coulomb friction law

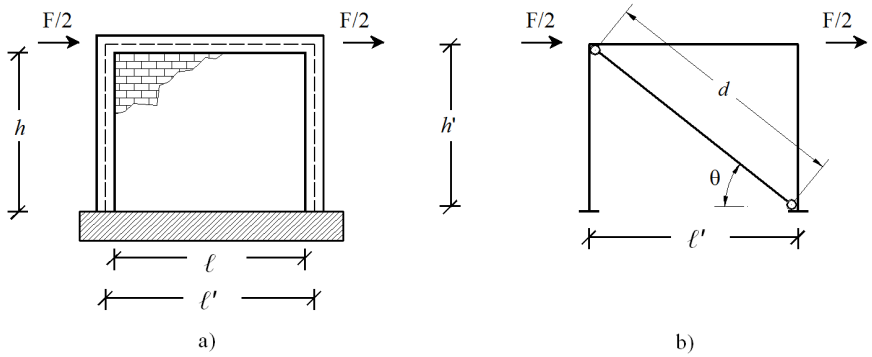

Fig. 1.20. Structural schemes: *a)* FEM-BEM Model; *b)* braced frame with equivalent strut.

If the problem is first solved by means of the micromodelling approach and subsequently by means of the simplified scheme then, by imposing the equivalence of the stiffness obtained from the two models, the dimension of the strut can be evaluated. Therefore, denoting as $\overline{D}_i$ and D_i the stiffness of the two different schemes, the condition of equivalence can be written as:

$$D_i = \overline{D}_i \tag{1.7}$$

The lateral stiffness of the braced system in Fig. 1.20-b, equivalent to the scheme in Fig. 1.20-a, can be evaluated in the unknown *w* by imposing the

condition that the horizontal forces to be applied to the schemes in **Fig. 1.21-b** and **Fig. 1.21-c** produce unitary displacement of the point P in the middle span of the beam.

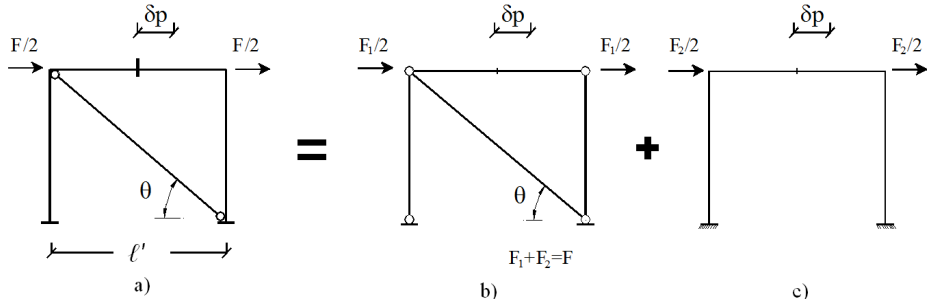

Fig. 1.21. Decomposition of later stiffness of macromodel.

It can easily be found that the equivalent stiffness of the braced system can be evaluated as sum of the stiffness of the systems in Fig. 1.21-a (D_d) and Fig. 1.21-b (D_f) as:

$$D_i = D_f + D_d = \frac{k_d \cos^2\theta}{1+\frac{k_d}{k_c} sen^2\theta + \frac{1}{4}\frac{k_d}{k_b}\cos^2\theta} + \\ + 24\frac{E_f I_c}{h'^3}\left(1-1.5\left(3\frac{I_b}{I_c}\frac{h'}{l'}+2\right)^{-1}\right) \tag{1.8}$$

where the following equivalencies hold:

$$k_d = \frac{E_d\, t\, w}{d}; \quad k_c = \frac{E_f\, A_c}{h'}; \quad k_b = \frac{E_f\, A_b}{\ell'} \tag{1.9}$$

In Eq. (1.9) E_d and E_f are the Young modulus of the infill along the diagonal direction and the Young modulus of the frame respectively and A_c and A_b the cross-sectional areas of the columns and the beam.

On the other hand the stiffness $\overline{D_i}$ of the micromodel response is determined by means of the FEM-BEM numerical procedure. If one impose the equivalence in Eq. (1.7) the with w of the equivalent strut can be determined by Eq. (1.8). The operation can be performed for any geometrical and mechanical characteristic assignments for the frame and the masonry infill.

If one sets the parameter λ^* as

$$\lambda^* = \frac{E_d}{E_f}\frac{th'}{A_c}\left(\frac{h'^2}{\ell'^2}+\frac{1}{4}\frac{A_c}{A_b}\frac{\ell'}{h'}\right) \tag{1.10}$$

the latter defines the geometrical and mechanical degree of coupling of the infill-frame system. The authors using the described procedure determined numerically a suitable correlation between this parameter and the dimensionless width *w/d* of the equivalent strut (**Fig.1.22**).

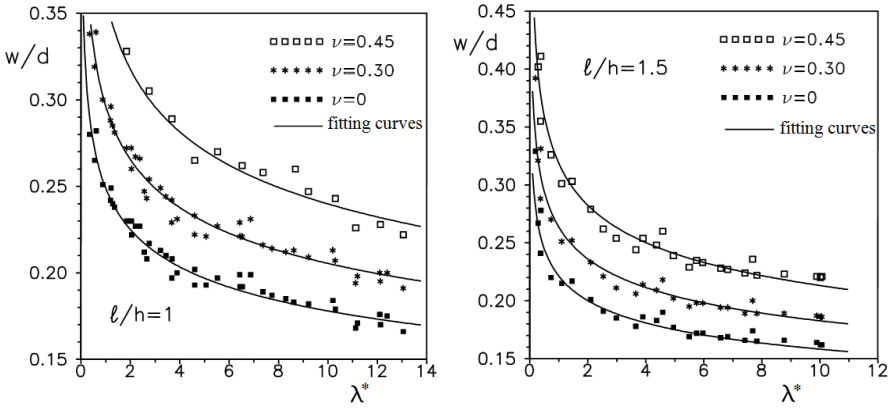

Fig. 1.22. Numerical values of *w/d* with variation of λ^* and fitting curves for aspect ratios $\ell/h=1.0$ and $\ell/h=2.0$.

The values of *w/d* obtained by the numerical investigation can be fitted by the analytical expression:

$$\frac{w}{d} = \frac{c}{z}\frac{1}{(\lambda^*)^{\beta}} \tag{1.11}$$

where c and β depend on the Poisson's ratio ν_d of the infill along the diagonal direction and can be evaluated as follows:

$$\begin{aligned} c &= 0{,}249 - 0{,}0116\,\nu_d + 0{,}567\,\nu_d^{\,2} \\ \beta &= 0{,}146 - 0{,}0073\,\nu_d + 0{,}126\,\nu_d^{\,2} \end{aligned} \tag{1.12}$$

and

$$z = \begin{cases} 1 & if\ \ell/h = 1 \\ 1.125 & if\ \ell/h = 1.5 \end{cases} \tag{1.13}$$

The Eq. (1.11) constitutes a tool for the direct estimation of the width of the equivalent strut by assigning the geometrical and mechanical features of the infill-frame system. The width of the structure depends on the Young modulus E_d and on the Poisson ration ν_d both calculated along the diagonal direction. In a further study Cavaleri *et al.* (2012) proposed a strategy for the evaluation of these values starting from the elastic properties of the masonry panel on its principal direction by means of the following relationships (Jones (1998))

$$\frac{1}{E_d} = \frac{1}{E_1}(\cos\theta)^4 + \left[\frac{1}{G_{12}} - \frac{2\nu_{12}}{E_1}\right](sen\,\theta\cos\theta)^2 + \frac{1}{E_2}(sen\,\theta)^4 \tag{1.14}$$

$$\nu_d = E_d\left[\frac{\nu_{12}}{E_1}((sen\,\theta)^4 + (\cos\theta)^4 - \left[\frac{1}{E_1} + \frac{1}{E_2} - \frac{1}{G_{12}}\right](sen\,\theta\cos\theta)^2\right] \tag{1.15}$$

An updated form of the Eq. (1.11) was provided by Amato *et al.* (2008, 2009) introducing the dependence of the stiffness of the equivalent strut also on the level of vertical load transferred frame the frame to the infill as follow

$$\frac{w}{d} = \kappa\frac{c}{z}\frac{1}{(\lambda^*)^\beta} \tag{1.16}$$

The coefficient κ depends on the value of the vertical deformation of columns ε_v produced by the total vertical load F_v acting at their top

$$\kappa = 1 + (18\lambda^* + 200)\varepsilon_v;\ \varepsilon_v \frac{F_v}{2A_cE_f} \tag{1.17}$$

In the same paper Papia *et al.* (2003) provided also a numerical study to modify the expression to take into account the loss of stiffness due presence of openings on the infill. The model have demonstrated a great agreement with experimental results and allows one to determinate really accurately the equivalent stiffness of any typology of infilled frame system.

1.5 The issue of the definition of a constitutive law for the equivalent strut in macromodeling approach

When is necessary to carry out nonlinear analyses of infilled frame stricter un which macromodels are used it is necessary to define a complete constitutive law for to attribute to equivalent strut. Since the latter is an idealization of a real physical problem (and doesn't actually exist) in this relationship cannot be performed by a direct experimental approach but only observing the nonlinear behaviour of an infilled frame system. Therefore the derivation of a constitutive law should be pursued by determining a relationship for the strut which allow one to reproduce the actual overall behaviour.

Several approaches have been proposed, some of them provide first the determination of a monotonic constitutive law to be used also as backbone curve for cyclic analyses among those **Panagiotakos** and **Fardis** by means of experimental cyclic tests on scale samples of frames with brick infill panels defined a simplified tetra-linear relationship (**Fig. 1.23**). If no residual resistance is assumed, the segments are reduced to 3. The branch describes the initial shear behaviour of the uncracked panel. The second corresponds to the formation of the equivalent strut in the panel, after the detachment of the infill from the surrounding frame.

The third describes the softening response of the panel after the critical displacement S_m and is characterized by the K_3 slope. The last horizontal segment defines the final state of the panel, and is characterized by a constant residual resistance. Actually, the results of the experimental tests show non-zero values of the residual resistance only for few samples, so that some authors decide to neglect it, assuming a softening line that reaches a zero residual strength at the displacement S_u (dashed line) in Fig. 1.23. Anyway the adoption of a residual strength has the advantage to improve the numerical stability of the analyses.

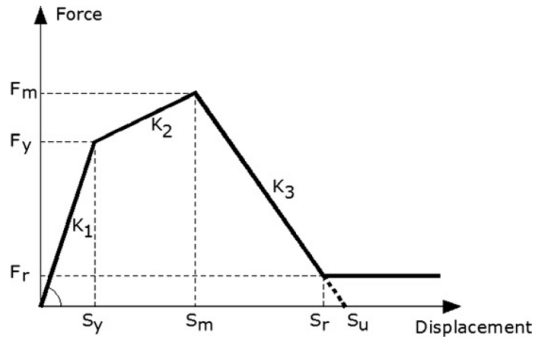

Fig. 1.23. Force-Displacement relationship for the equivalent strut model (Panagiotakos and Fardis(1996).

The determination parameters necessary to define the different branches of the curve are below described:

- Initial stiffness $\boldsymbol{K_1}$

$$K_1 = \frac{G_m t \ell}{h} \tag{1.18}$$

in which $\boldsymbol{G_m}$ is the tangential elastic modulus of the masonry infill, ℓ, h and t are the length, the height and the thickness of the panel respectively.

- Yielding force $\boldsymbol{F_y}$

$$F_y = f_{tp} t \ell \tag{1.19}$$

in which f_{tp} is the tensile strength of the panel, evaluated by a diagonal compressive test.

- Post yielding stiffness $\boldsymbol{K_2}$

$$K_2 = \frac{E_m t w}{d} \tag{1.20}$$

Being E_m the mean Young modulus of masonry and w the equivalent width calculated by means of Eq. 1.4.

- Maximum force $\boldsymbol{F_m}$ assumed as $1.25F_y$
- Displacement at maximum force $\boldsymbol{S_m}$

$$S_m = S_y + \frac{F_m - F_y}{K_2} \tag{1.21}$$

- Stiffness of the softening branch K_3 to be assumed in the range:

$$0.005\,K_1 \le K_3 \le 0.1K_1 \tag{1.22}$$

- Residual force F_r to be assumed in the range:

$$0 \le F_r \le 0.1F_y \tag{1.23}$$

- Displacement corresponding to the residual force S_r (or S_u)

$$S_r = S_m + \frac{F_m - F_r}{K_3} \tag{1.24}$$

This relationship represents a really general and flexible instrument to describe the nonlinear behavior of the equivalent strut in order to reproduce the one of the frame-infill system being this suitable for different ways of calibration. Some authors adopted this law in their studies proposing different criteria to determine some parameters to have a better agreement with their experimental results.

The constitutive law proposed by **Bertoldi** *et al.* (1993) was obtained by analyzing the seismic behavior of 10 different frames having two bays with equal span and a varying number of storeys (from 2 to 24) of equal height. The pushover analyses were performed both for the bare and for the infilled configuration, by adopting the model of the equivalent strut for the panels, defined by the subsequent equation due to Bertoldi *et al.* (1993).

$$\frac{w}{d} = \frac{K_1}{\lambda h} + K_2 \tag{1.25}$$

Where values of K_1 and K_2 can be evaluated by **Tab. 1.1** and the parameter λh is determined by the expression of Mainstone (1974). The Force–Displacement relationship of each equivalent strut is to the reported in **Fig. 1.24**.

	λh<3.14	**3.14< λh<7.85**	**λh>7.85**
K_1	1.3	0.707	0.47
K_1	-0.178	0.01	0.04

Tab. 1.1. Determination of parameters K_1 and K_2 (Bertoldi *et al.* (1993)).

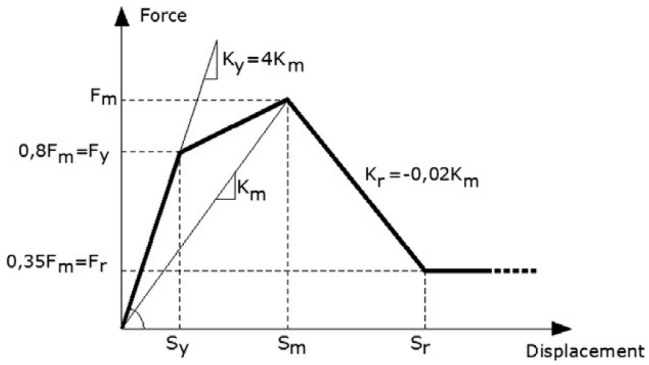

Fig. 1.24. Force-Displacement relationship for the equivalent strut model (Bertoldi *et al.* (1993).

The main parameters to be defined are K_m and F_m, which respectively are the maximum strength and the stiffness of the equivalent strut.

The stiffness K_m is given by

$$K_m = \frac{E_m wt}{d} co^{s2}\theta \tag{1.26}$$

In order to evaluate the maximum strength F_m, four possible collapse mechanisms of the panel are considered being the most recognizable by the experimental evidence and by the actual damage detected in infilled frame structures: crushing at the center of the panel, crushing of the corners, sliding of the horizontal mortar bed joints and diagonal shear failure.

A specific value of the ultimate stress σ_w acting uniformly on the cross section of the equivalent strut is associated to each of these mechanisms

- crushing at the center of the panel;

$$\sigma_{w1} = \frac{1.16\sigma_{m0}\tan\theta}{K_1 + K_2\lambda h} \tag{1.27}$$

- crushing of the corners;

$$\sigma_{w2} = \frac{1.12\sigma_{m0}\sin\theta\cos\theta}{K_1(\lambda h)^{-0.12} + K_2(\lambda h)^{0.88}} \tag{1.28}$$

- sliding of the bed joints;

$$\sigma_{w3} = \frac{(1.2 \sin\theta + 0.45 \cos\theta)u + 0.3\sigma_{m0}}{\frac{K_1}{\lambda h} + K_2} \tag{1.29}$$

- diagonal shear failure;

$$\sigma_{w4} = \frac{0.6\tau_{m0} + 0.3\sigma_0}{\frac{K_1}{\lambda h} + K_2} \tag{1.30}$$

In the above reported equations σ_w is the normal compressive strength of the masonry infill; τ_{m0} is the shear strength provided by a diagonal compressive test; u is the sliding resistance of the bed joints; σ_0 is the average normal stress on the panel. The identification of the width w is obtained by eq. 1.25 while the coefficients K_1 and K_2 are still obtained by Tab. 1.1. The horizontal component of the corresponding critical force is associated to the minimum of those strengths

$$F_m = (\sigma_w)_{\min} tw \cos\theta \tag{1.30}$$

This kind of approach is certainly more related to the mechanic of the system considering all main possible failure modalities but a large validation, based on several infilled frames typologies should be done to assess the actual applicability to every system.

Other formulations have been proposed to define the constitutive law of the equivalent strut. The two here proposed represent the most followed in the research application. In particular the definition of the strength of the equivalent strut constitutes the most significant issue when defining the constitutive law since it does not depend simply on the strength shear strength pane but more realistically on the infill-frame coupling and also on the portion of vertical load carried by the infill. For this reason a further relationship for the evaluation of the maximum strength to attribute to the equivalent strut due to Žarnić and Gostič (1997) is here given in order to provide a wider overview

$$F_{\max} = 0.818 \frac{\ell t f_{tp}}{C_1}(1+\sqrt{C_1^2+1}); \quad CI = 1.925 \frac{\ell}{h} \tag{1.31}$$

where the symbols have the same significance of the one used before.

1.6 The issue of the definition of a cyclic law for the equivalent strut i*n macromodeling approach

In order to extend the use of macromodels to perform nonlinear time history analyses several hysteretic models have been developed. The cyclic behaviour of an infilled frame is not easy to capture so the models that have been proposed from time to time had to introduce more complex rules to account the actual behaviour. Also in this case the definition of the cyclic law for the strut has to be determined observing the results of experimental cyclic tests on the overall infill-frame system in order to perform an indirect determination. The experimental evidence of tests shows that the overall behaviour has these general characteristics:

- both strength and stiffness degradation is recognized at each cycle depending on the previous inelastic excursion;
- the cycles show a significant dissipation capacity of the infilled frame system with respect to the bare ones if a brittle failure doesn't occur;
- the cycles are affected by pinching at the in proximity to the axes origins due to the fact that the cracks occurred in the previous loading phase have to be closed to regain strength and stiffness at the reloading.

One of the first hysteretic models to be used in macromodel approach is due to **Klingner and Bertero** (1978). The infill wall is replaced by two struts acting in compression only. The initial stiffness is obtained considering the diagonal *d* having a cross section of thickness equal to the actual one and width *w* calculated according to Mainstone (1971). The degradation of stiffness is then related to geometrical and mechanical parameters of the system, and is calibrated experimentally. The envelope curve provides a softening branch beyond the peak strength.

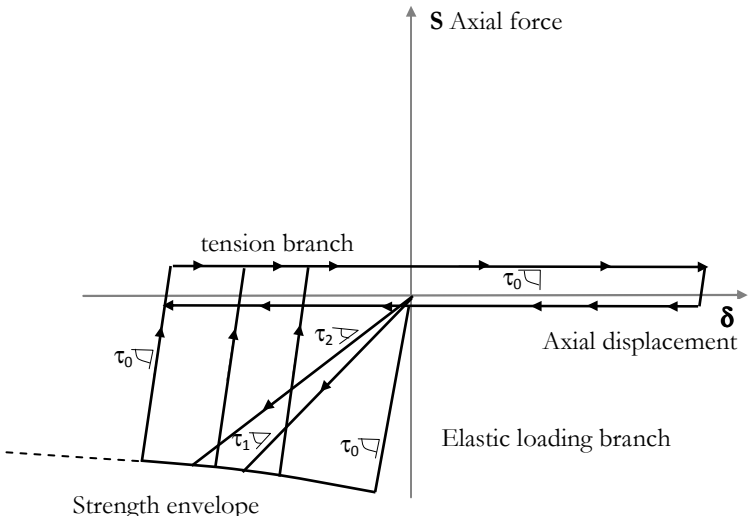

τ_o =angle defining initial stiffness and first branch of unloading curve
τ_i = arctg(S^*/δ^*), reloading angle after peak strength reaching
δ^* = maximum displacement of the cycle;
S^* = strength value on the enveloper curve corresponding to the maximum displacement of the cycle δ^*

Fig. 1.25. Hysteretic law for the equivalent strut proposed by Klingner and Bertero (1978).

In this model it can be observed that: 1) the strut has a limited strength; 2) the unloading stiffness in compression is equal to the elastic loading one; 3) each reloading branch starts from axes origin and is linear with a slope that depends on the previous maximum positive or negative displacement reached.

The model have been calibrated, and provides good results, for infilled frames in which the panel is connected to the surrounding frame by means of a diffused steel reinforcement. This typology of infills have anyway a limited spread in the building practice. Moreover, the model is not always suitable for an accurate reproduction of the experimental results, especially in the case of tests providing large displacements.

This limitation is due to the fact that the model does not account for the damage accumulation that produces the shrinkage of the panel and have as effect a shifting of the reloading branch at each cycle.

Doudoumis and Mitsopoulou (1986), to account for this fact, proposed a cyclic law in which the strut is inactive in tension and also in compression until reaching a certain level of deformation (**Fig. 1.26**). However the stiffness of the strut, is defined through an envelope curve and has constant loading-unloading slope that is not updated accounting for the history of deformation of the strut.

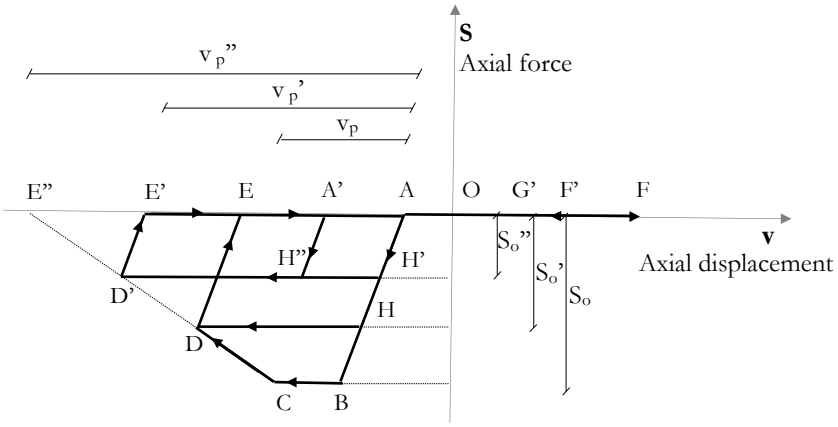

Fig. 1.26. Hysteretic law for the equivalent strut proposed by Doudoumis and Mitsopoulou (1986).

Panagiatakos and Fardis (1996) proposed a lateral force- lateral displacement law for the strut showing a good agreement with the experimental results obtained on infilled frames without connectors between frame and infill.

In this model (**Fig. 1.27**) the initial stiffness depends on the masonry panel (geometry and shear modulus equal to those of the material that constitutes the infills) but is not clarified how it applies to large buildings in which the introduction of a diagonal strut requires definition of its geometry and mechanical properties

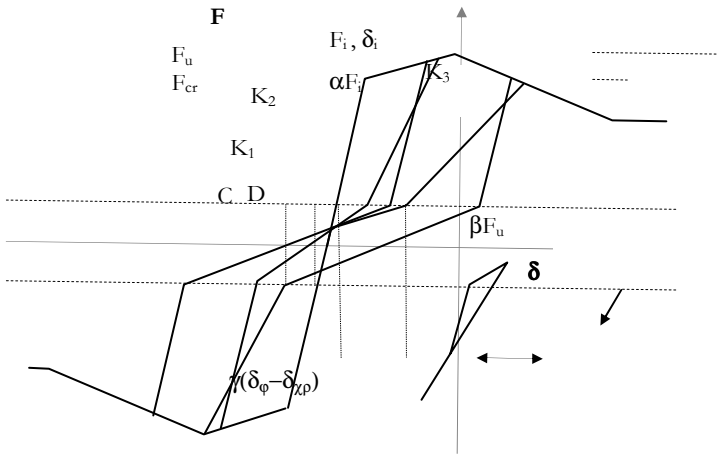

Fig. 1.27. Hysteretic law for the equivalent strut proposed by Panagiatakos and Fardis (1996)

Madan *et al.* (1997) developed an hysteretic model with parameters calibrated to simulate the stiffness and strength degradation of, as well as the effect of pinching for masonry infilled frames subjected to monotonic, cyclic, quasi-static and dynamic actions.

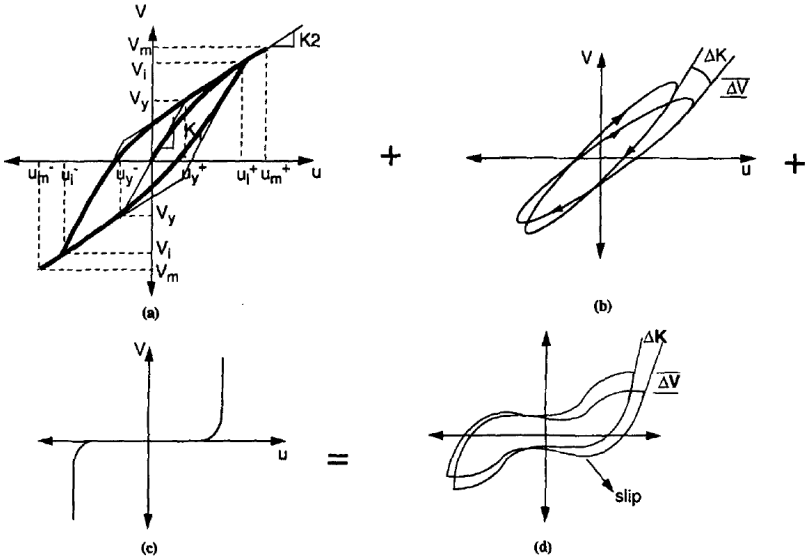

Fig. 1.28. Hysteretic law for the equivalent strut proposed by Madan *et al.* (1997).

In the proposed procedure the masonry panel is replaced by struts characterized having a strength envelope derived by the procedure of Saneinejad and Hobbs (1995). It is a parabolic law with initial stiffness equal

to twice the secant stiffness calculated in correspondence of the peak strength. The model of Saneinejad and Hobbs is integrated by Madan with an hysteretic Bouc-Wen model. The parameter calibration is performed on the basis of experimental results. The decomposition of the model is illustrated on **Fig. 1.28**. The resulting model (Fig. 1.28-a) is composed by the sum of a Bouc-Wen hysteresis model, a classic strength and stiffness degradation model and a slip lock model to include the pinching effect.

One of the most complete models is due to **Crisafulli** (1997) and in a subsequent work to **Crisafulli and Carr** (2007).

The model is able to simulate the contribution of the infill walls with different levels of precision, as a function of the input data available. The local effects due to the interaction between the panel and the frame may also be taken into account in a simplified way by adopting the approach of two diagonal equivalent struts for each direction (**Fig. 1.29-b**), which can be considered as an intermediate solution between a model with three struts, more accurate but also more complex (**Fig. 1.29-c**), and the model to a single strut (**Fig. 1.29-a**), more simple but also less precise.

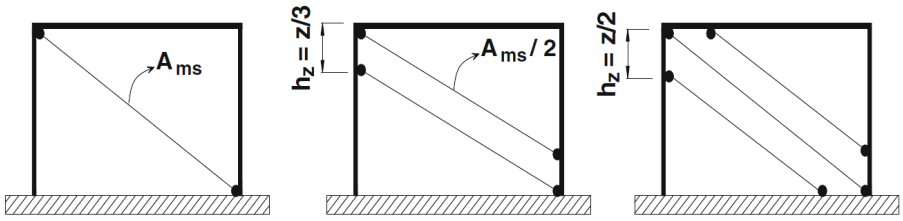

Fig. 1.29. Possible multiple strut configuration (Crisafulli (1997)): a) single strut; b) double strut; c) triple strut.

The cyclic behavior of masonry in compression (**Fig. 1.30**) is represented by different hysteresis rules to consider the load history. The link between stress and strain depends on the current deformation and various parameters relating to previous stress-strain stages. The model can also account for the effects of local contact, small intermediate cycles and tensile behavior of masonry.

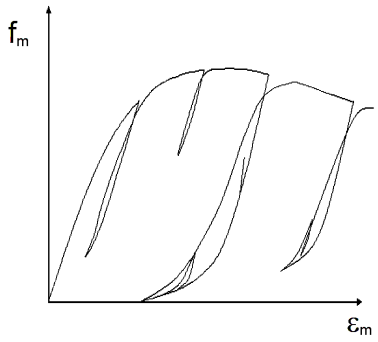

Fig. 1.30. Hysteretic law for masonry (Crisafulli (1997)).

One important characteristic of the model is the introduction of a special shear spring (**Fig. 1.31-a**) to account for frictional effects between mortar bed joints. It is assumed that the shear behavior of mortar is linear elastic before reaching the maximum shear strength in both loading and unloading phases (**Fig. 1.31-b**). In the elastic branch the shear stress τ is therefore obtained by the product of the deformation γ multiplied by the shear modulus of masonry G_m. The shear strength depends on the limit bond value τ_0, the friction coefficient μ and the compression stress acting perpendicularly to the mortar joints. The values of μ and τ_0 have to be calibrated in order to characterize properly the actual capacity of masonry. Once limit shear stress is reached, the bonding between mortar and bricks is lost and only frictional effects remain active.

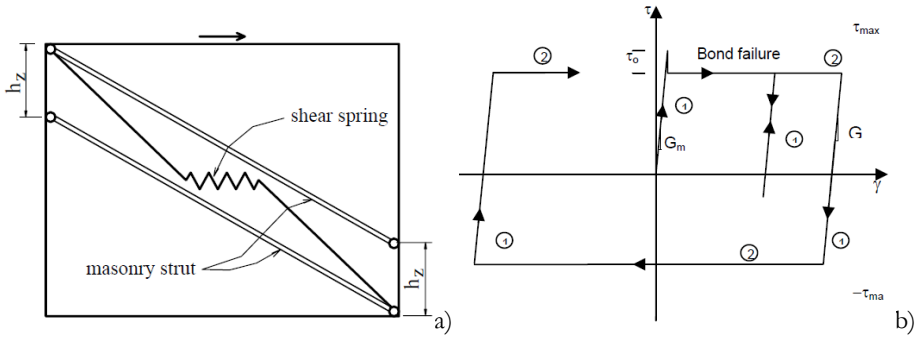

Fig. 1.31. Shear spring strut (Crisafulli (1997)): a) geometrical collocation; b) cyclic behavior.

The model of Crisafulli is probably the most complete infill-frame macromodel ever developed, being able to account directly for different

failure mechanisms, frictional effects and local infill-frame interaction. However the employment of this approach provides the calibration of a wide quantity of parameters that are really difficult to determine in most of the cases.

Finally the hysteretic model of **Cavaleri** *et al.* (2005) is here discussed. The model will be explained more in detail since it is the one adopted for the research purposes of this thesis.

The original idea have been developed basing on the law proposed by Klingner and Bertero (1978) introducing several modifications in order to improve the accuracy of loading and unloading branches.

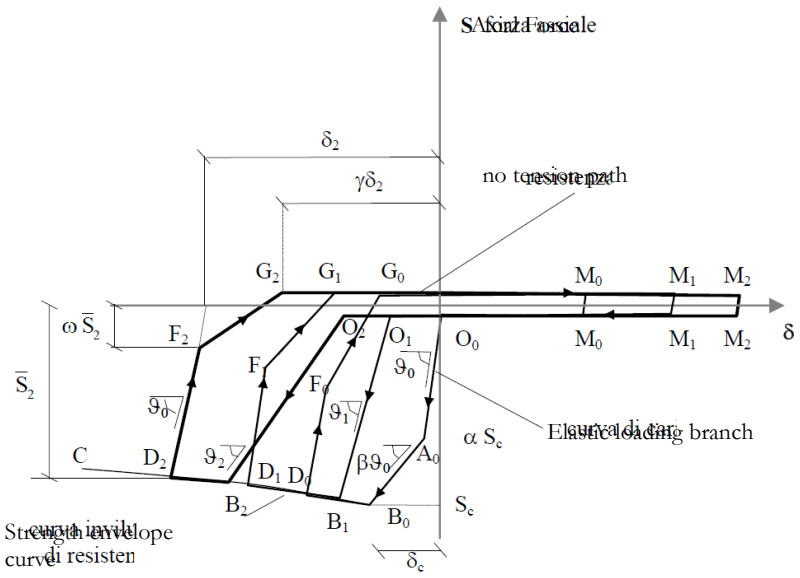

ϑ_0 = angle defining initial stiffness
α = parameter defining the extension of the elastic loading branch
β = parameter defining the reduction of stiffens before peak strength reaching
ζ = parameter defining the slope of strength envelope after peak strength reaching
ϑ_i = angle defining the slope of each loading branch (depending on parameter ρ)
$\bar{S}_i$ = restoring force at the displacement reversal
δ_i = displacement corresponding to zero restoring force during unloading in the hypothesis of constant stiffness equal to initial stiffness
ω = parameter defining the reduction of stiffness at the unloading
γ = parameter defining the reduction of stiffness at the unloading
ξ = parameter defining the extension of the loading branch in compression characterized by zero restoring force
ρ = parameter calibrating the slope of loading branch

Fig. 1.32. Hysteretic model for the equivalent strut (Cavaleri *et al.* (2005))

The cycles are guided by a strength envelope that corresponds to the ideal monotonic behavior. The main features of this model which makes it a rally flexible instrument regard the possibility to define a double slope for the first loading branch and for all the unloading branches. Moreover the model accounts for the pinching effect during the reloading caused by the shrinkage of the panel with a zero force branch before regaining strength and stiffness. The cycle shapes are updated at each cycle having since the parameter have memory of the previous displacement history.

The analytical law describing all branches and the parameters involved are below reported having as reference the **Fig. 1.32**.

(1) Linear elastic loading (path OA)

It is defined by the equation

$$S(\delta)=\frac{E_d A_i}{L}\delta \tag{1.32}$$

in which S is the axial force in the strut; E_d is the Young's modulus for the infill material in the diagonal direction; δ is the axial displacement (positive values corresponds to an extension); L is the length of the strut, taken here as the distance between diagonally opposite nodes; and A_i is the product of the panel thickness (assumed equal to the thickens of the strut) by the width of the equivalent strut itself; this path is covered at the first loading and may be covered at each reloading if the deformation of the strut (positive or negative) does not over-come the maximum deformation corresponding to point *B*. The point A_0 corresponds to the restoring force αS_c, S_c being the compressive strength in diagonal direction, while α is a parameter lower than 1 calibrated on the basis of the experience.

(2) Nonlinear loading (path AB)

It is covered when the deformation corresponding to point *A* is overcome and features the begin of the nonlinear behaviour of the strut. The branch AB is covered at the first loading and may be covered at each reloading until the maximum deformation of the strut (positive or negative) does not overcome the deformation corresponding to point B.

The slope of this linear branch is established by means of the calibrating parameter β. The equation that characterises this branch is

$$S(\delta)=\alpha S_c \frac{L}{E_d A_i}+\left(\delta-\alpha S_c \frac{L}{E_d A_i}\right)\beta \frac{E_d A_i}{L} \tag{1.33}$$

where each symbol has been described above.

The unloading from each point of the branch AB follows the same rules of the unloading as explained at the following points (4) and (5).

(3) Strength envelope curve (path BC)

The curve is defined by

$$S(\delta)=\frac{S_c}{\exp(\zeta\delta_c)}\exp(\zeta\delta) \tag{1.34}$$

in which δ_c is the deformation corresponding to S_c, that is

$$\delta_c=\frac{\alpha S_c}{K_0}+\frac{S_c-\alpha S_c}{\beta K_0} \tag{1.35}$$

Further, ζ is a parameter that defines the strength degradation, selected on the basis of experience, K_0 is the axial stiffness of the strut in the branch OA ($K_0=tan(\tau_0)=E_d A_i/L$).

(4) Unloading curve (path DF)

It is featured by a slope equal to that one of the first loading elastic branch. The point *F* corresponds to a level of the force equal to $\omega\bar{S}$, $\bar{S}$ being the restoring force at the inversion of the load and ω being a calibrating parameter lower than 1. The governing equation is

$$S(\delta)=\bar{\delta}-(\delta-\bar{\delta})\frac{E_d A_i}{L} \tag{1.36}$$

$\bar{\delta}$ being the deformation at load reversal.

(5) Unloading curve (path FG)

In this branch the slope is reduced with respect to the branch DF. The reduction of the slope is calibrated by the parameter γ. Referring, for sake of

simplicity, to the cycle 2 of Fig. 1.32 the slope $\tilde{K}_2$ of the branch F_2G_2, is defined as

$$\tilde{K}_2 = \frac{\omega \bar{S}_2}{\bar{\delta}_2 - \gamma\delta_2 - \frac{\bar{S}_2 - \omega\bar{S}_2}{K_0}} \tag{1.37}$$

where $\bar{\delta}_2$ is the deformation experienced by the strut at the load reversal point D_2, $\bar{S}_2$ is the force at the point D_2, δ_2 is the deformation that would assume the strut at the zero restoring force under the hypothesis of unloading with constant slope from point D_2. The parameter γ is calibrated on the basis of experience.

(6) Tensile curve (path GM)

In this stage the strut does not exhibit any strength (the branches GM depicted in Fig. 1.32 are not properly coincident with the axis of the displacements for a higher clarity, thus the figure is only apparently in contrast with the above statement).

(7) Reloading curve (path MO)

Also in this case the strut does not exhibit any strength until the point O is reached , featured by a level of deformation in compression different from zero. The position of the point O depends on the previous deformations. In details, referring for example to the cycle 2, the extension of the branch O_0O_2 is equal to $\xi\delta^*$, ξ being a parameter to be calibrated on the basis of the experience and δ^* the maximum deformation value (positive) experienced by the strut.

(8) Reloading linear curve (path OB)

This branch is covered after the deformation corresponding to point O is overcome and the deformation corresponding to point B_0 (positive or negative) is also previously overcome. The slope of this linear branch is influenced by the maximum deformation (positive or negative) experienced by the strut. In specific the governing equation is

$$S(\delta)=\xi\delta^{*}+(\delta-\xi\delta^{*})\rho Tan(\vartheta_{FG}) \tag{1.38}$$

ρ being a calibrating parameter to be chosen on the basis of the experience (generally greater than 1) and ϑ_{FG} the angle defining the slope of the unloading branch nearer to the zero value of the restoring force (branch FG) experienced by the strut.

The model above described can be also used to perform monotonic pushover analyses. In this case only the parameters α, β and ζ have to be calibrated since the latter define the shape of the strength envelope.

The predictive capacity of the model been have proved by the authors by means of a comparison with experimental quasi-static cyclic tests carried out on infilled frames infilled with different typologies of masonry and a first calibration of the parameters involved have been also provided.

Despite the flexibility of the model, that is suitable to be used in every general case, it depends on several parameter needing a wide experimental calibration. For this reason a further experimental campaign on the cyclic behaviour of infilled frames arranged with 3 different typologies of masonry infills have been programmed and completed during the research period of this PhD.

Basing on the partial results of this experimental campaign Amato (2008) provided some updated values of the calibrating parameters.

The complete results are reported in the subsequent chapter together with the one of the previous campaigns.

In this research thesis the results of those experimental tests have been used to calibrate a monotonic constitutive law to be used in static pushover analyses and, define a new simplified hysteretic model for the equivalent strut and validate the numerical models proposed.

2 EXPERIMENTAL INVESTIGATION ON THE CYCLIC BEHAVIOR OF INFILLED FRAMES

Two experimental campaigns on single-storey, single-bay RC fully infilled frames subjected to lateral cyclic actions are presented in this chapter. They represent the main experimental reference for the validation and the comparison of the numerical models developed in the subsequent sections.

Masonry infills selected for the execution of experimental tests (arranged with calcarenite blocks, clay blocks, and lightweight concrete blocks) represent three main traditional typologies used to realize infill panels. It is clear that each kind of masonry may present several sub-typologies in actual cases, therefore data here presented constitutes only a part of the possible results for each masonry infill typology.

2.1 Experimental investigation

The experimental campaigns were carried out at two different times. Regarding the more recent, experimental program included 8 infilled frames (S1 series) designed to represent a typical configuration recognizable in existing buildings designed for gravity loads and without any seismic detail. Geometrical ratios between beam and column cross-sections define a weak

column-strong beam scheme. The ratio between the bay length and the storey height was approximately 1. Specimens were arranged with three different kinds of masonry among the most widespread in practical applications: 2 specimens were infilled with calcarenite masonry (S1A specimens), 2 with clay masonry (S1B specimens), and 4 with lightweight concrete masonry (S1C specimens). The mean concrete strength, measured after 28 days, was 25 MPa, while the elastic Young modulus was about 23000 MPa. The reinforcement steel bars had a medium strength of 450 MPa. Mechanical and typological characteristics of specimens are summarized in **Tab. 2.1**.

Code	Masonry infill	N° of Specimens	Columns dimensions (cm)	Beam dimensions (cm)	
S1A	Calcarenite masonry	2	20x20	20x40	Actual investigation
S1B	Clay masonry	2	20x20	20x40	
S1C	Lightweight concrete masonry	4	30x30	30x40	
S2A	Calcarenite masonry	2	20x20	20x40	Older investigation
S2B	Clay masonry	2	20x20	20x20	

Table 2.1. Specimen geometrical characteristics description.

Experimental results and geometrical details for 4 additional infilled (S2 series) frame specimens, tested in a previous experimental campaign (Cavaleri et. al. 2005), are also considered here in order to enhance the data and comparing results. Of these four frames two were infilled with clay masonry and the further two with calcarenite masonry. Mechanical characteristics of concrete and rebars were similar to those previously mentioned. The details of the first and second series of specimens with specifications of the reinforcements are reported in Figs. **2.1-2.4**.

Masonries used to arrange the specimens were preliminarily subjected to experimental tests in order to assess their mechanical properties. Ordinary, lateral and diagonal compressive tests were carried out. Compressive tests on mortars and units (in both orthogonal directions) were also performed. This preliminary experimental campaign is exhaustively discussed in Cavaleri et al. (2012). All the significant results in terms of mechanical elastic properties and strengths are summarized in **Tab. 2.2**.

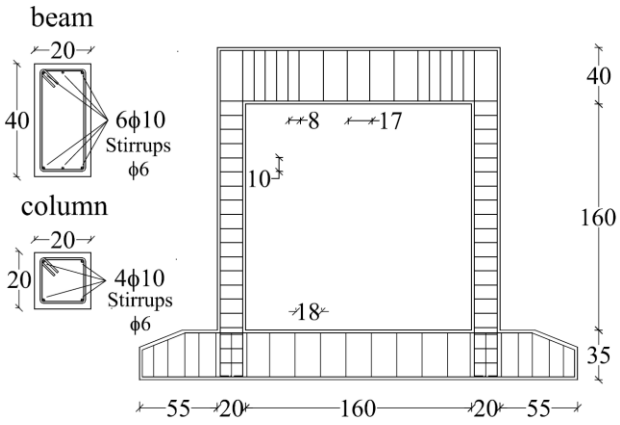

Fig. 2.1. S1A and S1B specimens details

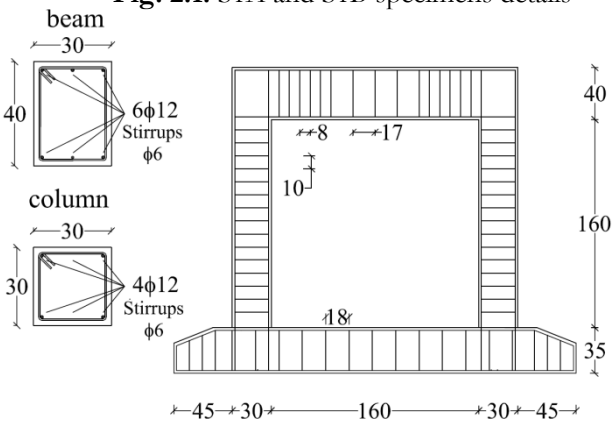

Fig. 2.2. S1C specimens details.

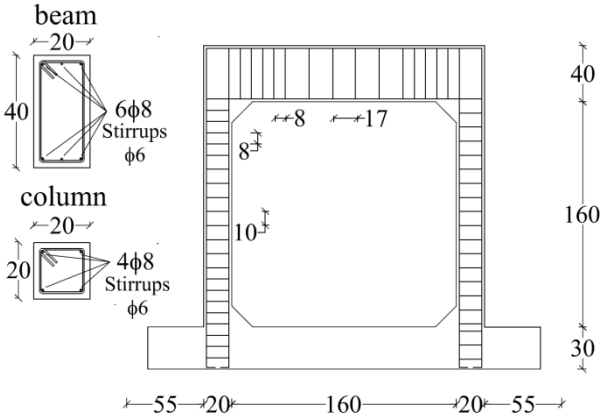

Fig. 2.4. S2A and S2B specimens details.

Calcarenite masonry	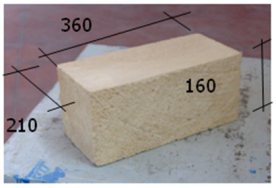			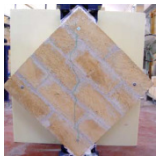
S1A	Mortar - f_m=3.06 Units - f_{bm} =7.06	E_2=3933 f_m=2.67	E_1=7408 f_m=3.08	G_{12}=1348 ν_{12}=0.22; ν_{21}=0.10 f_{vm}=0.73
S2A	Mortar - f_m=9.89 Units - f_{bm} =4.00	E_2=7106 f_m=4.57	E_1=9528 f_m=3.92	G_{12}=2937; ν_{12}=0.10; ν_{21}=0.085 f_{vm}=0.89
Clay masonry	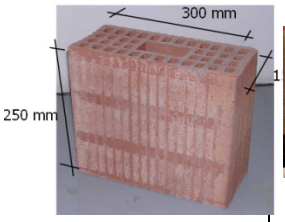		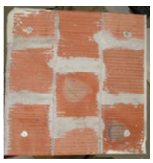	
S1B-S2B	Mortar - f_m=9.16 Units - $f_{bm,v}$=37.68 $f_{bm,h}$=2.06	E_2=6401 f_m=8.66	E_1=5038 f_m=4.18	G_{12}=2547 ν_{12}=0.07; ν_{21}=0.09 f_{vm}=1.07
Lightweight concrete masonry	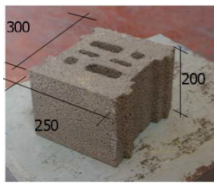			
S1C	Mortar - f_m=9.57 Units - $f_{bm,v}$=4.07 $f_{bm,h}$=3.15	E_2=4565 f_m=1.74	E_1=1944 f_m=0.30	G_{12}=2042; ν_{12}=0.13; ν_{21}=0.22 f_{vm}=0.29
Masonry mechanical properties reference system	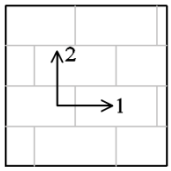			

Table 2.2. Mechanical properties of masonry employed to arrange infills.

2.2 Test setup and instrumentation

The test setup is shown in **Fig. 2.5**. Specimens were primarily subjected to an axial vertical constant load (200 kN on each column), applied by four manually controlled hollow hydraulic jacks (**Fig. 2.6**). The device for the application of vertical loads was constrained with respect to the horizontal displacement in order to maintain the verticality and to permit free sliding of the head of the frame. The resulting force applied was monitored by measuring the oil pressure in the jacks. Lateral loads were applied by a horizontal double-acting jack (**Fig. 2.7**) monitored by a load cell having 500 kN as the nominal load interfaced with the acquisition system. A special system of constraints was provided at the base of specimens to avoid rigid translations and rotations (**Fig. 2.8**). Displacements at the top of the specimen were measured by means of a transducer having measuring range 0-200 mm (**Fig. 2.9**). In addition to the lateral displacement of the frame head, the horizontal displacement and the rotation (in the plane of the frame) of the base were monitored by 4 digital gauges having measuring range 0-12.5 mm; in this way constraining efficacy was verified. In **Fig. 2.10-2.12** a real view of some specimens in the test apparatus is shown.

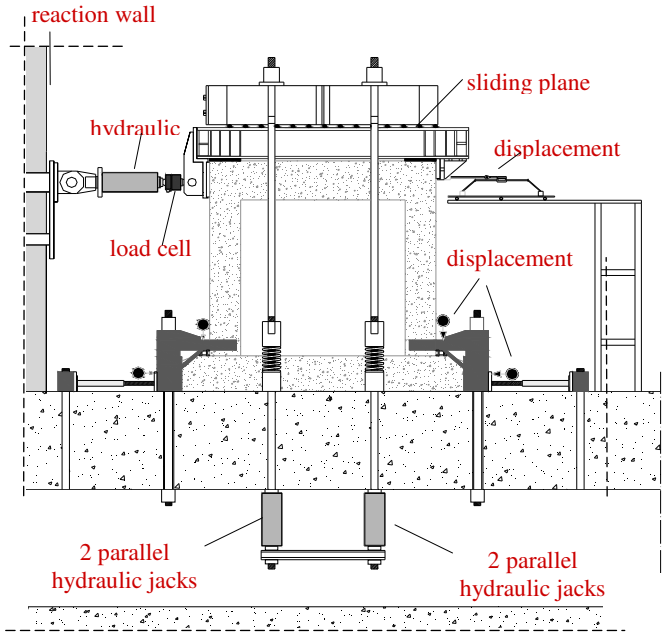

Fig. 2.5. Test set up.

Fig. 2.6. Hollow hydraulic jacks for vertical load application.

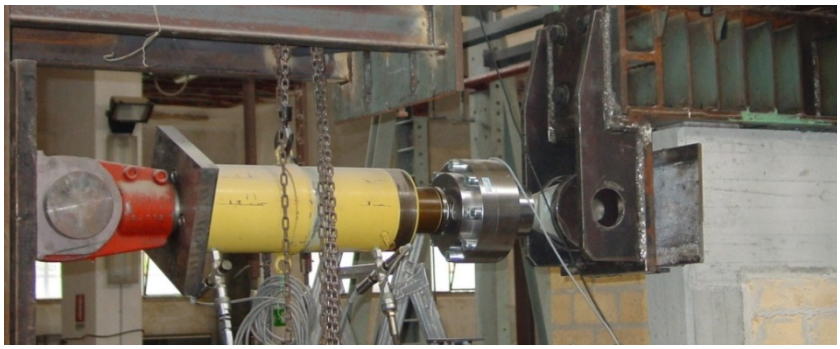

Fig. 2.7. Hydraulic jack for lateral load application.

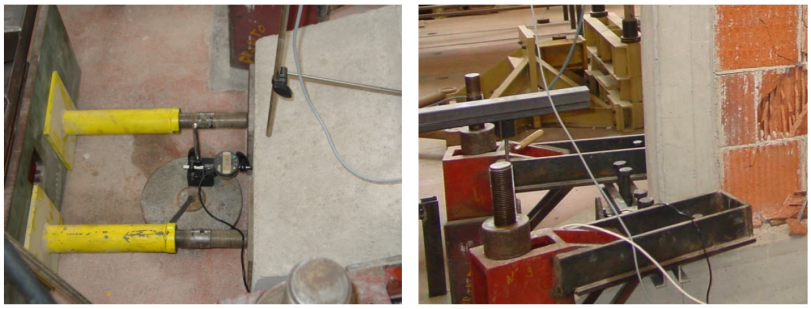

Fig. 2.8. Specimen translation and rotation constraints.

Fig. 2.9. Gauge for the top lateral displacement measuring.

Fig. 2.10. Calcarenite masonry infilled frame specimen in the test apparatus.

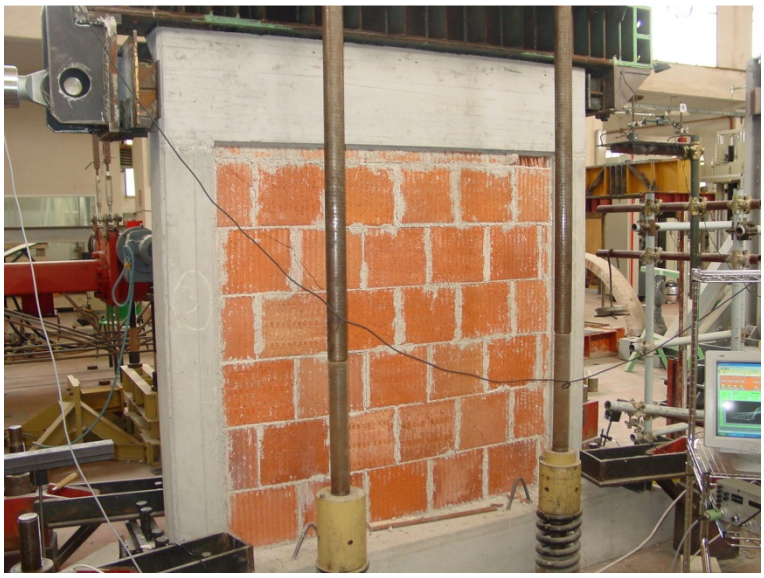

Fig. 2.11. Clay masonry infilled frame specimen in the test apparatus.

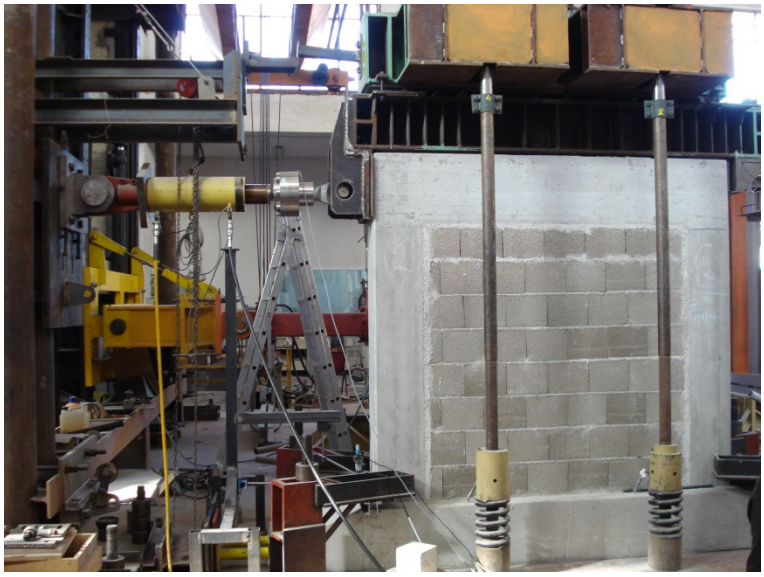

Fig. 2.12. Lightweight concrete masonry infilled frame specimen in the test apparatus.

2.3 Bare fames

Bare frames stiffness was measured before infills were made in order to compare it with that gained once infills were realized. Once evaluated the shear strength of the columns and it was recognized that flexural mechanisms anticipate shear mechanisms, the strength of the bare frames was predicted by a simplified model corresponding to a limit equilibrium associated with plasticization of the top and base sections of columns. In calculating the ultimate moments of the columns M_u, the presence of an axial load on columns N_c (*200 k*N) was taken into account. Referring to **Fig. 2.13**, the bare frame strength F_{ub} was evaluated by the limit equilibrium condition leading to the following expression:

$$F_{ub} = \frac{4M_u(N_c)}{h^*} \tag{2.1}$$

in which h* is the net height of the bare frame. The predicted values of lateral strength for the S1 and the S2 series are reported in **Tab. 2.3**. In the same table the mean experimental stiffness are inserted.

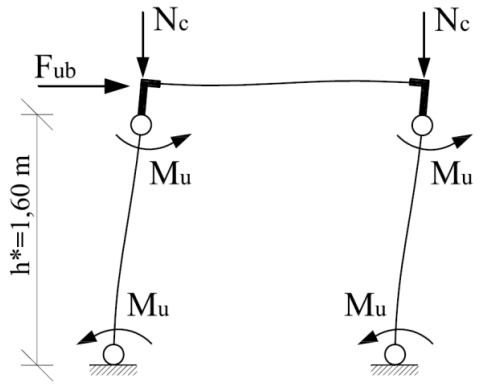

Fig. 2.13. Simplified scheme for evaluation of lateral strength of bare frames.

	M_u [kNm]	F_{bu} [kN]	K_b experimental average [kN/mm]
SIA-S1B-S2	24	60	11
S1C	48	120	43
S2	22	55	-

Table 2.3. Plastic moments of columns cross sections, analytical lateral strength and experimental lateral stiffness of bare frames.

2.4 Cyclic response of infilled frames

The S1 series specimens were tested by increasing the displacement at each cycle up to a drift of 2.5 %. The cycle amplitude increment was variable during the loading pattern up to a maximum of 10 mm for the last cycles. Damage mechanisms were monitored during the tests in order to detect propagation of cracks on infills and frames. Stiffness, strength, and ductility evaluations were carried out. The S2 series specimens were tested up to a drift of 0.6%. The cyclic responses for S1 and S2 series specimens are reported in **Figs. 2.14-2.25**.

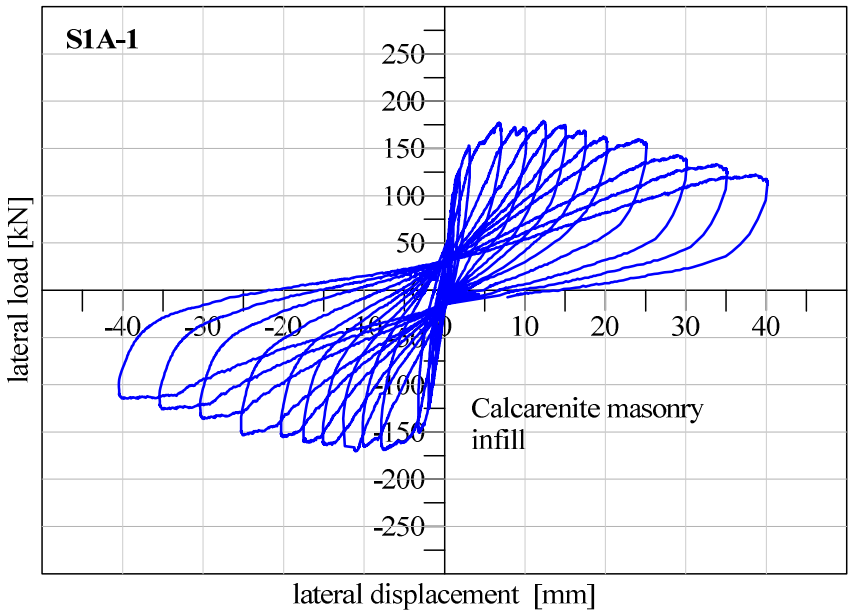

Fig. 2.14. Force-displacement experimental curves of clay calcarenite infilled specimen: S1A-1.

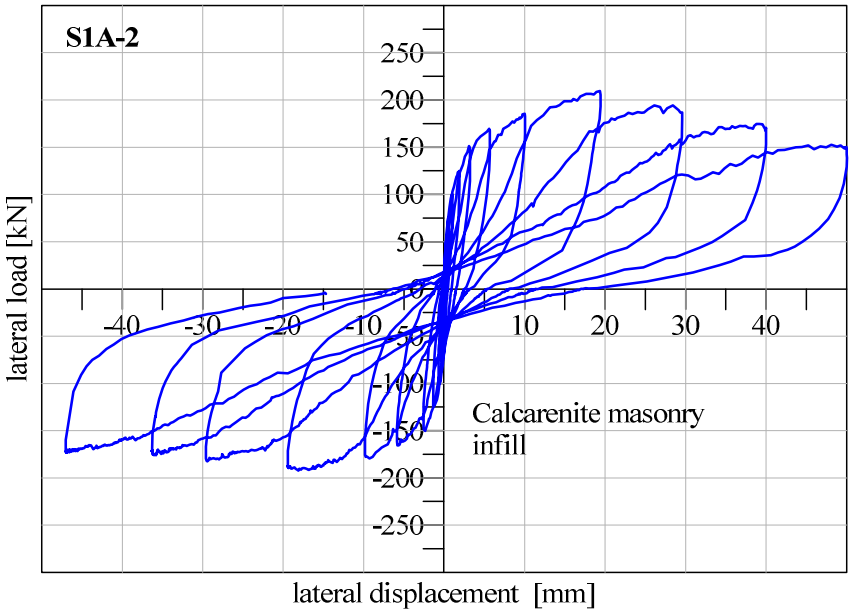

Fig. 2.15. Force-displacement experimental curves of clay masonry infilled specimen: S1A-2.

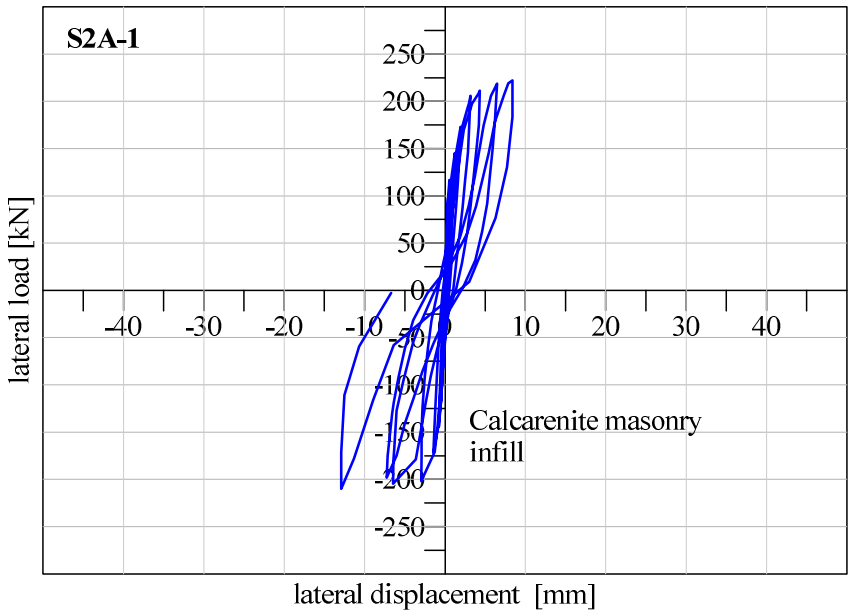

Fig. 2.16. Force-displacement experimental curves of clay calcarenite infilled specimen: S2A-1.

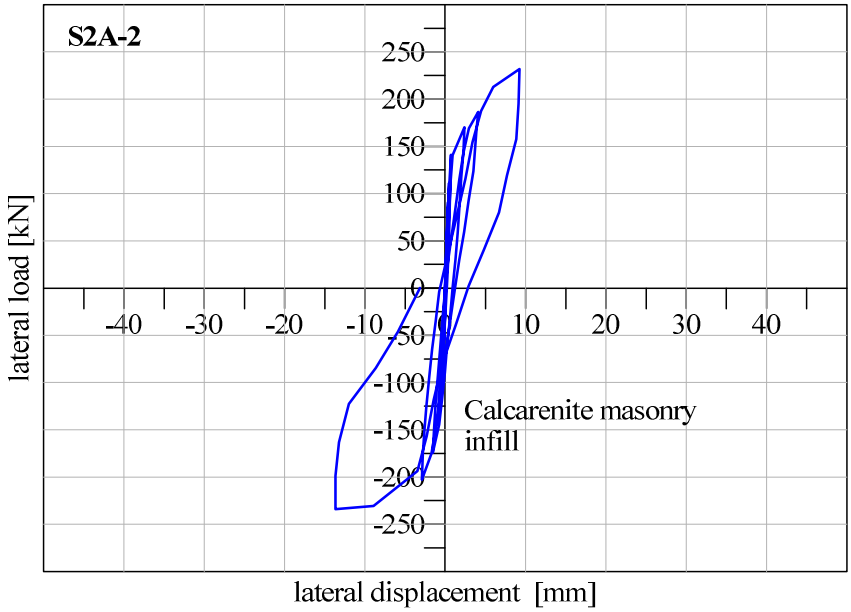

Fig. 2.17. Force-displacement experimental curves of clay masonry infilled specimen: S2A-2.

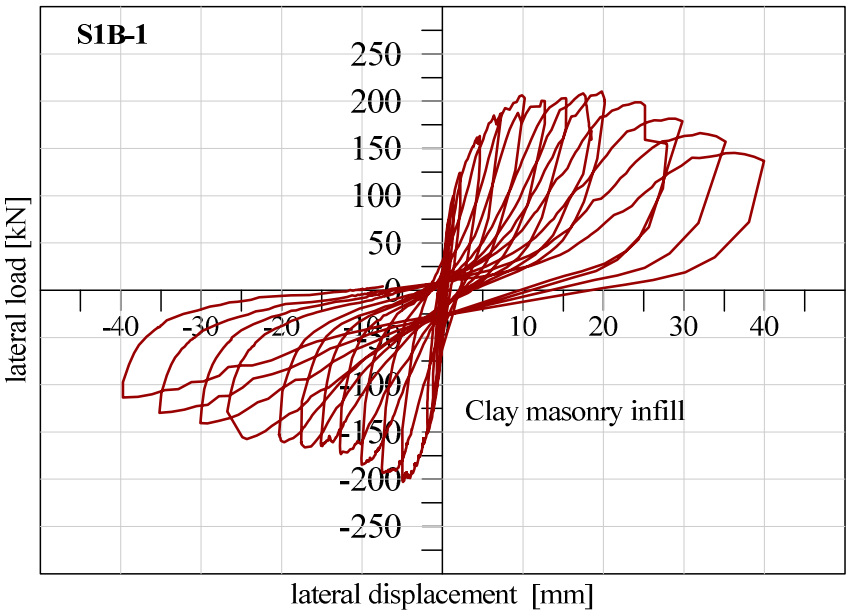

Fig. 2.18. Force-displacement experimental curves of clay masonry infilled specimen: S1B-1.

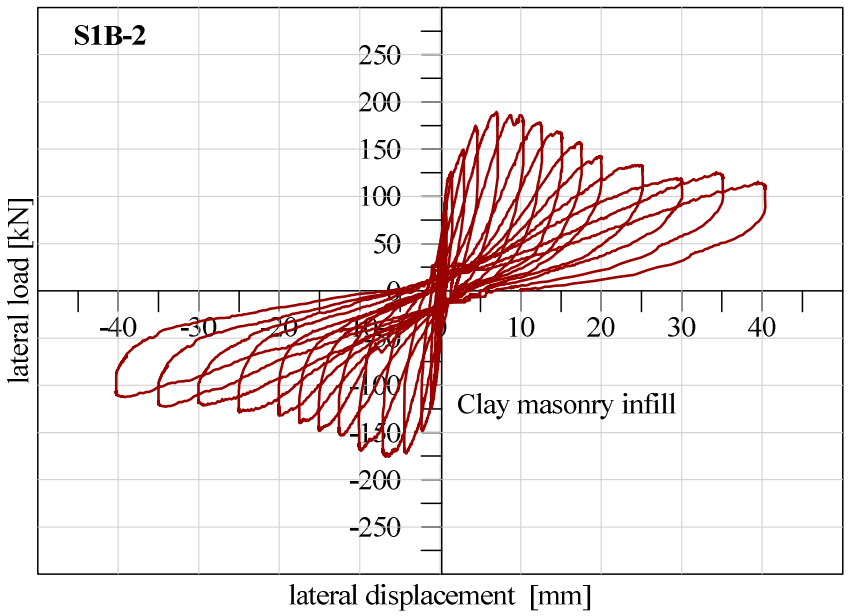

Fig. 2.19. Force-displacement experimental curves of clay masonry infilled specimen: S1B-2.

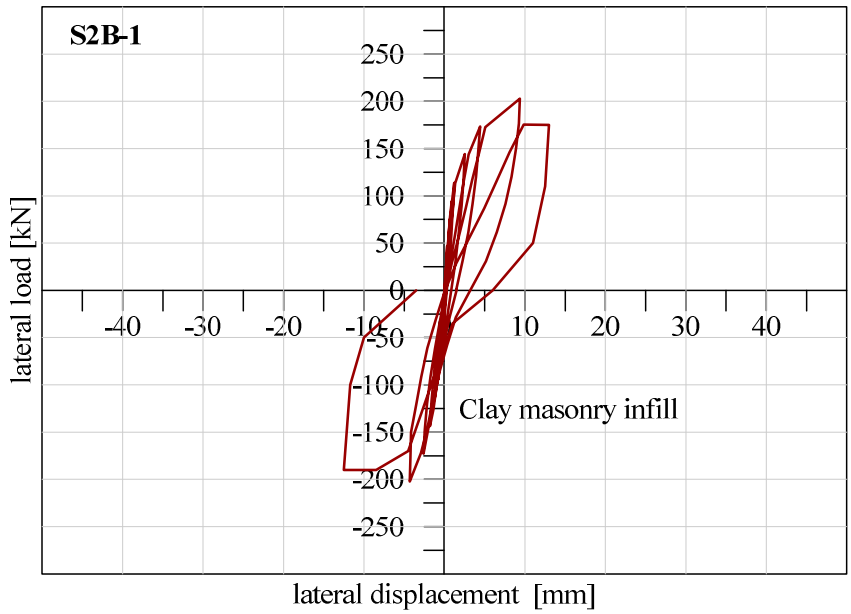

Fig. 2.20. Force-displacement experimental curves of clay masonry infilled specimen: S1B-1.

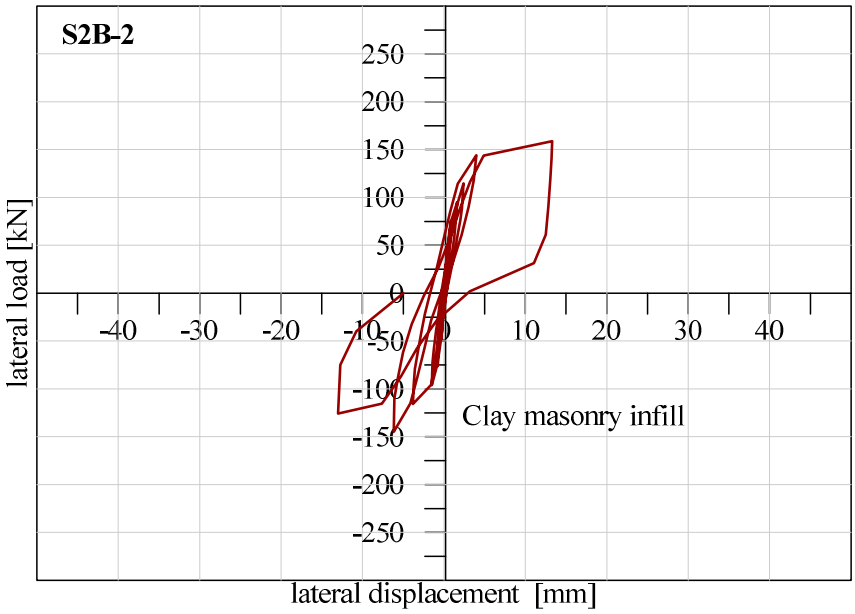

Fig. 2.21. Force-displacement experimental curves of clay masonry infilled specimen: S1B-2.

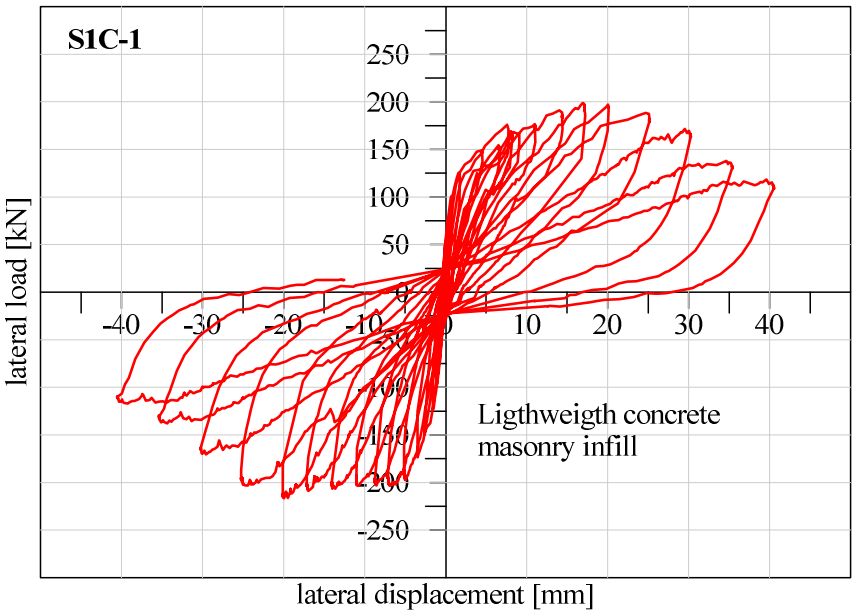

Fig. 2.22. Force-displacement experimental curves of clay masonry infilled specimen: S1C-1.

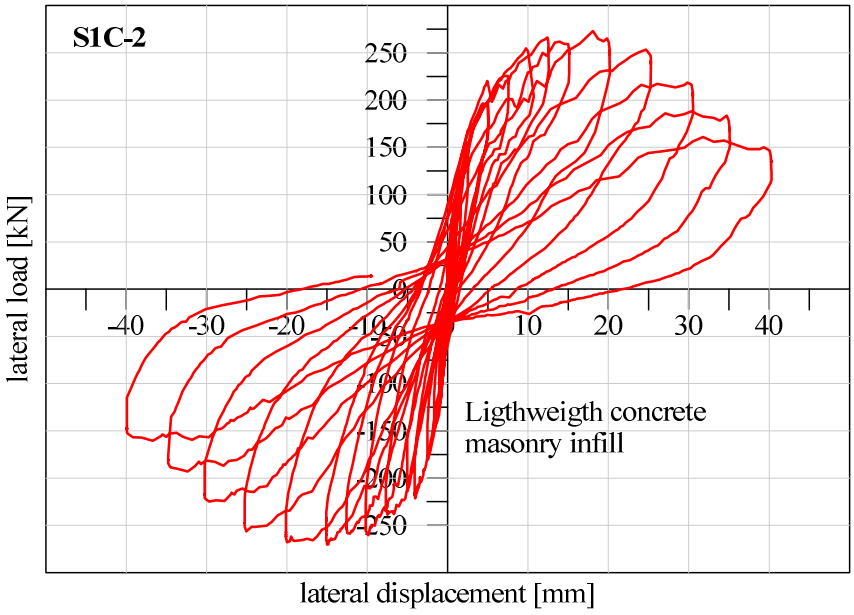

Fig. 2.23. Force-displacement experimental curves of clay masonry infilled specimen: S1C-2

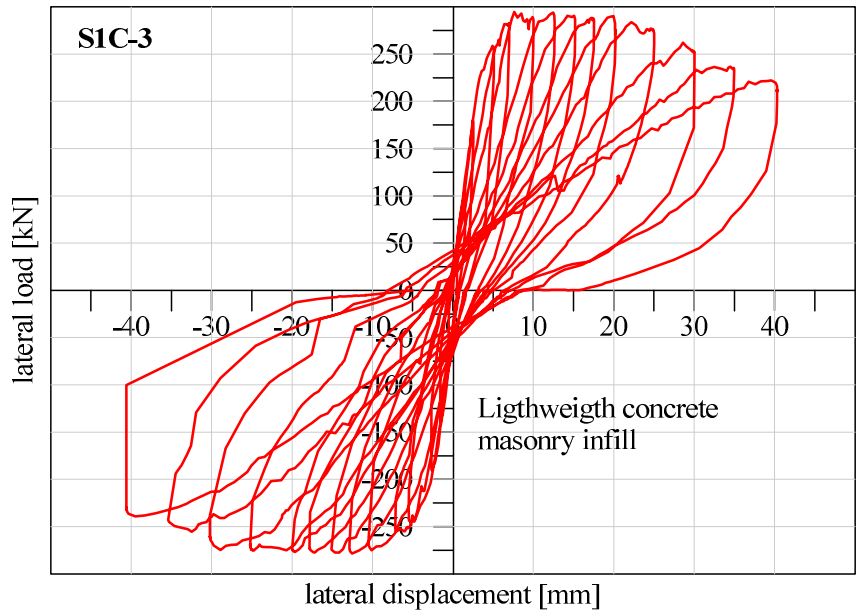

Fig. 2.24. Force-displacement experimental curves of clay masonry infilled specimen: S1C-3.

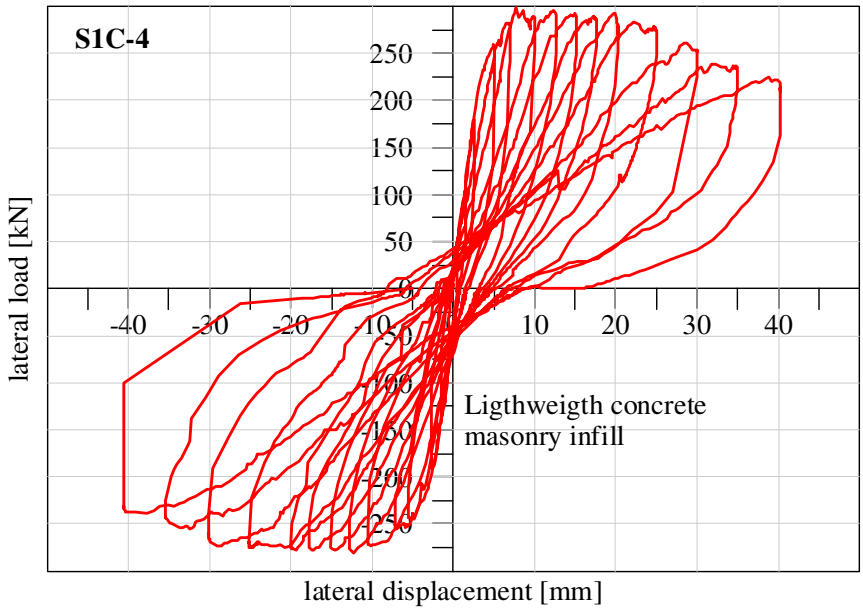

Fig. 2.25. Force-displacement experimental curves of clay masonry infilled specimen: S1C-4.

In terms of maximum average lateral strength, calcarenite and clay masonry infilled specimens showed a global increase of about 3.4 times compared to the bare frames. Lightweight concrete masonry infills had a lower, but not negligible, influence on strength, showing an increase of about 2.2 times due first of all to lower shear strength, which is typical of this kind of masonry. A low strength degrading after peak reaching was observed for all specimens, demonstrating an efficient confinement effect exercised by the frames on the infill panels.

For the S1 series specimens significant loss of strength is observable only after a drift of 1.8%. Cracking propagation affected both frames and infills. First approximately diagonal cracks formed on frames at the upper joints. Corresponding diagonal cracks affected infills mainly following mortar joints. For larger displacements (over 20 mm) more evident cracking propagation, corresponding to the beginning of strength decay, was observed, accompanied by formation of sub-horizontal cracks in the middle of columns and more severe damage at beam column joints (**Fig. 2.26**). Clay and lightweight concrete masonry infills were affected by partial crushing of units placed at the corners and along the two diagonal directions while more diffused cracking patterns were recognized on calcarenite masonry infills, demonstrating a better global capacity of stress redistribution. In **Fig. 2.27-2.29**, some infilled frame specimens at the end of tests with the cracking pattern detected are shown.

Regarding to stiffening effects, specimens infilled with calcarenite and clay masonry showed the most significant increment, exhibiting respectively an average increase of 8.3 and 11.4 times. Lightweight concrete masonry infills showed instead a lower influence on overall stiffness, recording an increment of 1.9 times compared to the bare frames. However all specimens exhibited a significant stiffness degradation at each cycle, especially after the peak strength was reached. On the other hand the peak strength did not significantly decrease until large displacements occurred. Cycles experimental curves showed for all tested specimens a significant pinching effect at load reversal, justified by the fact that the entire plastic excursion, previously accumulated, had to be recovered to regain stiffness and bearing capacity.

Ideally enveloping the cycles of the responses, global ductile behaviour was observed, though the collapse of the whole system was governed by failures of RC column mechanisms not clearly recognizable as ductile.

Fig. 2.26. End of column and beam – column joint damaging.

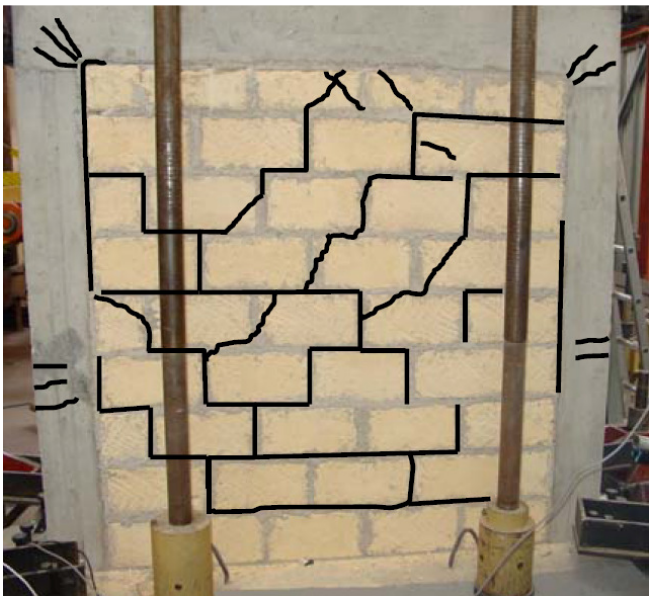

Fig. 2.27. Specimen cracking patterns at the end of test.

Fig. 2.28. Specimen cracking patterns at the end of test.

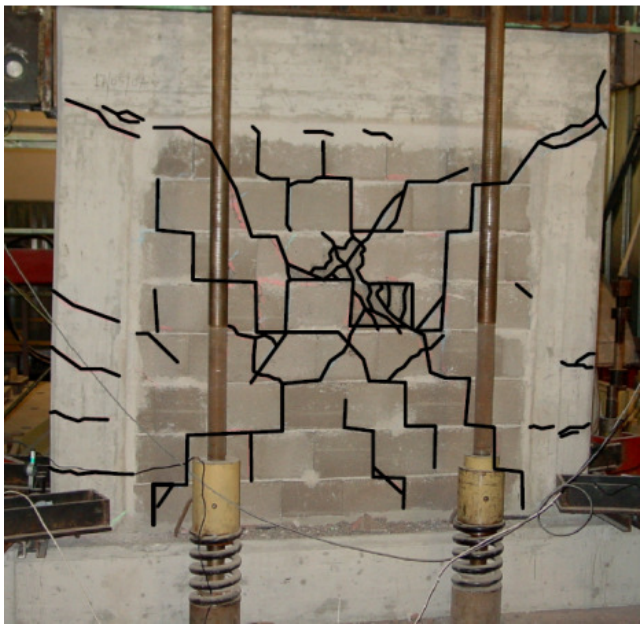

Fig. 2.29. Specimen cracking patterns at the end of test.

2.5 Considerations on strength increment due to infills

As shown by the experimental results, infill panels play a major role in global strength and stiffness. Regarding strength, an increase of 2-4 times compared to the bare frame was detected for the different infill typologies.

It is not simple to predict the global strength of infilled frames, which depends on the degree of coupling between frame and infill and involve a high numbers of variables. Nevertheless, the final strength of infilled frames is important for the definition of adequate mechanical properties to assign to equivalent strut. As well exposed in the subsequent sections, in order to attribute for each case a monotonical constitutive law, representing the backbone curve for Pivot model, may be useful the definition of a tool being able to predict the final strength of infilled frame systems. For this purpose it is possible to establish, basing on experimental results, a correlation between global strength increment and frame/infill mechanical properties. If one defines the strength increment ratio δ_s, due to the presence of the infill panel as

$$\delta_s = \frac{F_{ui}}{F_{ub}} \tag{2.2}$$

in which F_{ui} is the maximum strength exhibited by the infilled frame and F_{ub} is the bare frame lateral strength, an expression for δ_s, including the mean shear strength f_{v0m} of masonry infills, can be established by observing the best fitting of experimental results as reported in **Fig. 2.30**, that is

$$\delta_s = 2.75 \, (\alpha_s f_{v0m} \,)^{0.17} \tag{2.3}$$

where the parameter α_s is expressed as

$$\alpha_s = \frac{F_{up} \cos\theta}{F_{ub}} \tag{2.4}$$

θ being the angle defining the slope of the diagonal of the frame while F_{up} represents a conventional diagonal strength of the panel, classically obtained as

$$F_{up} = f_{v0m} t d \tag{2.5}$$

where t is the thickness of the panel and d the length of its diagonal dimension.

As noticeable in **Fig. 2.30**, single and mean experimental values appear fairly condensed around this proposed correlation law which expresses substantially that the overall strength increment depends not only on shear strength of the panel but is significantly modulated by the panel – frame strength ratio α_s.

Experimental values employed for the construction of these analytical relationships include the results of the S1 and S2 series of specimens and also the strength values reported in Kakaletsis *et al.* (2009) and Koutromanos *et al.* (2011) who tested different typologies of brick masonry infills. In **Tab. 2.4** the strength values and detected ratios are summarized.

A simple way to use the above defined correlation for providing and estimating the equivalent diagonal strut peak strength is discussed afterwards.

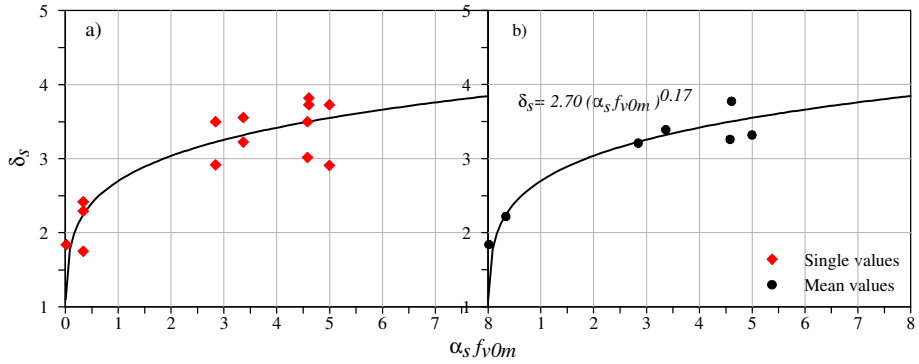

Fig. 2.30. δ_s–$\alpha_s f_{v0m}$ correlation. *a)* Values of δ_s referred to each specimen; *b)* mean values of δ_s referred to each typology of infilled frame.

Spec. Code	Infill units	f_{v0m} [Mpa]	F_{ub} [kN]	F_{ui} [kN]	δ_s	δ_s mean	$F_u Cos\,\theta$ [kN]	α_s	$\alpha_s f_{v0m}$ [Mpa]
S1A-1	Calcarenite	0.73	60	175.0	2.92	3.21	233.6	3.89	2.84
S1A-2	Calcarenite	0.73		210.0	3.50		233.6		
S1B-1	Clay	1.07	60	210.0	3.50	3.26	256.8	4.28	4.58
S1B-2	Clay	1.07		181.0	3.02		256.8		
S1C-1	LW conc.	0.29	120	210.0	1.75	2.22	139.2	1.16	0.34
S1C-2	LW conc.	0.29		275.0	2.29		139.2		
S1C-3	LW conc.	0.29		290.0	2.42		139.2		
S1C-4	LW conc.	0.29		290.0	2.42		139.2		
S2A-1	Calcarenite	0.89	55	210.0	3.82	3.77	284.8	5.18	4.61
S2A-2	Calcarenite	0.89		205.0	3.73		284.8		
S2B-1	Clay	1.07	55	205.0	3.73	3.32	256.8	4.67	5.00
S2B-2	Clay	1.07		160.0	2.91		256.8		
Ref. [28]	Clay Bricks	0.08	-	-	1.84	1.84	7.0	0.19	0.02
Ref. [33]	Clay Bricks	0.80	180	640	3.56	3.39	757.0	4.21	3.36
Ref. [33]	Clay Bricks	0.80	180	580	3.22		757.0	4.21	3.36

Table 4. Strength values exhibited by specimens varying shear strength of panels and infill/frame strength ratios.

2.6 Considerations on the ductility of infilled frames

Considering the strength envelopes of the experimental cyclic tests a global ductile behaviour can be observed. The strong nonlinearity of the initial branch and the low slope of the softening branches make it difficult to exactly identify the yielding and ultimate displacements to calculate the ductility factor. As suggested in Kakaletsis *et al.* (2009) a conventional ductility factor $\mu_{0.85}$ can be defined drawing a horizontal straight line at 85% of the peak strength, intersecting the envelope at two points, one on the ascending and one on the descending branch. The ductility strength envelope factor $\mu_{0.85}$ is calculated as the ratio of displacements corresponding to these two points, while the specimen ductility factor is the mean value of the two $\mu_{0.85}$ ductility factors evaluated for the positive and negative envelopes of the same specimen. The ductility factors calculated for the tested specimens are reported in **Tab. 2.5**, where the mean ductility values are also shown for each infill typology. The values vary from 5.08 for clay masonry infilled specimens to 7.61 for lightweight concrete masonry infilled specimens. Intermediate behaviour was exhibited by calcarenite masonry infilled specimens, for which the mean ductility factor is 6.15. It should be noticed that lightweight concrete masonry infilled specimens, which showed the highest ductility values, were subjected to a better confinement effect exercised by S1C frames. which have larger dimensions of the RC members. The ductility capacity detected for all specimens shows, as mentioned above, that though the failure of these systems was governed by mechanisms that were not exactly ductile, an overall ductile behaviour was exhibited by the infilled frame specimens.

	Infill masonry	**$\mu_{0.85}$** positive envelope	**$\mu_{0.85}$** negative envelope	**$\mu_{0.85}$** mean	**mean ductility**
S1A-1	Calcarenite	5.40	5.63	5.51	6.15
S1A-2	Calcarenite	6.67	6.92	6.79	
S1B-1	Clay	5.08	6.30	5.69	5.08
S1B-2	Clay	3.50	5.43	4.47	
S1C-1	LW conc.	5.88	12.00	8.94	7.61
S1C-2	LW conc.	5.50	6.98	6.24	
S1C-3	LW conc.	6.96	11.67	9.31	
S1C-4	LW conc.	6.00	5.88	5.94	

Table 5. Ductility factors calculated for the tested specimens.

3 CALIBRATION OF AN EQUIVALENT STRUT MACRO-MODEL FOR THE PREDICTION OF CYCLIC BEHAVIOR

The need to predict the cyclic behaviour of infilled frames becomes fundamental when the nonlinear time history analyses are used to assess the capacity of RC masonry infilled structures. Some investigations on this aspect have been carried out in some experimental and analytical works, such as Klingner and Bertero (1978) which studied the effects of cyclic loads by testing portions of multi-storey buildings, also providing a first hysteretic model. Doudoumis and Mitsopoulou (1986) introduced in their hysteretic model an initial non-loading branch due to shrinkage of contact zones. Experimental pseudo-dynamic tests on masonry infilled RC frames were carried out by Mander *et al.* (1993, 1994) and Mehrabi *et al.* (1996) who also provided a cyclic law based on the results of tested infilled frames specimens. Other hysteretic models were further proposed, each of them based on different assumptions. Madan *et al.* (1997) proposed a hysteretic single-strut model taking into account strength and stiffness decay and pinching, Crisafulli (1997) investigated the influence of different multiple-strut models on structural response, Kappos *et al.* (1998) presented a hysteretic model based on shear strength of infills. In the last years Cavaleri *et al.* (2005) proposed a highly detailed constitutive law for cyclical or

monotonic behaviour of an equivalent single strut and provided a first calibration of the parameters involved, while Crisafulli and Carr (2007) developed a new multi-strut macromodel including. in addition to classical truss elements, governed by axial compressive laws, a special shear frictional strut. Among the above mentioned models, those including the cyclic behaviour often depend on a large number of parameters, making it difficult to use them for practical applications. The problem becomes more relevant in the case of multiple-strut configurations (double, triple pin jointed struts or mixed axial and shear struts) without considering the different possible infill/frame couplings, which introduce further uncertainties. However, the necessity to assess the capacity of existing structures is today increasing, and as several studies demonstrate (Dolšek and Fajfar (2008), Kakaletsis *et. al* (2009), Stavridis, Koutromanos and Shing (2012), Uva *et al.* (2012), Fiore *et al.* (2012)), the analyses should be adequately performed including infill panels to avoid underestimation or overestimation of buildings' effective capacities.

The introduction of the infill panel contribution thus appears absolutely necessary as does the adoption of simplified models, also not too heavy from the computational point of view. This chapter of the thesis has the aim of discussing how the cyclic behaviour of infilled frames can be predicted with sufficient accuracy by a simple modelling. The modelling of the equivalent diagonal struts is performed by means of multilinear plastic link elements, available in the libraries of different FEM codes, governed by the Pivot hysteretic law proposed by Dowel *et al.* (1998). Parameters defining hysteretic behaviour are also provided for the investigated masonry infills typologies.

3.1 The "Pivot" hysteretic model

Many models have been developed to describe the cyclic nonlinear behaviour of diagonal struts equivalent to infills.

In order to perform dynamic nonlinear analyses for complex RC masonry infilled frame structures, flexible instruments requiring few parameters and a low computational effort, accompanied by sufficient reliability in the results, appear to be necessary.

The use the Pivot hysteretic model was introduced by Dowel, Seible and Wilson, (1998) as an instrument to predict RC columns hysteretic behaviour under cyclic actions with the aim to simplify the computational effort required by classical fibre numerical analysis of the cross section. The same authors suggested the model to reproduce force-displacement laws in general. The advantage of using the Pivot model is essentially due to the fact that this model is based mainly on geometrical rules that define loading and unloading branches rather than analytical laws, reducing not only computational effort but also the number of hysteretic parameters involved. Moreover, the Pivot model has great flexibility in modelling unsymmetrical tension-compression behaviours, as in the case of infill equivalent struts which are considered resistant only to compression stresses. An absolutely general outline of Pivot model is reported in **Fig. 3.1**. The model is completely defined when tension and compression strength envelopes are established (yielding tension and compression values F_{y1} and F_{y2}, initial stiffness and peak strength). Hysteresis rules are governed by parameters α_1, α_2, β_1 and β_2. Their significance is expounded below, with a brief summary of the Pivot model.

By the intersection of the horizontal lines through the ordinate values $\alpha_2 F_{y2}$, $\alpha_1 F_{y1}$, $\beta_1 F_{y1}$ and $\beta_2 F_{y2}$, and the lines containing the initial elastic branches, the primary Pivot points P_1, P_4 and P_2, P_3 and the Pivot pinching points PP_2 e PP_4 are identified. The quadrants Q_1, Q_2, Q_3 and Q_4 are delimited by the abscissa axis and the initial elastic branches defined before.

Starting a cycle from Q_1 (tension), once the yielding value is exceeded the unloading branch is directed toward point P_1 in Q_1 quadrant and toward pinching Pivot point PP_2 in the Q_2 quadrant until the initial elastic branch is reached. The cycle follows this branch (P_2 direction) up to the compression yielding stress. Beyond this point the cycle is in the $Q3$ quadrant where unloading goes toward point P_3 and, after reaching Q_4, goes toward pinching Pivot point $PP4$ on the initial elastic tension branch. At this state the cycle restarts in the Q_1 quadrant by following point R_1, which represents the last force value reached before the previous unloading in Q_1. The hysteresis parameters α_1, α_2, β_1 and β_2 should be appropriately fixed.

The application of Pivot hysteretic model undergoes major simplification when modelling infill equivalent diagonal strut cyclic behaviour, since the infill panels do not offer any contribution in terms of tensile strength and α_1 and β_1 parameters have to be considered null. Furthermore, experimental observation shows that infilled frame systems do not gain stiffness at load reversal until the whole plastic deformation (previously accumulated) is recovered. Basing on this hypothesis, the β_2 parameter is also null. The hysteretic law is therefore only governed by the α_2 parameter which is here experimentally calibrated for masonry infills which are object of the actual investigation. As reported in **Fig. 3.2** a strong simplification is occur with respect to the general case. Point P3, which becomes the *fundamental Pivot point*, guiding unload directions is identified once yielding compression value F_{y2} and α_2 parameter are assigned. Points S_1, S_2 and S_3 on the strength compression envelope respectively represent the yielding value, the peak value and 30% of the strength reduction value.

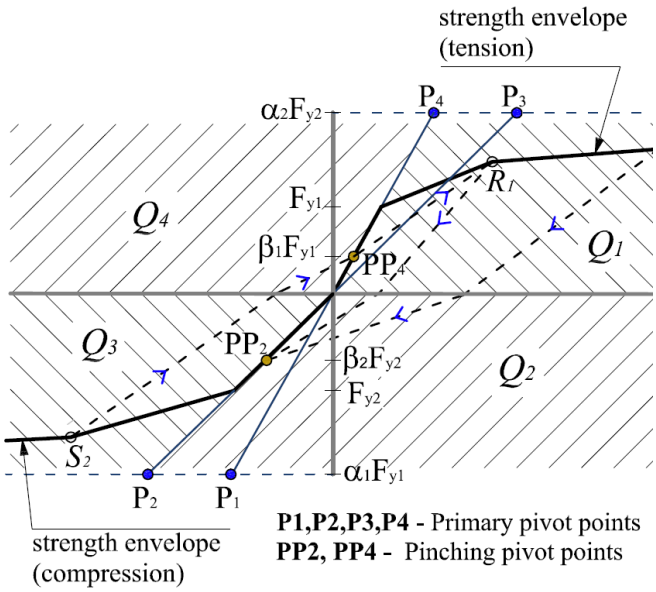

Fig.3.1. Hysteretic Pivot model for a generic unsymmetrical tension-compression law.

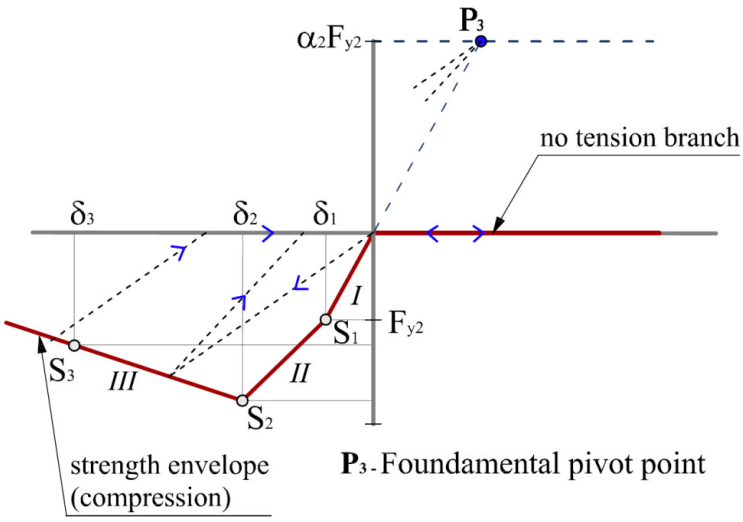

Fig.3.2. Hysteretic Pivot law particularization for the equivalent diagonal strut.

3.2 Definition of a macro-model for the infilled frame

The reference structural model (**Fig. 3.3**) was formulated using the SAP 2000 NL software. Beam elements for RC frame members were used. Taking into account the hierarchy in strength of columns and beams and the adequate shear strength of the members, mechanical nonlinearities of frame were introduced by means of four interacting axial load-moment plastic hinges placed at the ends of the columns. Beam-column joints were modelled as rigid links. Referring to plastic hinges, an elastic perfectly plastic envelope of the moment-curvature law was assigned with maximum moment and ultimate curvature obtained depending on the reinforcement and concrete characteristics (as a consequence of the stirrup confinement an ultimate strain for the concrete equal to 6‰ was fixed). The cyclic moment-curvature degradation was governed by a Takeda law. The equivalent diagonal struts, representing the different kinds of infill panels, were modelled through multilinear plastic link elements for which the general Pivot model is implemented in SAP 2000 NL.

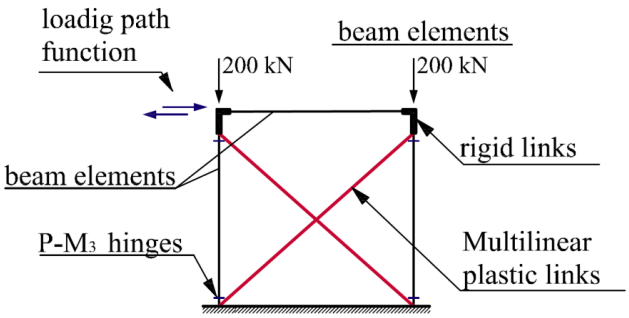

Fig. 3.3. Structural FEM model employed for the analyses.

It is important to notice that the attribution of the strength envelope for link elements, which guides the Pivot law, can be performed using any predictive model provided by the literature, therefore the afterwards discussed procedure constitutes only one of the alternatives.

In this case the initial stiffness was assigned through the expression proposed by Papia et al. (2003), in which the cross-section height w is evaluated depending on the parameter λ^* that each time identifies the frame/infill system by means of the following expression:

$$w = dk\frac{c}{z}\frac{1}{(\lambda^*)^{\beta}} \tag{3.1}$$

where c and β depend on the Poisson's ratio ν_d of the infill along the diagonal direction and can be evaluated as follows:

$$\begin{aligned} c &= 0{,}249 - 0{,}0116\nu_d + 0{,}567\nu_d^{\,2} \\ \beta &= 0{,}146 - 0{,}0073\nu_d + 0{,}126\nu_d^{\,2} \end{aligned} \tag{3.2}$$

The coefficient z takes on the value 1 since the panels are square ($l/h=1$) while the coefficient κ depends on the level of the vertical loads acting on the columns, varying from 1 (negligible vertical loads) to 1.5 (high vertical loads). In this case κ was set equal to 1.3 since medium levels of vertical loads were acting on the columns. A more accurate evaluation strategy for κ is discussed in Amato *et al.* (2008 and 2009).

Finally, the parameter λ^* can be evaluated as:

$$\lambda^* = \frac{E_d}{E_f}\frac{th'}{A_c}\left(\frac{h'^2}{l'^2}+\frac{1}{4}\frac{A_c}{A_b}\frac{l'}{h'}\right) \tag{3.3}$$

where E_d and E_f are respectively the Young modulus of the infill along the diagonal direction and the Young modulus of the concrete frame, A_c and A_b are the areas of the cross-sections of the frame columns and beams, while the geometrical features of the infill frame system *t, l, l', h, h'* are defined in (**Fig. 3.4**).

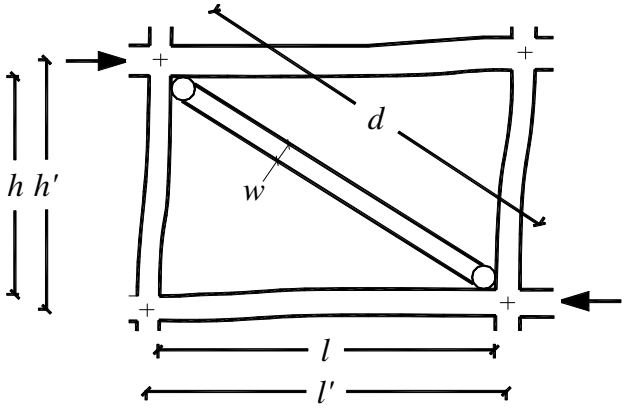

Fig. 3.4. Geometrical features of frame with strut equivalent to infill.

According to this formulation, the elastic moduli of masonry panels E_d and Poisson's ratios ν_d should be identified along the diagonal direction in which the equivalent pin-jointed strut lies. Prediction of these values was carried out according to the strategy proposed by Cavaleri et. al (2013) which is based on knowledge of the elastic properties E_1, E_2, G_{12}, ν_{12} for masonries, along the two principal directions, which are predictable starting from the strength of masonry along the same directions.

The peak strength of the equivalent struts S_2 of the specimens can be iteratively determined or not by using correlation (2.3) as discussed below.

If a prediction of the global strength of the infill/frame system F_{ui} is approximately performed as the sum of the bare frame strength F_{ub}, evaluated as in Eq.(2.1), and the horizontal component of the strut strength S_2^I, that is

$$F_{ui} = F_{ub} + S_2^I \cos\theta \tag{3.4}$$

where the angle θ defines the slope of the diagonal strut, then by means of Eq.(3.4), an approximation of the equivalent strut strength can be obtained as:

$$S_2^I = \frac{F_{ui} - F_{ub}}{\cos\theta} \tag{3.5}$$

Clearly Eq.(3.4) is only an approximate expression because 1) it is not certain that the collapse of the system will overlap the collapse of the frame and of the infill, 2) the infilled frame strength is conditioned by the level of coupling between frame and infill so the collapse mechanism is more complex than a scenario in which a frame collapses as if it was bare and an infill collapses as if it was an axially loaded strut.

By taking Eq.(2.2) into account, Eq.(3.5) becomes

$$S_2^I = \frac{F_{ub}(\delta_s - 1)}{\cos\theta} \tag{3.6}$$

Hence, after an estimation of F_{ub} by means of Eq.(2.1) and an evaluation of δ_s by Eq.(3.4) the strength of the equivalent strut can be obtained.

In order to consider the coupling between frame and infill the strength of the infilled frame can be more correctly evaluated by substituting in Eq.(3.4) the strength of the strut S_2^I with a fictitious strength S_2 which, summed with the strength of the bare frame, allows one to obtain the strength of the infilled frame exactly. The parameter that makes it possible to change S_2^I into S_2, namely to write

$$\omega_S = \frac{S_2}{S_2^I} \tag{3.7}$$

is here estimated by means of experimental observations. In **Fig. 3.5** is proposed a correlation between the parameter α_S, defining the ratio between horizontal component of the conventional diagonal strength of the infills F_{up} and bare frame strength F_{ub} and the value ω_S which multiplied by S_2^I allow one to obtain S_2 fictitious infill panel strength.

It can be observed that the dependence of ω_S on the ratio α_S can be fitted by the equation:

$$\omega_S = 0.90\alpha_s^{0.26} \tag{3.8}$$

Hence if α_S is known, ω_S, δ_S and S_2 can also be obtained. Eq. (3.7) makes it possible to predict the fictitious strength to be attributed to the equivalent strut and to make more accurate Eq.(3.4) and all derived analytical expressions.

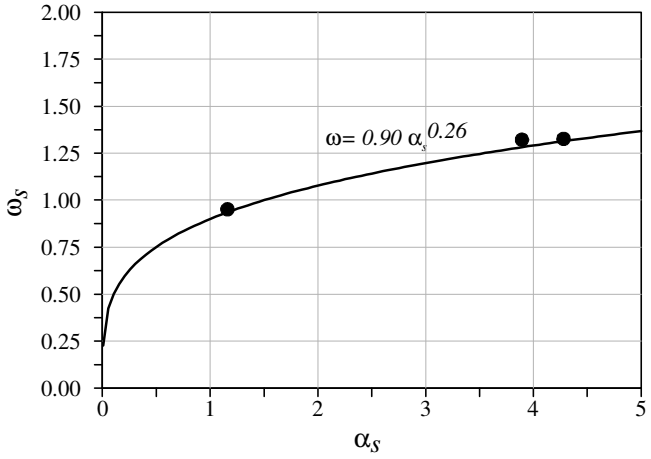

Fig. 3.5. ω_S-α_S correlation.

The strength envelope law was finally defined as reported in Cavaleri *et al.* (2005) for a monotonic curve, and only depends on 3 parameters α, β and ζ. The initial stiffness (branch I) was defined as:

$$K_1 = \frac{E_d tw}{d} \tag{3.9}$$

The stiffness in branch II was related to the parameter β as:

$$K_2 = \beta K_1 \tag{3.10}$$

Once the peak strength S_2 was assigned, the yielding strength S_1 was defined through the parameter α as:

$$S_1 = \alpha S_2 \tag{3.11}$$

The yielding and peak displacements were therefore directly identified:

$$\delta_1 = S_1 / K_1; \qquad \delta_2 = \delta_1 + (S_2 - S_1)/K_2 \tag{3.12}$$

The softening branch was linearized by connecting points S_2-δ_2 and S_3-δ_3 (branch III), assuming that $S_3=0.7S_2$, and δ_3 was obtained by the following expression (Cavaleri et al. (2005)):

$$\delta_3 = \frac{1}{\zeta}\ln\left[\frac{S_2}{S_3}\exp(\zeta\delta_2)\right] \tag{3.13}$$

The calibration of the parameters α, β and ζ which characterize the envelope curve, was provided for each infill typology by using the results of pushover analyses on the different types of systems tested. The values selected for the α, β and ζ parameters are those that allow the best fitting of the pushover curves on the mean experimental strength envelopes for each specimen typology. Pushover curves, used for calibration of the equivalent strut model law, are reported in **Fig. 3.6**. All the properties identifying the equivalent struts are summarized in **Tab. 3.1**.

Infill of	Dimensionless cross section	Strength envelope axial Force-Displacements law values			Strength envelope parameters			Pivot hysteretic parameters
	w/d	**S_1** [kN] / **δ_1** [mm]	**S_2** [kN] / **δ_2** [mm]	**S_3** [kN] / **δ_3** [mm]	α	β	ζ	α_2
Calcarenite	0.39	148 / 0.50	248 / 11.6	173 / 27.8	0.60	0.030	0.022	0.10
Clay	0.30	101 / 0.40	254 / 4.44	178 / 22.3	0.40	0.150	0.020	0.25
LW concrete	0.32	98 / 0.28	196 / 14.2	138 / 23.1	0.50	0.020	0.040	0.05

Table 3.1. Identification parameters for equivalent struts.

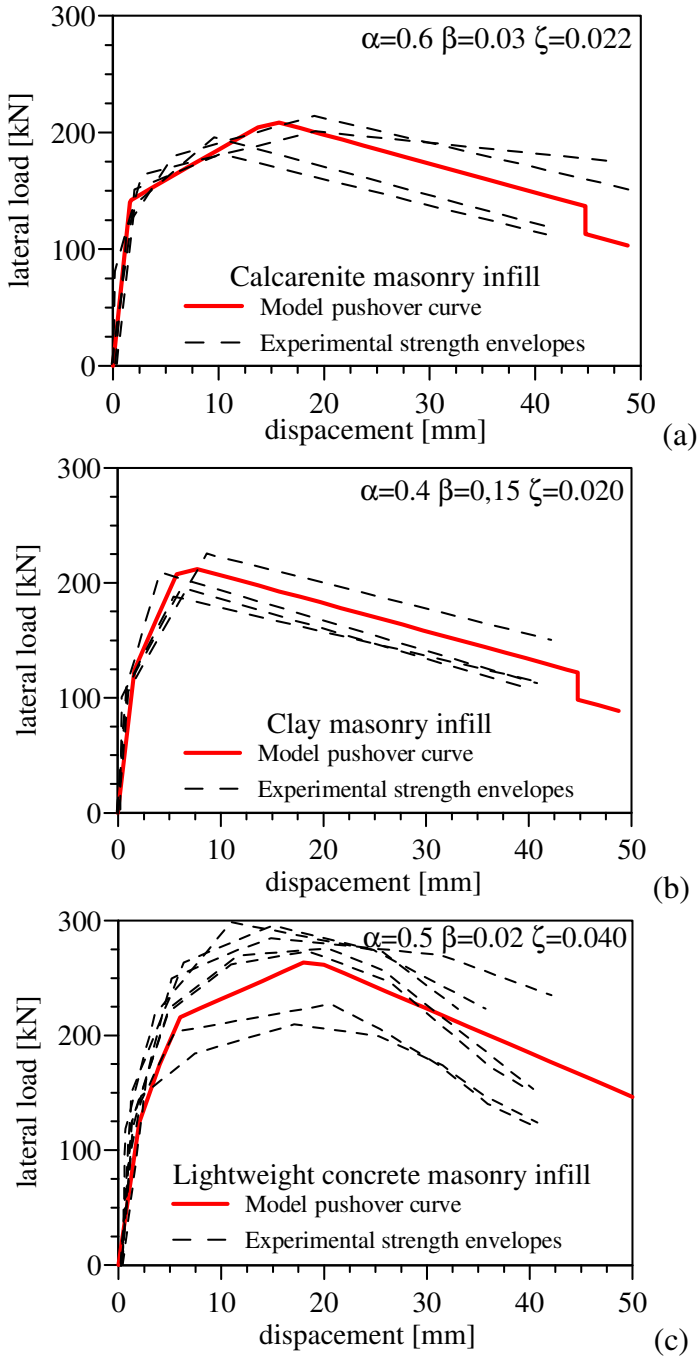

Fig. 3.6. Calibration of parameters trough best pushover-fitting curves. a) calcarenite masonry infill; b) clay masonry infill; c) lightweight concrete masonry infill.

3.3 Model validation: Experimental/Analytical comparison

Simulations of the tests were carried out by assigning as the input the history of displacements of the top of each specimen. The calibration of the parameter α_2 which defines the fundamental Pivot point P_3 was performed, for each of the 3 typologies of infilled frames, by the execution of several trial analyses. The values selected for α_2, which gave the best fitting of the experimental results, are shown in **Tab. 3.1** and are also suggested for masonry infill typologies having similar characteristics.

In **Figs. 3.7-3.9** experimental/analytical comparisons of the cyclic force-displacement responses of 3 different specimens, one for each infill/frame typology, are shown.

By observation of the cycle shapes, the results appear to be acceptable for each of the three cases. Regarding the experimental/analytical strength and stiffness matching, the role of the correct prediction of the strength envelope, which guides the cycles, appears to be fundamental to obtain suitable results. The more relevant differences in terms of strength and stiffness with respect to the experimental results are limited to a restricted number of cycles and do not exceed 15% for strength and 20% for stiffness. The consistency of the Pivot model becomes more evident observing the experimental/analytical responses obtainable by developing the lateral displacements (**Figs. 3.10-3.12**), that is by plotting the force versus the distance covered by the top of each frame.

As final reference for validation a comparison in terms of dissipated energy was carried. For both real experimental test and test simulation by means of Pivot model, the energy dissipated by each cycle, respectively W_e and W_p, and the cumulative dissipated energy, respectively ΣW_e and ΣW_p, were calculated. The comparisons are shown in **Figs. 3.13-3.15**. Energy dissipation, evaluated analyzing Pivot model test simulation at each cycle, shows good correspondence with the effective experimental dissipation. The comparison in terms of cumulative energy dissipation also shows that the global experimental behaviour is well fitted by the model, demonstrating the good reliability in predicting also global dissipative capacities. Normalized cumulative energy dissipation was also calculated dividing this dissipation by the term ΣD, which represents the cumulative sum of the

displacements, giving information about the energy dissipation capacities of the single infill/frame systems. The frames infilled with lightweight concrete masonry and calcarenite masonry seem to have the best dissipative properties with respect to the frames infilled with clay masonry. The energy dissipation values and the prediction errors are summarized in **Tab. 3.3**.

		Experimental		Pivot model		
Specimen	**ΣD** [mm] Cumulative displacements	**ΣW_e** [kNmm] Cumulative dissipated energy	**$\Sigma W_e/\Sigma D$** [kNmm/mm] Normalized cumulative dissipated energy	**ΣW_p** [kNmm] Cumulative dissipated energy	**$\Sigma W_p/\Sigma D$** [kNmm/mm] Normalized cumulative dissipated energy	**$(\Sigma W_p-\Sigma W_e)/\Sigma W_e$** [%] Model prediction error
S1A-2 (Calcarenite)	430	15369.4	35.74	17242.4	40.10	+ 12.2
S1B-1 (Clay)	580	15185	26.18	17561	30.28	+ 15.6
S1C-2 (LW concrete)	550	21697	39.45	22810	41.47	+ 5.1

Table 7
Experimental/analytical comparison of dissipated energy and percentage of error.

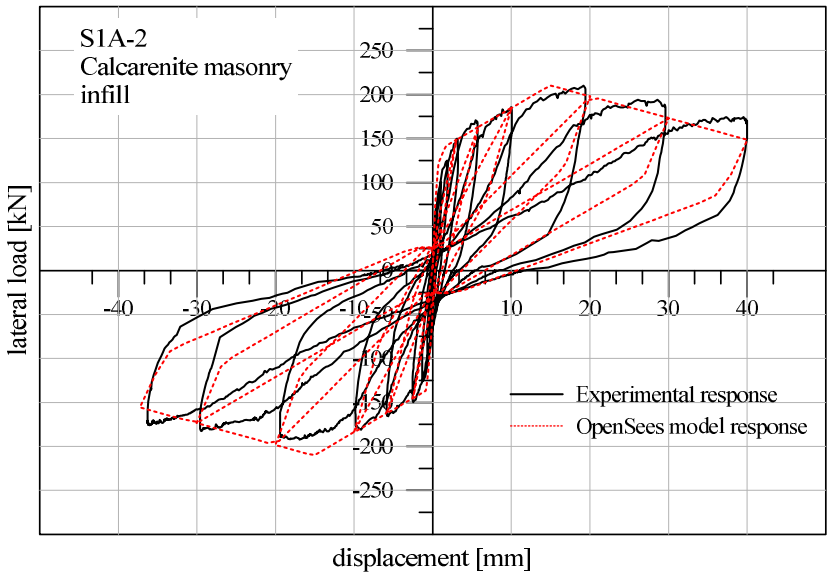

Fig. 3.7. Experimental/analytical cyclic response for a calcarenite masonry infilled frame specimen.

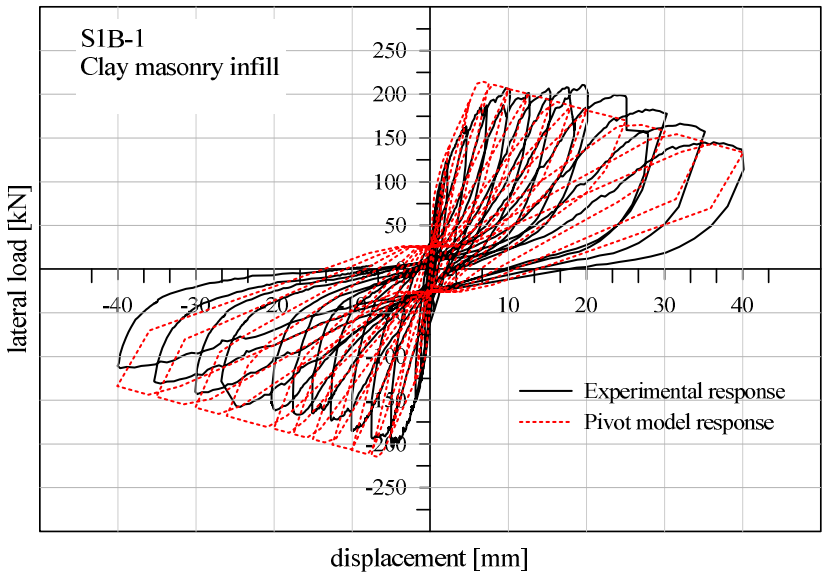

Fig. 3.8. Experimental/analytical cyclic response for a clay masonry infilled frame specimen.

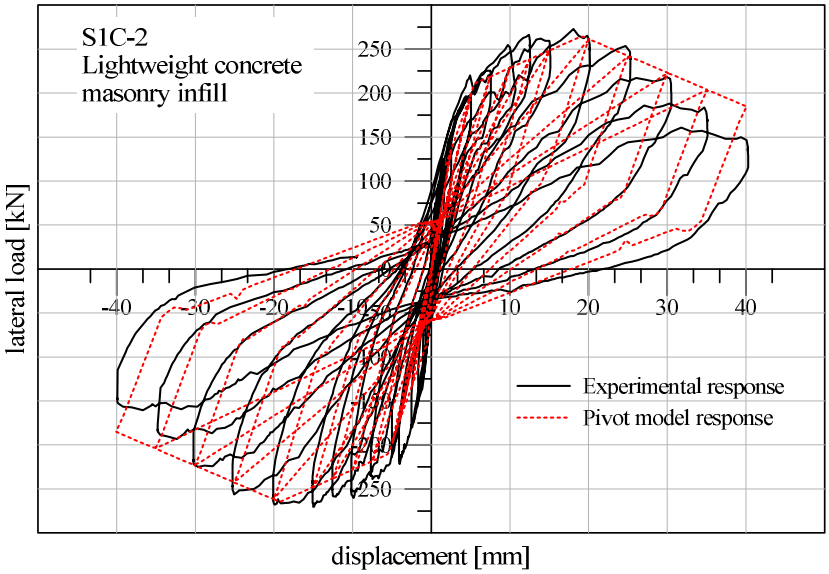

Fig. 3.9. Experimental/analytical cyclic response of lightweight for a concrete masonry infilled frame specimen.

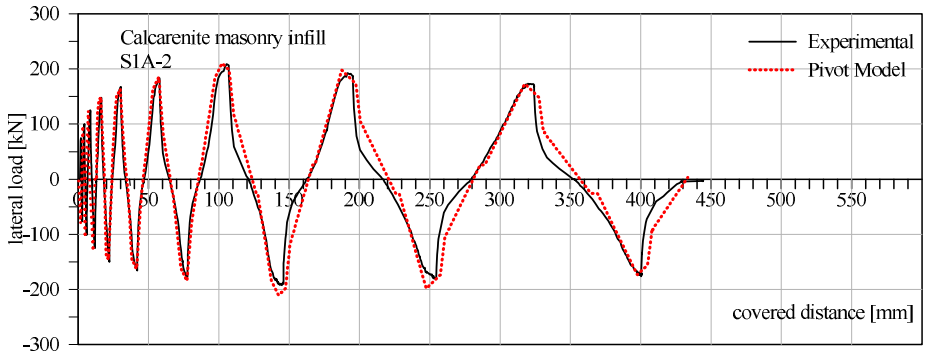

Fig. 3.10. Experimental/analytical force-lateral covered distance comparison test for a calcarenite masonry infilled frame specimen.

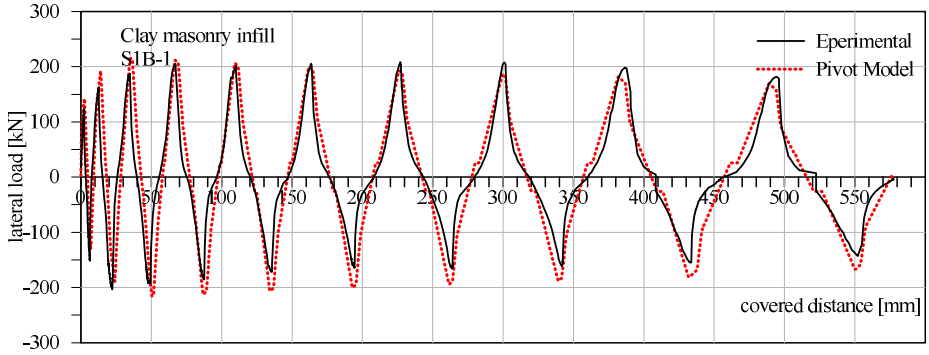

Fig. 3.11. Experimental/analytical force-lateral covered distance comparison test for a clay masonry infilled frame specimen.

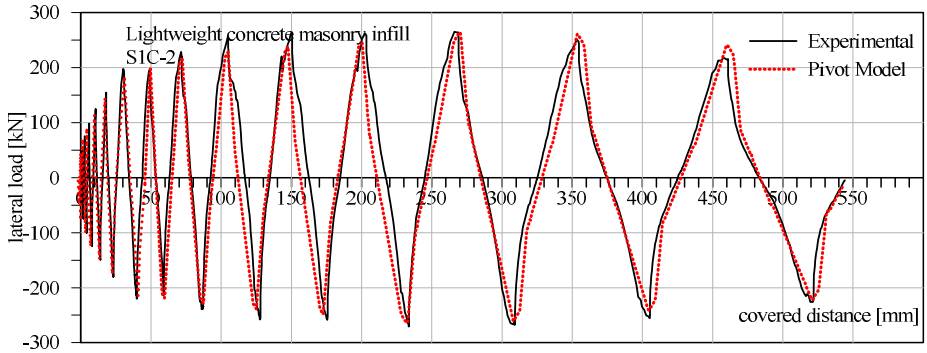

Fig. 3.12. Experimental/analytical force-lateral covered distance comparison test for a lightweight concrete masonry infilled frame specimen.

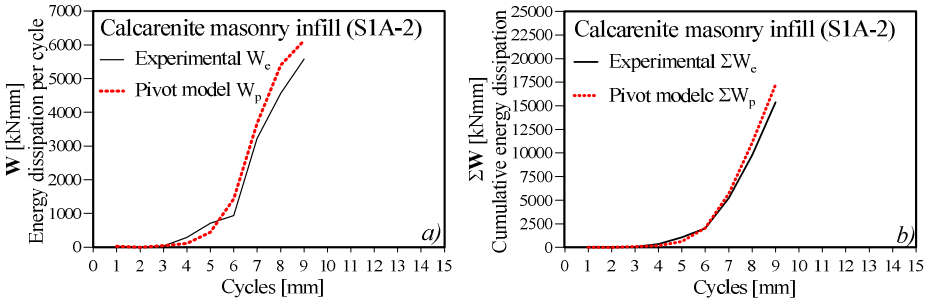

Fig. 3.13. Experimental/analytical energy dissipation comparison. a) Energy dissipation per cycle; b) Cumulative energy dissipation. S1A-2 specimen.

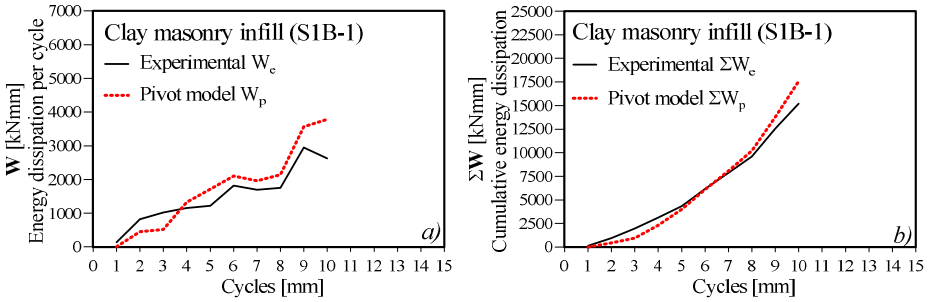

Fig. 3.14. Experimental/analytical energy dissipation comparison. a) Energy dissipation per cycle; b) Cumulative energy dissipation. S1B-1 specimen.

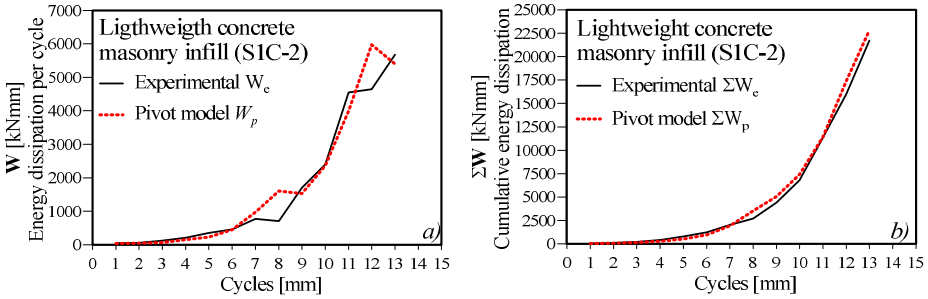

Fig..3.15. Experimental/analytical energy dissipation comparison. a) Energy dissipation per cycle; b) Cumulative energy dissipation. S1C-2 specimen.

3.4 Conclusions on the modelling of cyclic behaviour of infilled frames

The results are based on an experimental campaign on the cyclic response of RC fully infilled frames arranged with 3 different kinds of masonry infills presented in the previous chapter. It evidences the well-known major influence of infill panels on strength, stiffness and ductility of

the whole system compared to bare frames. By the observation of experimental evidence a predictive strategy for the assessment of cyclic response of infilled frames systems in structural models was developed, identifying the Pivot hysteretic model as a simple analytical cyclic law that can be employed to perform nonlinear time history analyses when equivalent diagonal strut macromodels are used to include infill presence in structural models. Basing on the experimental and the analytical studies here described, considering that the presence of infills produces a significant modification of the whole system behaviour of frames depending not only on the mechanical characteristics of the infill panels but also on the infill/frame couplings in terms of ratio of strength and ratio of stiffness, the following conclusions can be drawn:

1. an adaptation of the Pivot hysteretic model for the analytical evaluation of the cyclic response of infilled frames structures is possible and radically simplifies the modelling approach, being governed by only one parameter (α_2); the computational effort is also reduced since the Pivot model is based on a few geometrical rules rather than analytical laws;

2. identification of the parameters α_2 which define the degrading of the Pivot cycle, for the masonry infills involved in this study, gave optimal results, and experimental/analytical comparisons of the responses showed good reliability in the prediction of the responses themselves: limited differences of strength and stiffness with respect to the experimental tests were recorded; further, dissipation energy comparisons revealed good matching with very limited overestimations;

3. definition of the parameters of strength, ultimate deformability and stiffness, which are necessary for complete characterization of the Pivot model, can be obtained using models already available in the literature, which confirms the versatility of the Pivot model;

4. taking into account the results of the present study, the application of the model is suggested when it is necessary to assess the global response in terms of displacements, ductility and energy dissipation in nonlinear time history analyses;

5. this work, besides the enlargement of the experimental knowledge on cyclic behavior of RC infilled frames, is aimed to demonstrate that a simple modeling of equivalent struts is possible by means of Pivot hysteretic

model. Suggested values for α_2 parameter are relative to masonry infill typologies involved in actual experimental campaign. Anyway each user can perform a proper calibration if needed on the basis of its own experimental results and sensitivity.

4 LOCAL INTERACTION BETWEEN MASONRY INFILLS AND RC FRAMES

Infill masonry walls in framed structures make a significant contribution to the response under seismic actions. With special regard to reinforced concrete structures, it is known that internal forces modifications caused by the frame-infill interaction may be not supported by the surrounding frame because of the additional shear forces arising at the ends of beams and columns. Such additional forces may lead to the activation of brittle collapse mechanisms and hence their prediction is basic in capacity assessment, especially for structures that disregard the details for seismic zones. A parametric study, addressed to the prediction of the shear forces mentioned before, is here carried out. The results of this study can be used as a support when the simplified model is adopted consisting in the substitution of infill with an equivalent pin jointed concentric strut, because in this case the structural analysis fails in the prediction of the shear forces in question.

Through this chapter, in which existing RC infilled frames designed only for vertical loads are discussed, analytical laws, depending on the level of the axial force arising in a concentric strut equivalent to infill, are proposed, the above analytical law allowing to correct the local shear forces in the frame

critical sections, which are not predictable in the case of substitution of infill with an equivalent concentric strut.

4.1 Introduction to the local interaction issues

The contribution of infills in seismic response of framed reinforced concrete structures is significant; nevertheless, they are usually neglected in models assuming a non-structural function. The seismic damage on this kind of structures suggests, as widely discussed in literature, the fact that frames and infills have a strong interaction when involved in seismic events, not always being beneficial for structural safety and not negligible in general.

Though an infilled frame exhibits a significant increase in lateral strength and stiffness with respect to the corresponding bare one this fact cannot be extended to the whole structural behaviour depending on the distribution of infills. It can be generally stated that, if the planar and elevation distributions are regular and approximately symmetric, the contribution of infill panels is beneficial; contrariwise infills are potentially dangerous, often causing activation of additional torsional effects and soft story mechanisms. Regarding a single frame, the increase in strength mentioned before is associated with an increase in the demand for shear capacity in some specific sections. This aspect of the frame-infill interaction constitutes the central issue of this chapter.

As is well known, in the presence of lateral actions, the infill panel partially disconnects from the frame, remaining in contact with it only near two opposite corners (**Fig. 4.1**).

Strength increase occurring on infilled frames is allowable, however, if RC members adjacent to panels (beams, columns and joints) have sufficient shear overstrength

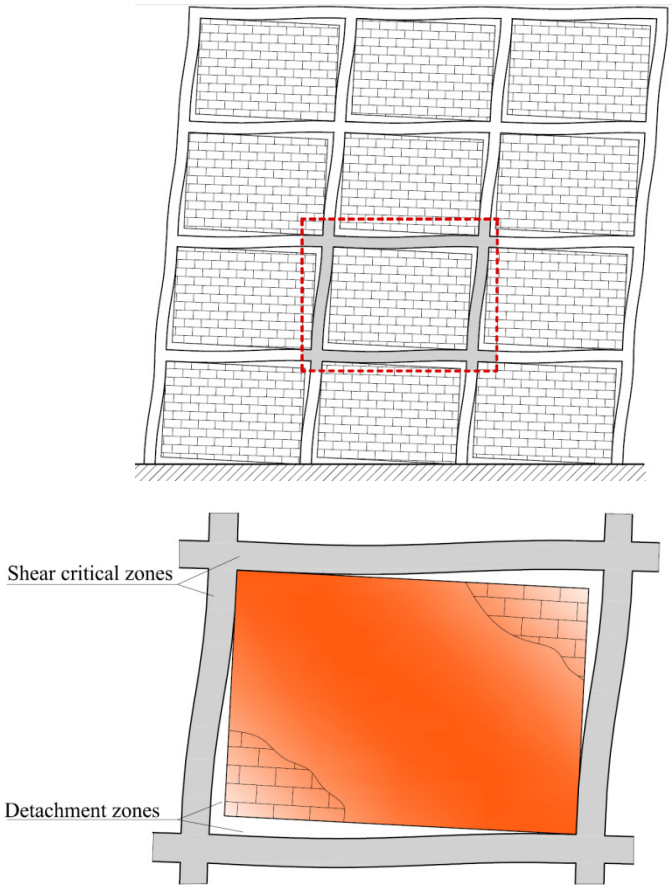

Fig. 4.1. Transmission of local shear forces close to the beam-column joints in presence of lateral actions.

When especially strong masonry infill panels are combined with frames having low shear reinforcement, the activation of local brittle collapse mechanisms, able to compromise the capacity and safety of the entire structure becomes a major question. In **Fig. 4.2** a picture referring to local shear failure mechanism due to frame-infill interaction is reported. The frame-infill interaction has been treated by several authors which have proposed strategies to introduce the effects of infills in structural models.

A very successful technique is based on the replacement of the infill with one or more equivalent diagonal struts. This technique, belonging to the macromodel approaches, was first introduced by Holmes (1961) and then developed by other researchers Stafford Smith (1966), Stafford Smith and Carter (1969), Mainstone (1974), Angel et al. (1994).

Fig. 4.2. Local shear failure of frames due to interaction with infills under seismic loads.

In the most simple case one equivalent pin-jointed concentric strut is used by means of that it is possible to obtain good reliability in modelling the stiffening effects produced by infill panels (e.g Papia et al. (2003)). Unfortunately, as a counterpart of its simplicity, this approach is unable to provide the internal forces in beams and columns, close to the joints, arising because of frame-infill interaction.

More complex macromodels making use of multiple diagonal struts (two or three), able to reproduce these effects, have also been developed (Crisafulli *et al.* (2000), Crisafulli and Carr (2007), Fiore *et al.* (2012)). However, identification of the mechanical properties to attribute to each strut is not a simple question since these depend not only on masonry mechanical properties but also on the frame-infill stiffness ratios and on the geometrical characteristics of the system (Asteris (2003, 2008).

The difficulties in managing multi-strut approaches grow when nonlinear (static o dynamic) analyses are required since the attribution of specific monotonical or cyclic nonlinear laws is necessary for each strut.

A substantially different approach has been instead followed by other authors (Mallik and Severn (1969), Mehrabi and Shing (1997), Shing *et al.* (2002), Gosh *et al.* (2002), Koutromanos *et al.* (2011) which have adopted an

"exact representation" of infills (micromodeling) to better reproduce frame-infill interaction. According to this modelling approach, panel and frames are modelled by means of planar shell finite elements while interface elements able to reproduce frictional effects and frame-infill detachment are considered for frame-infill contact regions. Such typology of approach, which is aimed at providing a more accurate response, is able to capture well local interaction effects and frame global internal force distribution, but in this case too, calibration of the analytical models, especially in terms of nonlinear laws for shell elements and interfaces, is not easy to accomplish. Furthermore, analyses of framed structures which make use of micromodels require a higher computational effort which is not always acceptable for practical engineering uses.

Also technical codes point out the need to take into account the frame-infill interaction. Eurocode 8 when furnishing indications about modelling in structural analysis prescribes that infill walls which contribute significantly to the lateral stiffness and resistance of building have to be considered. Unfortunately no reference models for infills are provided.
In a similar way in the Italian technical code neither are modelling criteria given nor is a strategy suggested to predict the local increase of shear in the columns and in the beams of infilled frames close to the nodal regions.

Differently from Eurocode 8 and the Italian codes, the Federal Emergency Management Agency (FEMA) code 356 dedicates a significant attention to describe how to take infills into account and how to predict the local effects on beams and columns. One possible choice that is offered is to model an infill by an equivalent pin-jointed strut that should have the same thickness and modulus of elasticity as the infill panel while the width w is given by

$$w = 0.175\left(\lambda_1 h'\right)^{-0.4} d \tag{4.1}$$

where, referring to **Fig. 4.3**, h' is the height of the frame, measured between the centre-lines of the beams, d is the measure of the diagonal dimension of the infill and λ_1 is given by

$$\lambda_1 = \left[\frac{E_d\, t \sin 2\theta}{4\, E_f I_c h} \right]^{\frac{1}{4}} \tag{4.2}$$

in which t is the thickness of the infill and h and ℓ are its height ancross-sections and E_d and E_f are the Young's modulus of the infill and of the material constituting the frame, respectively.

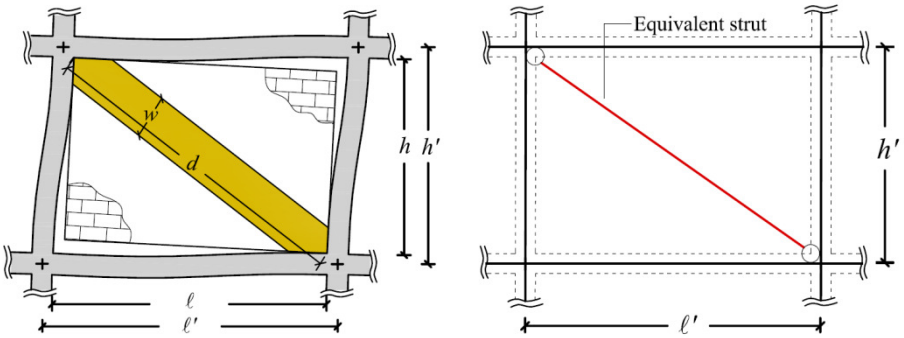

Fig. 4.3. Geometrical features of a frame-infill system and of the equivalent diagonal strut.

Referring to local interaction effects, the FEMA code specifies that beams and columns adjacent to infills should have sufficient strength to support local shear effects. According to the strategy proposed, in absence of more accurate models and analyses, the FEMA code–states that the flexural and shear strength of beams and columns close to nodal regions should exceed the internal forces evaluated by the application, at the specified lengths l_{ceff} and l_{beff}, of the horizontal and vertical components of the expected axial force value for an equivalent strut (**Fig. 4.4**). The lengths l_{ceff} and l_{beff} can be obtained as

$$l_{ceff} = \frac{w}{\cos\theta_c}; \quad \tan\theta_c = \frac{h - l_{ceff}}{\ell} \tag{4.3}$$

$$l_{ceff} = \frac{w}{\cos\theta_c}; \quad \tan\theta_c = \frac{h - l_{ceff}}{\ell} \tag{4.4}$$

Although the question of local failure of RC members adjacent to infills is treated in FEMA 356 more than in other codes, the strategies suggested, not deriving from a specific analysis and basing on expected values for equivalent strut strength may lead to an unreliable estimation.
Considering all premises above, it is here provided a study in which the relevance of the local shear interaction effects is pointed out, giving the basis for a tool as rigorous as it is simple for the prediction of the real distribution of shear demand in the critical sections of frames when a single equivalent concentric strut is used.

The study, regarding a single infilled frame that can be viewed as a part of a more complex framed structure, is based on the comparison of the results derived from two modelling approaches: one *(M1 model)* providing the simple single-strut approach; the other one *(M2 model)* using plane-shell elements to model infills, nonlinear beam elements at the contour and multilinear elastic links (*MElink*) resisting in compression only at the frame-infill interface. Comparisons are carried out, with variation in mechanical features, geometry , stiffening and strength ratios between frame and infill, in order to determine, for fixed interstorey drifts, the relationship between the axial force evaluated on the equivalent strut and the shear forces (negligible in the M1 model) evaluated in critical sections of beams and columns in the M2 model. The final aim is to permit use of the simple equivalent concentric strut approach for the analysis, this approach being able to provide adequate correction coefficients for local shear forces arising in the beams and in the columns near the joints.

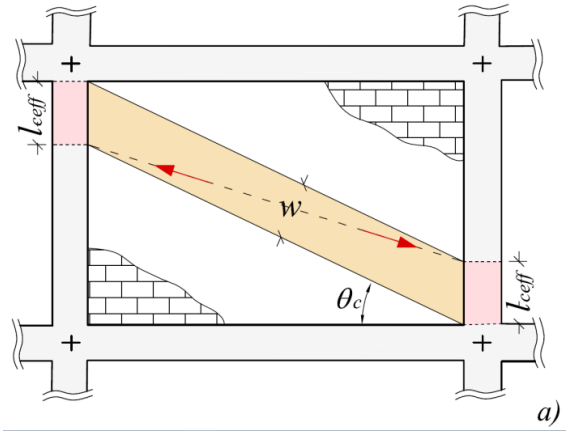

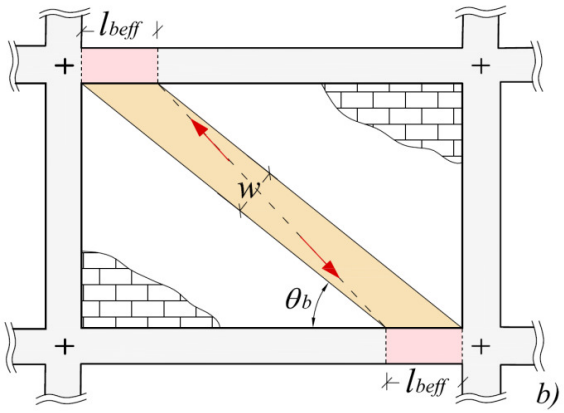

Fig. 4.4. Schemes for the evaluation of local effects according to FEMA 356: a) on columns; b) on beams.

4.2 Modelling approaches

As mentioned above the results of this work are based on a comparative procedure between two different approaches used to model the same structural system. Having as reference the generic infilled frame, whose geometrical features are indicated in **Fig. 4.5**, the structural responses at fixed interstorey drifts are compared in detail. The M1 model (**Fig. 4.6**) is based on the classical assumption of replacing an infill with an equivalent diagonal concentric strut. This model requires a very low computational effort and is really efficient when nonlinear analyses have to be carried out, although it is affected by a significant defect due to the impossibility of evaluating the interferences of infills in local internal force distribution on the RC members. The M2 model (**Fig. 4.7**), which instead requires a higher computational effort, allows one to evaluate the influence of the infill on the internal forces in RC members thanks to the modelling of the infill in finite elements connected to beams and columns through interfaces elements able to transfer normal forces to the surrounding frame. Models M1 and M2 can be considered equivalent and results can be compared under monotonic loading when they exhibit the same stiffness in both the linear and nonlinear fields. More generally, the stiffness equivalence can be defined as a function of interstorey drift (d_r) and expressed by the equation

$$K_{M1}(d_r) = K_{M2}(d_r) \tag{4.5}$$

$K_{M1}(d_r)$ and $K_{M2}(d_r)$ being the lateral secant stiffness of the M1 and M2 models for a generically assigned d_r.

Analyses and modelling were performed using SAP 2000 NL. The characterization of the M1 and M2 models is indicated below, while the details of comparisons procedures and results are discussed in the following sections.

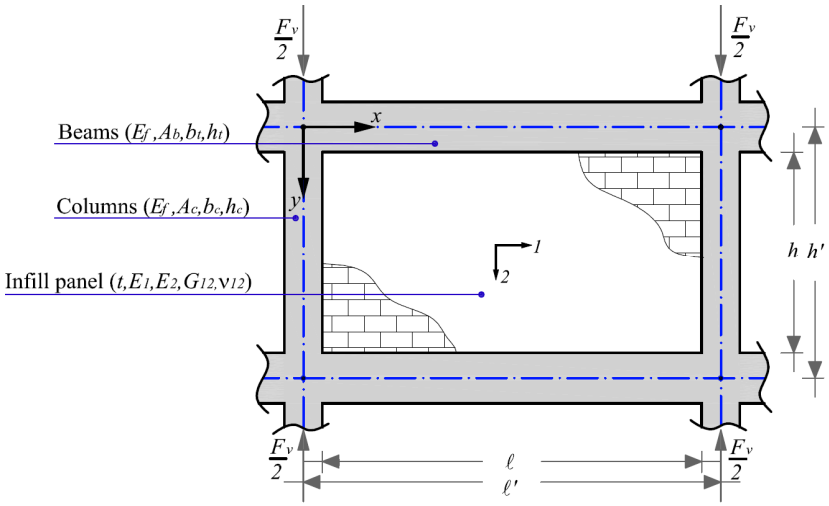

Fig. 4.5. Geometrical and mechanical features of an infilled frame.

4.3 The M1 Model

The M1 model (**Fig. 4.6**) is obtained by the application of the equivalent strut approach. The geometrical and mechanical characteristics of the RC infilled frame from which it is originated are shown in **Fig. 4.5**. There, b_b and h_b are the width and the depth of the beam cross-sections respectively and A_b the corresponding area, while b_c and h_c are the width and the depth of the column cross-sections respectively and A_c the area. Regarding to the elastic parameters, the concrete constituting the frame is identified by the Young modulus E_f. while masonry constituting infills is mechanically characterized by the parameters E_1, E_2, G_{12}, ν_{12} which are respectively the

Young moduli, rigidity modulus and Poisson ratio referred to directions 1 and 2.

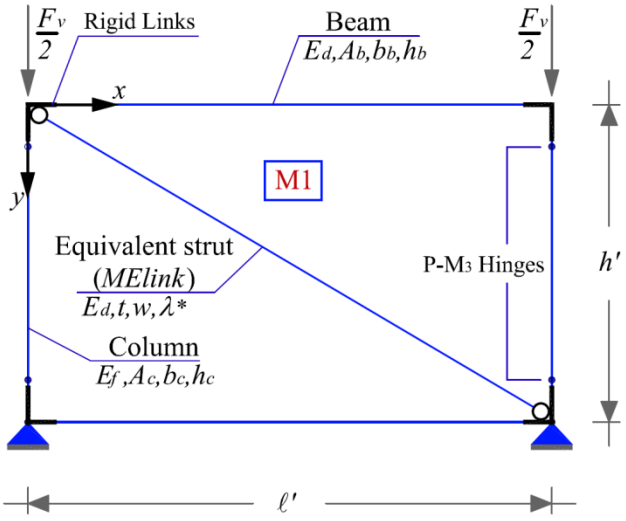

Fig. 4.6. M1 model geometrical and mechanical scheme.

The identification of the equivalent diagonal strut cross-section width w is performed by means of the expression below (Papia *et al.*, 2003).

$$w = d\,\kappa\frac{c}{z}\,\frac{1}{(\lambda^*)^{\beta}} \tag{4.6}$$

where coefficients c and β depend on the Poisson ratio ν_d along the diagonal direction (along which the equivalent strut lies) and are defined by the equations

$$c = 0.249 - 0.0116\,\nu_d + 0.567\,\nu_d^{\,2} \tag{4.7}$$

$$\beta = 0.146 + 0.0073\,\nu_d + 0.126\,\nu_d^{\,2} \tag{4.8}$$

while the coefficient z depends on the panel shape and can be evaluated as

$$z = 1 + 0.25(\ell / h - 1) \tag{4.9}$$

The coefficient κ appearing in Eq. (4.6) takes into account the effect of the vertical loads which generically act con columns and involve infill panels. This coefficient can be obtained as a function of the vertical

deformation ε_v experienced by columns as effect of the compressive load F_v (Amato *et al.* 2008), through the equation

$$\kappa = 1 + (18\lambda^* + 200)\varepsilon_v \tag{4.10}$$

in which ε_v is calculated as

$$\varepsilon_v = \frac{F_v}{2A_c E_f} \tag{4.11}$$

The parameter λ^* (Eqs. (4.6) and (4.10)), which is strongly representative of the frame-infill system and characterizes the stiffness ratios between infill and frame, is obtained as follows:

$$\lambda^* = \frac{E_d}{E_f}\frac{t}{A_c}\frac{h'}{}\left(\frac{h'^2}{\ell'^2} + \frac{1}{4}\frac{A_c}{A_b}\frac{\ell'}{h'}\right) \tag{4.12}$$

The evaluation of masonry elastic Young modulus E_d and the Poisson ratio ν_d along the diagonal direction can be easily carried out as a function of the mechanical parameters mentioned above (E_1, E_2, G_{12}, ν_{12}) according to the procedure proposed in Cavaleri *et. al* (2013).

The constitutive law that governs the equivalent strut is defined by a trilinear axial force-axial displacement compressive diagram having no tensile strength (**Fig. 4.7**) in which the initial elastic stiffness K_1 is evaluated as

$$K_1 = \frac{E_d tw}{d} \tag{4.13}$$

while the strength at the elastic limit F_1 is defined as a function of the parameter α, which defines the ratio between the peak strength and the level of the resisting force at the end of the elastic branch, that is

$$F_1 = \alpha F_2 \tag{4.14}$$

The stiffness in the post-elastic branch K_2 is instead related to the parameter β, which regulates the loss of stiffness after the yielding point with respect to the initial one:

$$K_2 = \beta K_1 \tag{4.15}$$

The displacements at the elastic limit and peak strength are therefore directly identified as

$$\delta_1 = F_1 / K_1 ;\ \delta_2 = \delta_1 + (F_2 - F_1)/K_2 \tag{4.16}$$

The trend of the softening branch is linearized and obtained by connecting points F_2-δ_2 and F_3-δ_3, assuming that $F_3=0.7F_2$ and calculating δ_3 by the expression below (Cavaleri *et al.*, 2005).

$$\delta_3 = \frac{1}{\zeta}\ln\left[\frac{F_2}{F_3}\exp(\zeta\delta_2)\right] \tag{4.17}$$

The equivalent strut peak strength F_2 is finally determined as a function of the mean shear strength of the masonry infill panel f_{v0m} as follows:

$$F_2 = f_{v0m} t \ell^* \tag{4.18}$$

in which ℓ^* represents the ideal length of the panel that coincides with the real length ℓ in the case of square infills ($\ell/h=1$) and undergoes a reduction down to 0.7ℓ when $\ell/h=2$. This assumption takes into account a strength reduction due to the aspect ratio of the infills, especially for rectangular long infills, experimentally observable.

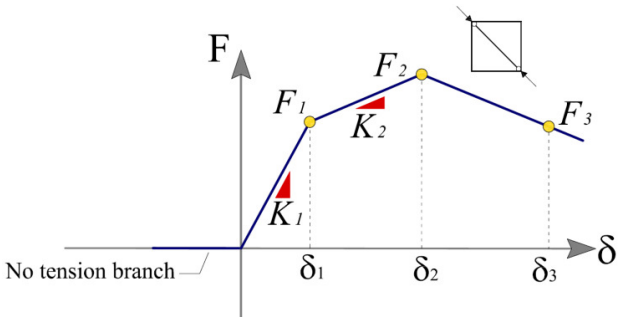

Fig. 4.7. Axial force – Axial displacement law for equivalent diagonal strut.

The case of collapse due to crushing of the corner units in contact with the frame is conservatively here not considered. The equivalent strut properties are introduced in the model by means of a Multilinear Elastic Link (MElink) element available in the SAP 2000 libraries.

The frame mechanical nonlinearities are introduced by means of 4 interacting axial force-bending moment plastic hinges (P-M) placed at the

ends of the columns to be representative of the case of a non-seismically designed strong beam-weak column frame.

The hinge properties depend in each case on the cross-section geometrical features and on the reinforcement. The concrete strength is assumed to be *25 Mpa* and an unconfined constitutive law is attributed to consider low transversal reinforcement. The steel rebar strength is set equal to *450 MPa* and an elastic perfectly plastic law is attributed. Nodal regions at the intersections between beams and columns are modelled as rigid links. The reinforcement geometrical ratio is set equal to *1%* for all column sections and it is furthermore assumed that the beams have a higher flexural strength than the columns, as in the case of structures designed to resist gravity loads only. Finally, a dimensionless axial force $n=0.2$ is assigned on top of the columns.

The values adopted for parameters α, β and ζ, calibrating the constitutive law shape for the equivalent diagonal strut were defined considering the experimental responses available in the literature (e.g. Cavaleri *et al.* 2005, 2012a) for frames infilled with different typologies of masonries. Besides, basing on results of experimental tests reported in (Cavaleri *et al.*, 2012b) for different typologies of masonries, it is assumed that the elastic Young modulus ratio $\gamma=E_1/E_2$ is equal to *0.75*, the shear modulus $G_{12}=0.4E_2$ and the Poisson's ratio $\nu_d=\nu_{12}=0.1$. Different values for the shear strength f_{v0m} of the panels (from *0.50* to *1.07 Mpa*) are considered in the analyses. The abovementioned parameters governing the equivalent strut compressive law each time are summarized in **Tab. 4.1**.

α	β	ζ	f_{v0m} [*Mpa*]
0.5	0.15	0.02	0.5 - 1.07

Table 4.1. Parameters calibrating equivalent diagonal strut constitutive law.

4.4 The M2 Model

Referring to the generic infilled frame (**Fig. 4.5**), the M2 model was also defined (**Fig. 4.8**) characterized by detailed discretization of infill by means

of orthotropic elastic shell elements. The assumptions for the elastic properties of the masonry (Young moduli E_1 and E_2 along the two orthogonal directions, shear modulus G_{12} and Poisson ratio ν_{12}) are the same as those proposed for the characterization of the M1 model.

The RC frame at the boundary was modelled as the one included in the M1 model in terms of geometry and properties of concrete and steel rebars. The distance between the infill and the surrounding frame beam elements, which are positioned at the centrelines, is covered by means of null weight rigid links. The latter have the sole function of transmitting the interface forces. A similar approach is also proposed in Doudomis (2007). Interface elements are placed between shell contour nodes and rigid link ends and are modelled using multilinear elastic link elements having only axial stiffness, no tensile strength and a constitutive law that is assumed to be elastic in compression. As mentioned above the interface elements are used to simulate the mortar joints.

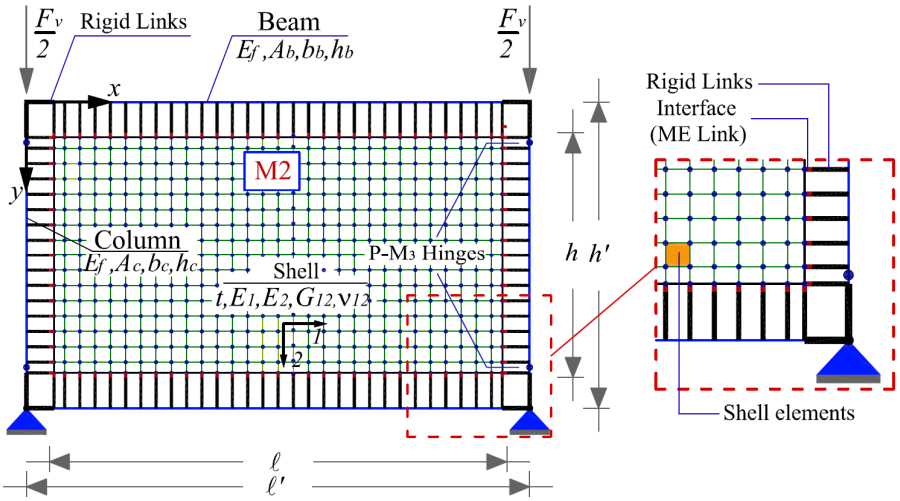

Fig. 4.8. M2 model: geometrical and mechanical scheme.

Taking into account the high manufacturing variability affecting these mortar joints, the conventional elastic Young modulus E_m=*3000 MPa* was set, and the conventional mortar joint thickness h_m=*20 mm* was assigned. Also considering-that under lateral loads the frame-infill contact lengths are strongly reduced and mortar joints are affected by significant damage, frictional effects were not included in the model (different studies (e.g.

Fiore *et al.,* 2007) show that friction arising in interfaces is not decisive for the overall response).

Nonlinearity of shell elements was introduced in the model by iteratively scaling (i.e. reducing) their thickness. The reduced thickness ideally represents that one allowing to obtain for the M2 model the same lateral secant stiffness as exhibited by the M1 model for a fixed interstorey drift level. This way the simple M1 model permits one to calibrate the M2 model at each selected prescribed displacement basing on a nonlinear law assumed for the equivalent strut.

The so defined M2 model furnishes more detailed results regarding frame internal force modification due to the frame-infill interaction, being able to simulate both interface detachment and local shear effects on RC member ends, unlike the M1 model, able to simulate the overall behaviour but not the distribution of the internal forces in the frame members.

4.5 Parametric study

As discussed in the previous section, the comparability of the two models used here is possible, under monotonic loading, when they exhibit the same stiffness at a generically assigned interstorey drift. Therefore the procedure used to evaluate internal force modification due to the presence of infill panels follows the steps shown above: *a)* assignment of the mechanical properties and geometry of the infilled frame; *b)* definition of the equivalent strut (M1 model); *c)* definition of the M2 model in which the thickness (t) of the infill is initially set equal to the real thickness; *d)* choice of an interstorey drift (d_r); *e)* analysis of the M1 model by imposing the fixed interstorey drift and evaluation of secant stiffness as the parameter identifying damage level; *f)* identification of the damage level in the M2 model (by reducing infill thickness) in such a way as to provide the same secant stiffness as exhibited by the M1 model; *g)* evaluation of RC frame internal force distribution on the M2 model. Once the internal force distribution is evaluated for both the M1 and M2 models it is possible to correlate the level of the shear forces acting in the critical sections of the frame members (obtained by the M2 model) and the axial force in the equivalent strut.

Parametric analyses were carried out to evaluate the responses, for an assigned damage level (identified by the interstorey drift ratio), of infilled frames modelled by means of both the approaches described above. The geometrical and mechanical properties of frames and infills (elastic moduli, aspect ratio, beam element cross-sections, masonry mechanical characteristics) were varied in order to evaluate their influence on the distribution of shear forces occurring on beam and column ends in contact with infills.

The shear force in the four critical sections indicated in **Fig. 4.9** (BNO-Beam North-West, BSE-Beam South-East, CNO-Columns North West, CSE-Columns South East) was considered. In these sections, equilibrium with forces transferred by the infill through the contact regions has to be granted, thus the shear demand is here highly concentrated.

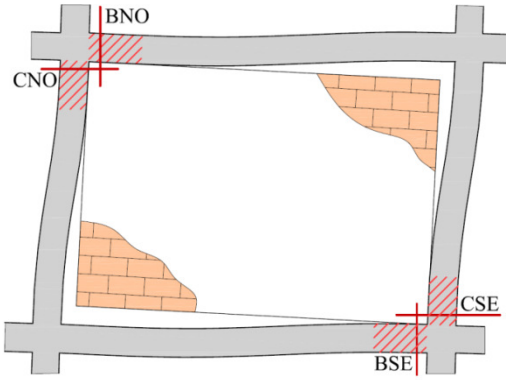

Fig. 4.9. Critical sections on RC frame.

For each infilled frame considered, M1 and M2 models were generated and analyzed for the drifts fixed above. Once the structural responses were obtained the dimensionless quantities reported below were evaluated:

$$\alpha_{BNO} = \frac{V_{BNO}^{(M_2)}}{N_p^{(M_1)}}; \alpha_{BSE} = \frac{V_{BSE}^{(M_2)}}{N_p^{(M_1)}} \tag{4.19}$$

$$\alpha_{CNO} = \frac{V_{CNO}^{(M_2)}}{N_p^{(M_1)}}; \ \alpha_{CSE} = \frac{V_{CSE}^{(M_2)}}{N_p^{(M_1)}} \tag{4.20}$$

in which $N_P^{(M_1)}$ is the axial force on the equivalent diagonal strut evaluated in the M1 model while $V_{BNO}^{(M_2)}$, $V_{BSE}^{(M_2)}$, $V_{CNO}^{(M_2)}$, $V_{CSE}^{(M_2)}$, are the shear forces acting in the critical sections evaluated using the M2 model.

The coefficients α_{BNO}, α_{BSE}, α_{CNO}, α_{CSE}, here called *shear distribution coefficients*, define the relationship existing between the shear forces acting on the frame critical sections and the axial force acting on the equivalent strut for a fixed interstorey drift ratio. If prediction of shear distribution coefficients is possible a priori as a function of the geometrical and mechanical variables of the infilled frame system, these coefficients become a useful tool to evaluate the real shear forces on frame sections as a quota of the equivalent strut axial force. In **Fig. 4.10** a qualitative comparison in terms of deformed shapes and distribution of shear demand between responses exhibited by the two models for the same interstorey drift is reported, evidencing the relevance of local shear effects detected in the contact regions by the M2 model and not by the M1 model.

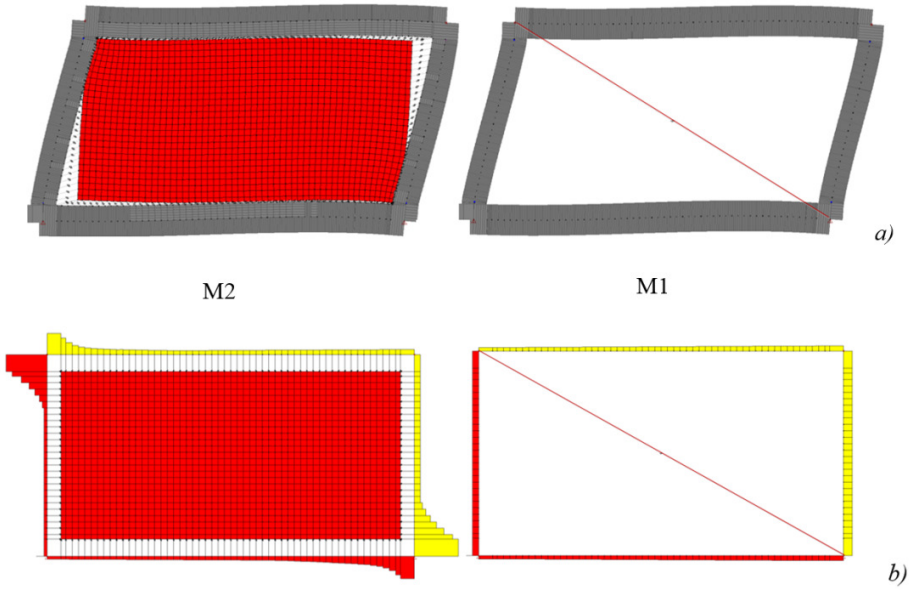

Fig. 4.10. Comparison between M1 and M2 model responses: a) deformed shape; b) shear distribution.

Since shear distribution coefficients can be defined at each interstorey drift reached by an infilled frame, a sensitivity analysis for different classes of infilled frames was primarily performed with an increase in the drift level from the elastic phase (d_r=*0.01-0.03%*) up to d_r=*1.2%* which for most non-ductile structural systems represents a near-collapse condition.

It is not easy to identify with a single parameter a class of infilled frame systems because a really wide quantity of variables is involved and the behaviour of each system depends not so much on the single mechanical properties of RC frame and masonry infills but more on their ratios. It is also important to underline that, since the analyses were carried out in a nonlinear field, parameters that usually are not significant in elastic studies, such as strengths and strength ratios, have to be taken into account. Therefore in this study the parameter ψ (Eq. 4.21) was considered as characterising the system; this parameter is the product of three terms that appear to be fundamental in the behaviour of an infilled frame.

$$\psi = \lambda^{*} \xi f_{v0m} \tag{4.21}$$

The parameter λ^{*} appearing in Eq. (4.21) has already been defined by Eq. (4.12). It carries information about the geometry of the system and the stiffness ratio between infill and frame. The term $\xi = M_{RB}/M_{RC}$, is the ratio between the resisting moments of the beam and column and is introduced since it is related to the plastic hinge formation sequence that significantly influences frame secant stiffness in the nonlinear field and therefore also the shear distribution coefficient trend. Since the resisting moment of the column does not have a univocal value but depends on the axial force, the term ξ can be more simply estimated, as was done in this case, by calculating the ratio h_b/h_c between the beam and column cross-section heights. Finally, f_{v0m} is the medium shear strength to be attributed to the masonry used for the infill. This medium shear strength plays a significant role because the forces that are transferred from the infill panel to the RC frame are strongly related to the panel strength.

In **Figs. 4.11-4.14** the results of the previously mentioned sensitivity analyses are shown. In detail the shear distribution coefficients are shown for different values of the ψ factor and for infilled frames having aspect ratios $\ell/h=1$ and $\ell/h=2$. From observation of the curves it appears evident that the shear distribution coefficients maintain a sub-horizontal trend after an unstable stage which is limited to low drift values. This trend occurs for shear distribution coefficients of both the beam and column critical sections and for the two aspect ratios of the infill considered. Another characteristic

of the shear distribution coefficients is that they assume the highest values when systems are characterized by low values of the ψ factor. This trend is explained by the fact that low values of the ψ factor are generally associated with weak infills combined with RC frames having significant stiffness. These conditions produce a reduction in the axial force N_p in the equivalent strut appearing in Eqs. (4.19-4.20) and the correlated growth of the α coefficients. In Tabs. (**2-3**) the characteristics of the specimens modelled for obtaining the curves α-d_r are included.

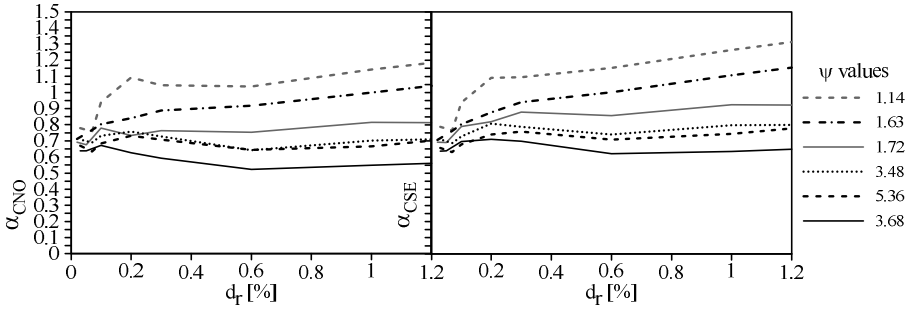

Fig. 4.11. Shear distribution coefficients α_{CNO} and α_{CSE} vs. drift ratio for different ψ values and $\ell/h=1$.

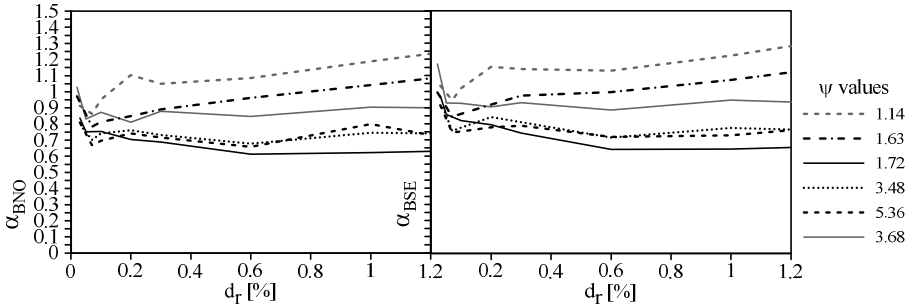

Fig. 4.12. Shear distribution coefficients α_{BNO} and α_{BSE} vs. drift ratio for different ψ values and $\ell/h=1$.

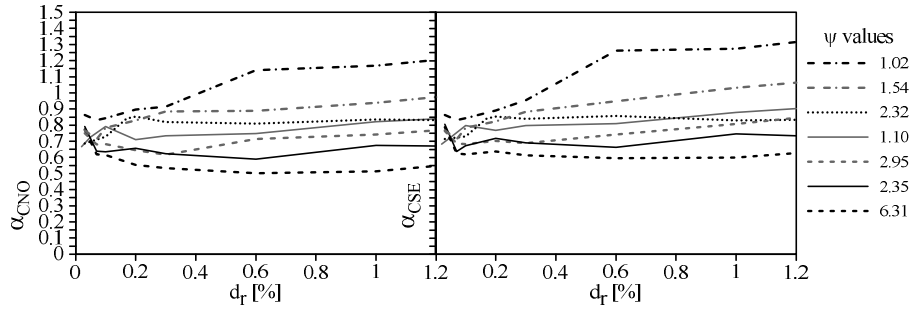

Fig. 4.13. Shear distribution coefficients α_{CNO} and α_{CSE} vs. drift ratio for different ψ values and $\ell/h = 2$.

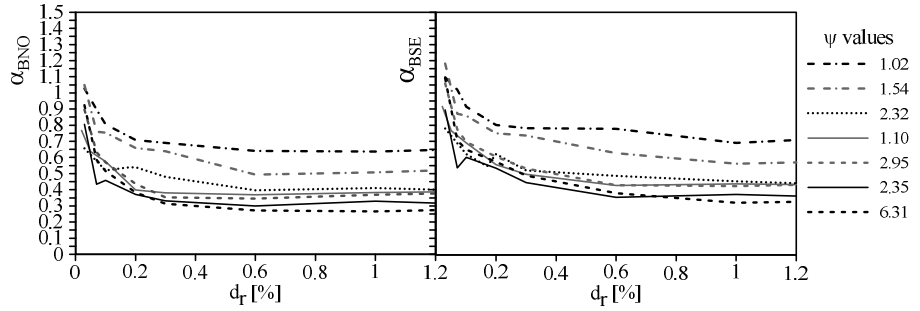

Fig. 4.14. Shear distribution coefficients α_{BNO} and α_{BSE} vs. drift ratio for different ψ values and $\ell/h = 2$.

#	b_c [mm]	h_c [mm]	b_t [mm]	h_t [mm]	h [mm]	ℓ [mm]	E_f [Mpa]	w [mm]	f_{v0m} [Mpa]	λ^*	ξ	ψ
#1	200	200	200	400	1600	1600	25000	623	1.07	1.72	2.00	**3.68**
#2	200	200	200	400	1600	1600	25000	623	0.50	1.72	2.00	**1.72**
#3	250	400	250	500	2700	2700	25000	1034	1.07	2.60	1.25	**3.48**
#4	250	400	250	500	2700	2700	25000	1190	1.07	0.85	1.25	**1.14**
#5	600	300	300	500	2700	2700	15000	1012	1.07	3.00	1.67	**5.35**
#6	250	400	250	500	2700	2700	25000	1034	0.50	2.60	1.25	**1.63**

Table 4.2. Characteristics of the specimens producing the results in Figs. (4.11-4.12).

#	b_c [mm]	h_c [mm]	b_b [mm]	h_b [mm]	h [mm]	ℓ [mm]	E_f [Mpa]	w [mm]	f_{v0m} [Mpa]	λ^*	ξ	ψ
#1	200	200	200	400	1600	3200	25000	757	1.07	1.10	2.00	**2.35**
#2	200	200	200	400	1600	3200	25000	757	0.50	1.10	2.00	**1.10**
#3	250	400	250	500	2700	5400	15000	1344	1.07	1.73	1.25	**2.31**
#4	200	200	200	500	1600	3200	15000	748	1.07	2.36	2.50	**6.31**
#5	200	200	200	500	1600	3200	15000	748	0.50	2.36	2.50	**2.95**
#6	200	300	200	400	1600	3200	15000	774	0.50	1.54	1.33	**1.03**
#7	200	300	200	400	1600	3200	15000	774	0.75	1.54	1.33	**1.54**

Table 4.3. Characteristics of the specimens producing the results in Figs. (4.13-4.14).

Since this study aims to provide the basis for a predictive general instrument able to estimate a reliable shear demand in critical sections a relationship was sought between the shear distribution coefficients and geometrical/mechanical features of the infilled frame summarized by the ψ factor. A further parametric analysis correlating α coefficients with ψ factors was therefore performed.

As previously observed, the α coefficients are almost drift independent after a certain drift level (typically a low value) is reached. Hence it is possible to choose a single interstorey drift value whose corresponding α coefficients can be considered representative of the frame-infill interaction for each value of the interstorey drift. In order to obtain the previously mentioned α–ψ correlation, the intermediate drift value d_r=0.6% was selected as a reference. Two sets of models having different infill aspect ratios (ℓ/h=1.0 and ℓ/h=2.0) were analyzed. The geometrical and mechanical features are indicated in **Tabs. 4.4-4.5** together with the terms λ^*, ψ and w. The results of the analyses are reported in **Figs. 4.15-4.16** and show the relationships between the ψ factor and coefficients α_{BNO}, α_{BSE}, α_{CNO}, α_{CSE}. Analytical best fitting functions (Eqs. 4.22-4.25) have also been provided in order to show the possibility of deriving effective tools for practical applications. The determination coefficients R^2 are also calculated to evaluate the agreement of the best fitting correlation law with the numerical results.

The laws for the α–ψ relationships are shown below (including R^2 coefficients) for ℓ/h=1 and for ℓ/h=2.

$$\alpha_{CNO} = 0.96\psi^{-0.37}\ (R^2 = 0.94); \quad \alpha_{CSE} = 1.03\psi^{-0.35}\ (R^2 = 0.91) \tag{4.22}$$

$$\alpha_{BNO} = 0.98\psi^{-0.33}\ (R^2 = 0.90); \quad \alpha_{BSE} = 1.03\psi^{-0.32}\ (R^2 = 0.93) \tag{4.23}$$

$$\alpha_{CNO} = 1.05\psi^{-0.36}\ (R^2 = 0.93); \quad \alpha_{CSE} = 1.08\psi^{-0.30}\ (R^2 = 0.90) \tag{4.24}$$

$$\alpha_{BNO} = 0.60\psi^{-0.39}\ (R^2 = 0.88); \quad \alpha_{BSE} = 0.68\psi^{-0.32}\ (R^2 = 0.82) \tag{4.25}$$

By means of the proposed laws α coefficients can be evaluated for each infilled frame system before analyses are made as a function of the ψ factor. The above coefficients can be used to correct shear forces detected in

critical sections when equivalent strut models are used to perform analyses. Finally, according to Eqs. (4.19-4.20) the shear value in critical sections can be evaluated by multiplying the previously calculated α coefficients by the axial force resulting in the equivalent strut.

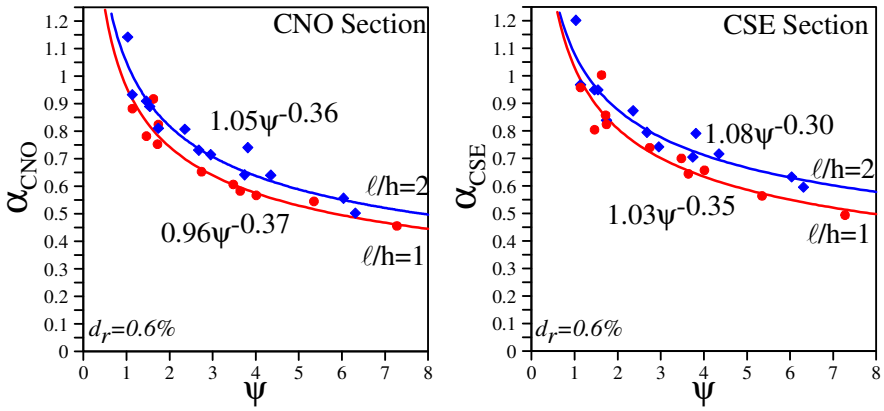

Fig. 4.15. Shear distribution coefficients α_{CNO} and α_{CSE} vs. ψ factor at $\ell/h=1$ and $\ell/h=2$. Numerical analysis results and interpolating functions.

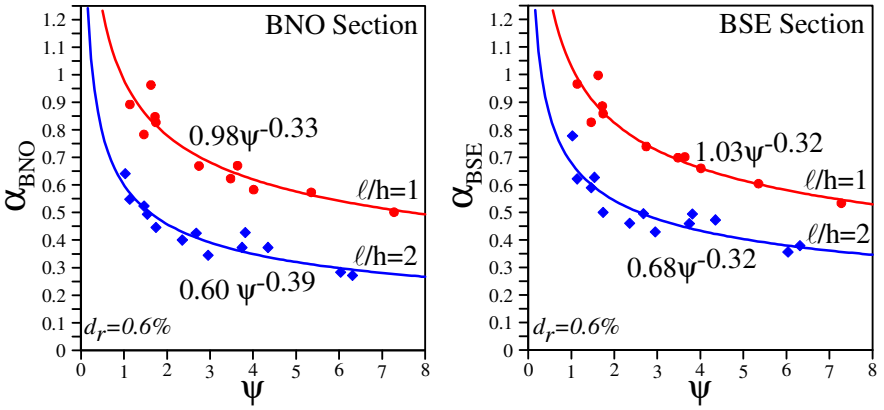

Fig. 4.16. Shear distribution coefficients α_{BNO} and α_{BSE} vs. ψ factor at $\ell/h=1$ and $\ell/h=2$. Numerical analysis results and interpolating functions.

By observing the $\alpha-\psi$ curves it appears evident, as observed before, that, for both aspect ratios considered, the α coefficients undergo a reduction when the ψ values increase. This expresses the general tendency of RC frames to receive shear forces on critical sections that increase as the stiffness of the frame increases with respect to the infill. The results also show that the influence of the infill aspect ratio (ℓ/h) has a major role,

especially for beams that are affected by significantly lower shear when the horizontal dimension of the panel ℓ prevails over the height h.

Spec.	b_c [mm]	h_c [mm]	b_b [mm]	h_b [mm]	h [mm]	ℓ [mm]	E_f [Mpa]	w [mm]	f_{v0m} [Mpa]	λ^*	ξ	ψ
C1A	200	200	200	400	1600	1600	25000	623	1.07	1.72	2.00	**3.68**
C2A	200	200	200	400	1600	1600	25000	565	1.07	3.40	2.00	**7.28**
C3A	250	400	250	500	2700	2700	25000	1190	1.07	0.85	1.25	**1.14**
C4A	250	400	250	500	2700	2700	25000	1190	1.07	1.30	1.25	**1.74**
C5A	250	400	250	500	2700	2700	25000	1034	1.07	2.60	1.25	**3.48**
C6A	250	400	250	500	2700	2700	25000	1012	1.07	3.00	1.25	**4.01**
C7A	250	400	250	500	2700	2700	25000	1067	1.07	2.05	1.25	**2.74**
C8A	600	300	300	500	2700	2700	25000	1192	1.07	0.82	1.67	**1.46**
C9A	600	300	300	500	2700	2700	15000	1054	1.07	3.00	1.67	**5.35**
C10A	200	200	200	400	1600	1600	25000	623	0.50	1.72	2.00	**1.72**
C11A	250	400	250	500	2700	2700	25000	1034	0.50	2.60	1.25	**1.63**

Table 4.4. Characteristics of the specimens producing the results in Figs. (4.15-4.16)- ℓ/h=1.

Spec.	b_c [mm]	h_c [mm]	b_b [mm]	h_b [mm]	h [mm]	ℓ [mm]	E_f [Mpa]	w [mm]	f_{v0m} [Mpa]	λ^*	ξ	ψ
C1B	200	200	200	400	1600	3200	25000	757	1.07	1.10	2.00	**2.35**
C2B	200	200	200	400	1600	3200	20000	707	1.07	2.82	2.00	**6.03**
C3B	200	400	200	500	2700	5400	20000	1362	1.07	1.30	1.25	**1.74**
C4B	200	400	200	500	2700	5400	20000	1368	1.07	2.00	1.25	**2.68**
C5B	200	400	200	500	2700	5400	20000	1121	1.07	2.80	1.25	**3.75**
C6B	200	400	200	500	2700	5400	20000	1450	1.07	0.85	1.25	**1.14**
C7B	200	400	200	500	2700	5400	20000	1200	1.07	3.25	1.25	**4.35**
C8B	600	300	300	500	2700	5400	20000	1453	1.07	0.82	1.67	**1.46**
C9B	600	300	300	500	2700	5400	20000	1293	1.07	2.14	1.67	**3.82**
C10B	200	200	200	500	1600	3200	15000	748	1.07	2.36	2.50	**6.31**
C11B	200	200	200	500	1600	3200	15000	748	0.50	2.36	2.50	**2.95**
C12B	200	300	200	400	1600	3200	15000	774	0.50	1.54	1.33	**1.03**
C13B	200	300	200	400	1600	3200	15000	774	0.75	1.54	1.33	**1.54**

Table 4.5. Characteristics of the specimens producing the results in Figs. (4.15-4.16) - ℓ/h=2.

The results of the analyses reported above can be a basis for assessment of the capacity of RC members of infilled frames when linear or nonlinear analyses are performed by means of equivalent concentric strut models. In practical applications, once the analysis is performed and the axial forces acting on the equivalent struts are known, the shear demand to consider for capacity assessment can be estimated by replacing shear forces on critical sections with the values V_{BNO}, V_{BSE}, V_{CNO}, V_{CSE} that can be calculated by means of the following expressions:

$$V_{BNO} = V_0 + \alpha_{BNO} N_P \; ; \; V_{BSE} = V_0 + \alpha_{BSE} N_P \tag{4.26}$$

$$V_{CNO} = \alpha_{CNO} N_P \; ; \; V_{CSE} = \alpha_{CSE} N_P \tag{4.27}$$

V_0 being the shear force due to the vertical loads on the beams and N_p the axial force in the equivalent strut.

4.6 Extensibility of the correlation laws

Considering that the laws in question, correlating the coefficients for the right estimation of the shear in the frame members, were obtained for a drift of 0.6%, it is natural to want to verify the extensibility of these laws to different drifts that can be experienced by frame-infill systems.
In this section an application is proposed to two cases of infilled frame having aspect ratios $\ell/h=1$ and $\ell/h=2$ respectively.
The response in terms of shear demand in the critical section is evaluated for different drift levels using the M2 model and is assumed to be *exact*. The shear distribution is calculated by means of the M1 model and corrected by using the laws in Eqs. (4.22-4.25), also for drifts different from 0.6% (lower and higher). Finally, the exact demand (M2 model) and the demand corrected by the proposed law (M1 model) are compared. For the sake of simplicity the term V_0 related to vertical loads is considered null in this example. The geometrical and mechanical characteristics of the models are reported in **Tab. 4.6** within the ψ factors and the related shear distribution coefficients calculated by Eqs. (4.22-4.25).

#	ℓ/h	b_c [mm]	h_c [mm]	b_b [mm]	h_b [mm]	h [mm]	ℓ [mm]	Ef [Mpa]	w [mm]	f_{v0m} [Mpa]	λ^*	ξ	ψ	α_{CNO}	α_{CSE}	α_{BNO}	α_{BSE}
#1	**1.0**	250	400	250	500	2700	2700	25000	1034	1.07	2.60	1.25	**3.48**	**0.605**	**0.666**	**0.649**	**0.691**
#2	**2.0**	200	300	200	400	1600	3200	15000	774	0.50	1.54	1.33	**1.02**	**1.043**	**1.074**	**0.595**	**0.676**

Table 6. Geometrical and mechanical characteristics of models used for validation tests.

The results of the tests are shown in **Figs. 4.17-4.18** in terms of shear on critical sections vs. interstorey drifts.

It appears evident that although the proposed strategy is based on shear distribution coefficients evaluated at d_r=*0.6%*, the resulting predictive capacity at each drift is quite reliable. Prediction errors for the drift levels considered are in most cases acceptable. Fig. (**17**) and Fig. (**18**) also show the level of shear obtainable by the procedure proposed by FEMA. It can be observed that this level of shear agrees conservatively with the maximum level of shear obtainable varying the drift. This result validates the procedure proposed by FEMA but confirms that the shear demand in the frame members may be lower, resulting in a lower effort in the measures to be implemented to obtain a fixed safety level.

As final result of analyses made on the two tested numerical specimens, and more generally to be representative the influence of local shear effects in RC masonry infilled structures, in Figs. **4.19-4.24** a graphical exemplification is provided comparing at different interstorey drift levels the effective shear demand determined by means of M2 and M1 model within the trend of principal compressive stresses on infill panels FE.

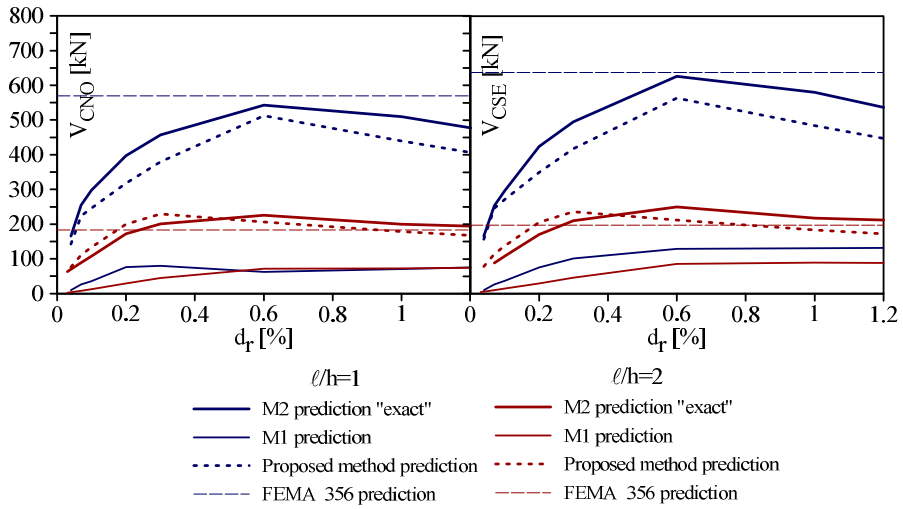

Fig. 4.17. Comparison of predictive capacity of shear forces on column critical sections in the M1 Model and proposed method with respect to the M2 Model for two ℓ/h=1 and ℓ/h=2 numerical specimens.

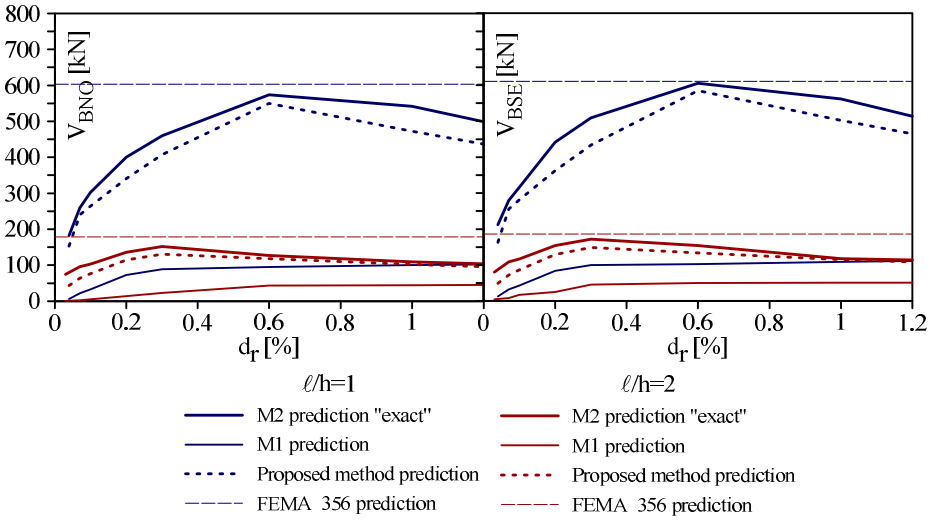

Fig. 4.18. Comparison of predictive capacity of shear forces on beam critical sections in the M1 Model and proposed method with respect to the M2 Model for two ℓ/h=1 and ℓ/h=2 numerical specimens.

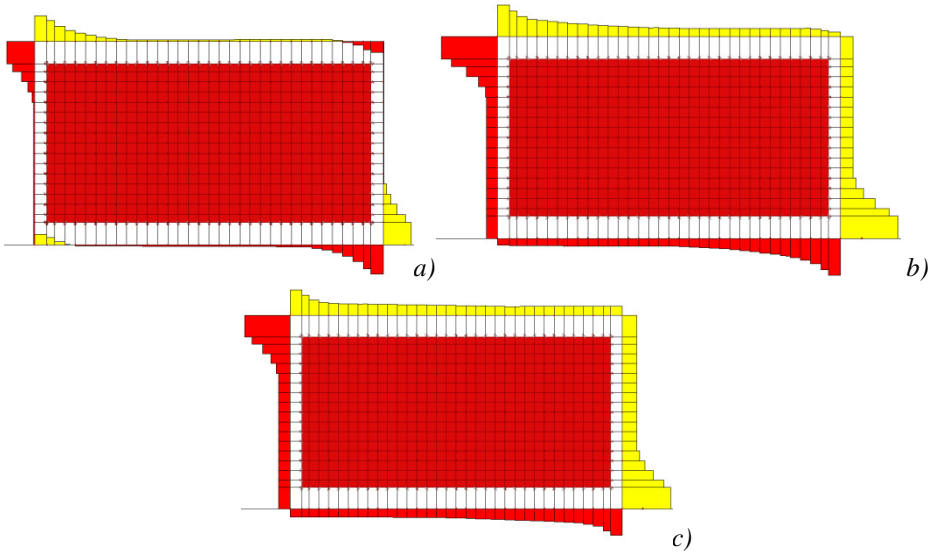

Fig. 4.19. Shear demand distribution evaluated by M2 model for ℓ/h=2 specimen at drifts: *(a) 0.1%; (b) 0.6%; (c) 1.2%.*

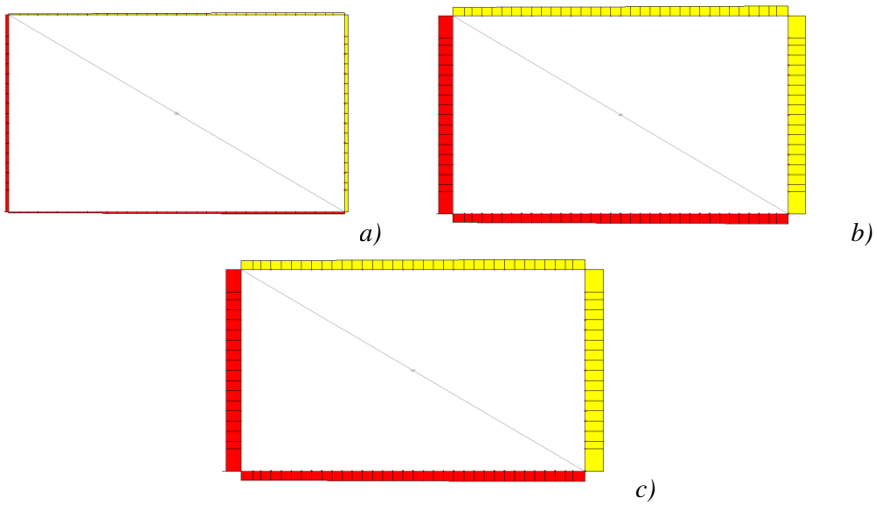

Fig. 4.20. Shear demand distribution evaluated by M1 model for ℓ/h=2 specimen at drifts: *(a) 0.1%; (b) 0.6%; (c) 1.2%.*

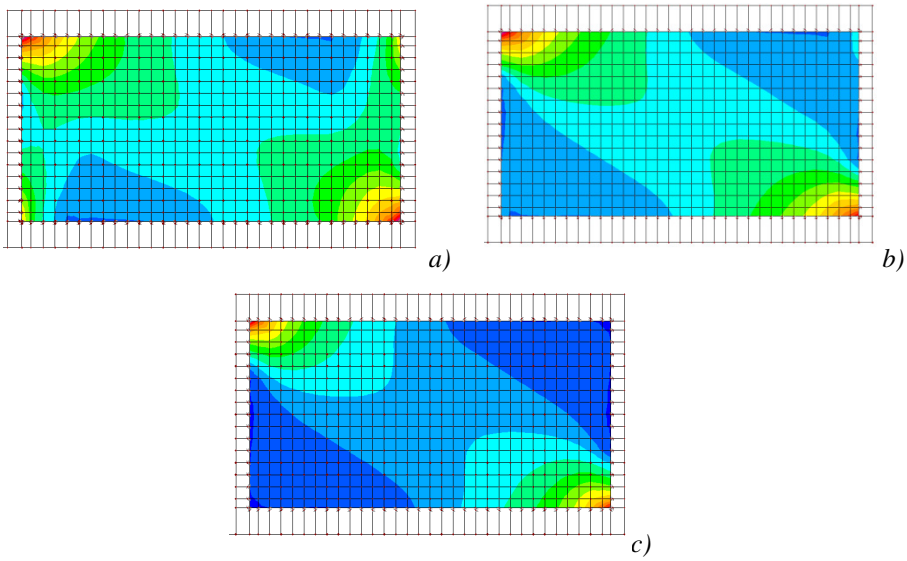

Fig. 4.21. Principal compressive stresses on infill panel evaluated by M2 model for ℓ/h=2 specimen at drifts: *(a) 0.1%; (b) 0.6%; (c) 1.2%.*

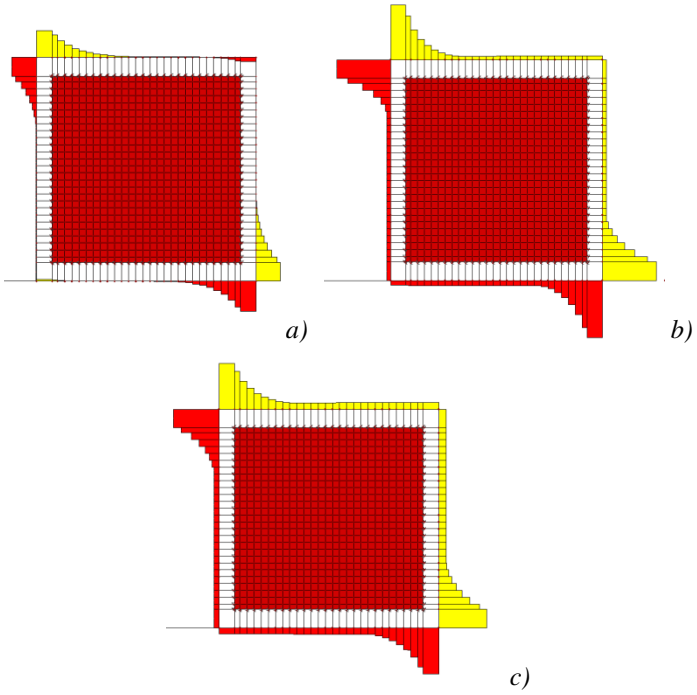

Fig. 4.22. Shear demand distribution evaluated by M2 model for ℓ/h=1 specimen at drifts: *(a) 0.1%; (b) 0.6%; (c) 1.2%.*

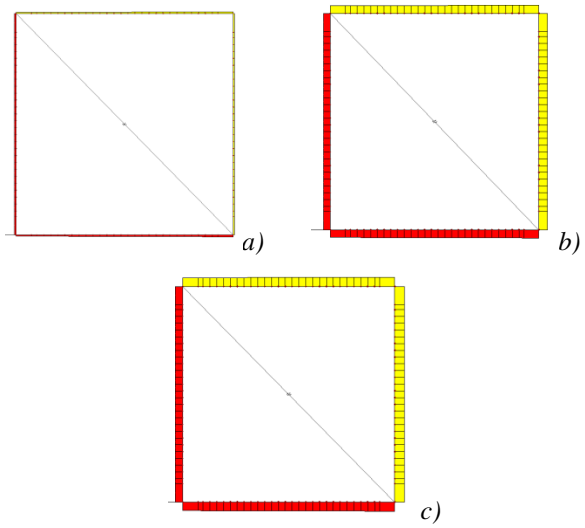

Fig. 4.22. Shear demand distribution evaluated by M1 model for ℓ/h=1 specimen at drifts: *(a) 0.1%; (b) 0.6%; (c) 1.2%.*

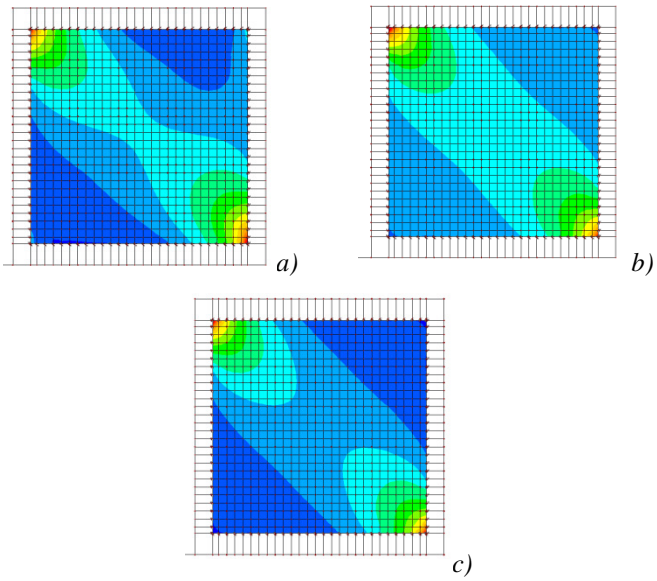

Fig. 4.24. Principal compressive stresses on infill panel evaluated by M2 model for ℓ/h =1 specimen at drifts: *(a) 0.1%; (b) 0.6%; (c) 1.2%.*

4.7 Conclusions on the local interaction between frames and infills and predictive strategies proposed

A study of the local shear effects produced at the ends of beams and columns of non-ductile RC infilled frames in the presence of lateral loads has been presented. This study has the aim of providing strategies for correcting the results in terms of shear demand obtained when, for the modelling, an infill is substituted with an equivalent concentric strut.

A comparison has been carried out between the force arising in the frame members in the case of an infill modelled as an equivalent concentric strut and in the case of an infill "exactly" modelled by finite shell elements, at different drift levels, for a single infilled frame. The comparison was repeated varying the geometrical and mechanical characteristics of the frame-infill system and a correlation law between a parameter synthesizing the characteristics of frame and infill and the real shear distribution in the critical sections was derived.

This law allows one to express the local shear forces acting on beam and column ends as fraction of the axial load experienced by the equivalent strut and for this reason it can be considered a basis for a predictive tool to be used for the assessment of shear demand on RC member critical sections that is otherwise undetectable when a simple equivalent concentric strut model is used.

The predictive capacity of the correlation proposed was tested on two numerical specimens having two different aspect ratios, demonstrating a good accuracy for all investigated drifts. Further, a comparison was made with the shear demand assessment proposed by FEMA, confirming on one hand the reliability of the approach proposed and on the other one the possibility of an overestimation of the FEMA approach for lower drifts than those for which the equivalent strut is affected by force equal to its resistance.

The proposed correlation is obtained considering mechanical properties and structure configurations representative of RC frames designed to resist vertical loads only, but the study can be improved by including a wider class of infilled frames. However, it reveals that more accurate assessment of local shear effects is achievable even if detailed and

onerous models are not used to perform analyses. Further, instruments supplementing technical codes which do not provide any predictive strategy for the evaluation of local frame-infill interaction effects or give very conservative approaches can be formulated.

5 CALIBRATION OF A FIBER IN PLANE – OUT OF PLANE MACRO-MODEL FOR MASONRY INFILLS

The content of this chapter was developed in collaboration with professor Benson Shing at *University of California at San Diego*. It is here discussed the definition of an equivalent strut macromodel to be used to simulate both in plane and out of plane behavior of infilled frames. The model provides the use of fiber beam elements with distributed plasticity, therefore the identification of the mechanical properties of the equivalents struts starts from the calibration of proper stress-strain relationships. The calibration is based on the procedure proposed by Shing and Stavridis (2014) which starts defining for each single-bay, single-story infilled frame a simplified force-displacement law. The equivalent strut is indirectly identified calibrating the constitutive law of the material in such a way to have a best fitting of the infilled frame in plane response with the predicted simplified curve. The effectiveness of the procedure, originally validated by the authors for low reinforced frames with strong infills, was updated to account infill-frame systems characterized by weak infills and adequate shear reinforcing. Validation was in this case performed by means of the results of the experimental investigation discussed in §.2. The predictive efficacy of the strategy resulted finally improved. Furthermore an updating of the model is provided to account simultaneously for in plane – out of

plane response of the infilled frame and reciprocal damage. The use of distributed plasticity beam elements is particularly suitable to account for out of plane response since they are able to simulate the arching mechanism developed by infill panels when subjected to lateral forces.

5.1 Procedure for the identification of the simplified force displacement curve of the infilled frame by Shing and Stavridis (2014) and proposed modifications

The procedure below described looks at the infilled frame macromodel in a more general sense calibrating them in such a way that they not only reflect the behavior of the infill walls but also the response of the frame members associated with mechanisms that are not represented in the model, such as the shear failure of the RC columns.

The calibration provides 2 steps. The first is to divide a multi-bay, multi-story, structure into multiple single-bay, single-story frames, and the second is to derive the lateral load-vs.-displacement curve for each of these frames. The second step could be accomplished by creating a detailed finite element model for each bay of the structure. However, this can be impractical for structures with many bays and stories. This question was circumvented using experimental data and finite element analysis results to derive a set of simple rules to define ASCE 41-type pushover curves for infilled frames. The original calibration focused on non-ductile RC frames with strong infill walls consisting of multiwythe solid clay brick units. The idealized lateral-vs.-displacement curve adopted is shown in **Fig. 5.1** and it is calibrated following the steps described in the subsequent sections.

The geometrical parameters characterizing the single infilled frame are reported **Fig.5.2.**

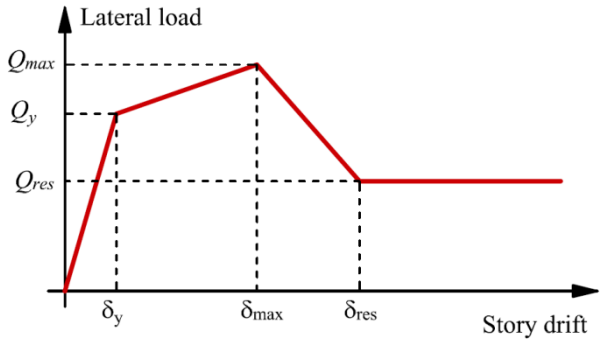

Fig. 5.1. Single infilled frame simplified force displacement law.

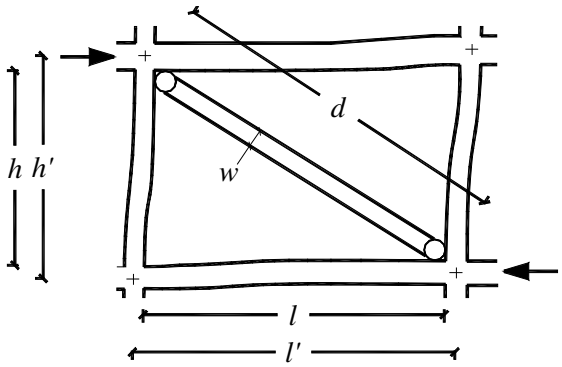

Fig. 5.2. Geometrical features of a single infilled frame with an equivalent strut.

5.1.1 Identification of the initial stiffness

The initial stiffness K_I is evaluated by means of the expression proposed by Fiorato *et al.* (1970) (Eq. 5.1a) in which the uncracked flexural and shear stiffness contributions of the (K_{fl} and K_{shl}) are considered.

$$K_I = \frac{1}{\frac{1}{K_{fl}} + \frac{1}{K_{shl}}} \tag{5.1a}$$

In order to have a better correspondence with the experimental results, which generally show a significant nonlinear behavior in initial branch, it was here preferred to use secant stiffness (Eq. 5.1b), obtained multiplying K_I by the reduction coefficient α that can assume values in the range 0.3-0.5.

$$K_{I\,\mathrm{sec}} = \alpha K_I \tag{5.1b}$$

The flexural stiffness of the infilled frame is calculated as $K_{fl}=3E_cI_{ce}/h$, being E_c the Young modulus of concrete, h the height of the infill and I_{ce} is the moment of inertia of the composite masonry-concrete section, with the masonry wall section replaced by an equivalent concrete section. The inertial properties of masonry section are obtained each time multiplying the actual moment of inertia for the homogenization coefficient $n=E_m/E_c$ weighing Young modulus of masonry E_m, with respect to concrete one. The shear stiffness can be calculated taking into account only the infill contribution as $K_{sh}=A_wG_wh$, in which A_w and G_w are the cross-sectional area and the shear modulus.

5.1.2 Yielding strength Q_y and Peak strength Q_{max}

The yield strength Q_y is the point at which there is a distinct reduction in stiffness due to the separation and sliding between the infill and the RC frame. It is assumed with good approximation that the yielding load can be estimated as

$$Q_y = {}^{2}\!/_{3}\, Q_{\max} \tag{5.2}$$

In the original procedure, developed for a non-ductile frame, considering a diagonal shear sliding crack mechanism occurring before shear failure of columns , the peak strength Q_{max} of an infilled frame can be estimated by means of the expression

$$Q_{\max} = \psi\left(Q_{lc} + Q_{rc}\right) + c_0 A_w + \mu P_w \tag{5.3}$$

in which Q_{lc} and Q_{rc} are the shear strengths of left and right columns respectively and ψ a reduction factor between 0 and 1 to account the fact that the two columns and the infill may not develop their peak resistances at the same time. Moreover the two columns support a quite different shear force at the base sections because of the interaction with the infill wall which has as consequence a shear force increasing on one section and a reduction on the other. Basing on these considerations it was set $\psi=0.5$ for the cases here studied. The coefficient c_0 represents the cohesive strength of the mortar joints, while μ is the friction coefficient. A value of *0.15 MPa* for

all kinds of masonries was considered in this study which was fixed for c_0 while it was assumed that the friction coefficient could vary in the range 0.5–0.6 in order to take into account the hollow percentage of the blocks. The term P_w represents the portion of the gravity load that is carried by the infill. The latter can be estimated basing on the elastic axial stiffness of the infill and columns calculating the distribution factor κ as

$$\kappa = \frac{K_{aw}}{K_{aw} + K_{ac}} \tag{5.4}$$

K_{aw} being the vertical axial stiffness of the infill wall evaluated as $K_{aw}=E_wA_w/h$ and $K_{ac}=2E_cA_c/h$ the axial stiffness of the two columns. Therefore the load P_w can be expressed as quote of the total vertical load P_v as

$$P_w = \kappa P_v \tag{5.5}$$

Equation 5.3 can be rewritten in a more general form accounting also for a ductile failure of the frame characterized by the formation of a 4 plastic hinge mechanism. If one considers that the strength contribution given by the frame S_f is given by the minimum of the lateral loads associated the possible ductile failure $S_{f,D}$ or non-ductile failure $S_{f,ND}$ as

$$S_f = \min\begin{cases} S_{f,D} = 4M_u / h \\ S_{f,ND} = \psi(Q_{lc} + Q_{rc}) \end{cases} \tag{5.6}$$

where $M_u=M_u(N_c)$ is the ultimate moment associated with the top and the bottom sections of the columns (subjected to the axial force N_c) when a ductile plastic hinge mechanism occurs.

Defining the term $S_w = c_0 A_w + \mu P_w$, equation 5.3 becomes thus more generally

$$Q_{\max} = S_f + S_w \tag{5.7}$$

5.1.3 Residual strength Q_{res}

The residual strength Q_{res} can be calculated as the sum of the residual strength of the infill due to friction along the bed joints, $Q_{w,res}$, and the

residual shear resistance of the columns, $Q_{c,res}$, after the development of dominant shear cracks as

$$Q_{res} = 2\,Q_{c,res} + Q_{w,res} \tag{5.8}$$

In order to extend the flexibility of the procedure and to capture eventually ductile behaviour of the infilled frame it is here proposed a relationship defining residual strength as function of the infill-frame strength ratio. The ratio ΔS between peak infill wall strength S_w and frame peak strength S_f is calculated as

$$\Delta S = \frac{S_w}{S_f} \tag{5.9}$$

When strong infills are present ($\Delta S \geq 1$) a typical load drop occurs after the peak strength of the infilled frame occurs. In this case the residual load can be approximately estimated as $0.75\ Q_{max}$. In the case of weak infills this reduction is lower and depend on the strength ratio ΔS. Equation 5.8 can be thus more generally rewritten accounting this aspect as

$$Q_{res} = \eta Q_{\max} \tag{5.10}$$

where the coefficient η is a reduction defined as

$$\eta = \begin{cases} 1 - 0.25\Delta S & (if\ \ \Delta S < 1) \\ 0.75 & (if\ \ \Delta S \geq 1) \end{cases} \tag{5.11}$$

Despite its simplicity the estimation of residual load by means of Eq. 5.10 has demonstrated to hold a sufficient accuracy in a comparison with experimental results.

5.1.4 Yielding drift δ_{Q_y} and Peak strength drift $\delta_{Q_{\max}}$

Combining the Eqs. 5.1b and 5.2 the percentage yielding drift is evaluated as

$$\delta_{Q_y} = \frac{Q_y}{K_{I\,\sec}} \left(\frac{100}{h'} \right) \tag{5.12}$$

h' being the reference gross height for the infilled frame.

The peak strength drift was estimated modifying the relationships proposed by Shing and Stavridis (2014) by the introduction of the coefficient β which takes into account the modification of the peak displacement as function of strength ratio ΔS previously defined in Eq. 5.9

$$\delta_{Q_{\max}} = 0.86 - \frac{1}{3}\frac{AR_w}{\beta} \tag{5.13}$$

β being

$$\beta = \begin{cases} \Delta S^{-0.5} & (if\ \Delta S < 1) \\ 1.0 & (if\ \Delta S \geq 1) \end{cases} \tag{5.14}$$

and AR_w the aspect ratio of the infill that was *1.0* for the analysed specimens.

The introduction of the coefficient β allows the shifting of the peak strength displacement consistently with the fact that in presence of weak infills the peak displacement is significantly higher.

5.1.5 Drift at residual strength reaching $\delta_{Q_{res}}$

In the study of Shing and Stavridis (2014) it is suggested to calculate the drift ratio at which the residual strength is reached as

$$\delta_{Q_{res}} = 1.40\delta_{Q_{\max}} \tag{5.15}$$

This choice leads to a sudden load drop of the simplified force-displacement curve after the peak and provides a good reliability only in the case of strong infills. However infilled frames may behave also in a ductile manner if infill is weaker. To extend the validity of Eq. 5.15 to recognize the possible behaviour of the infilled frame system the following linear relationship is proposed to determine $\delta_{Q_{res}}$ as function of the infill-frame strength ratio

$$\delta_{Q_{res}} = (4.3 - 0.82\Delta S)\delta_{Q_{\max}} = \gamma\delta_{Q_{\max}} \tag{5.16}$$

The coefficient γ represents therefore the generalized ratio between the residual strength drift and the peak drift. The expression in Eq. 5.16 allows one to consider infill-frame strength ratios in the range *0.35-4.0* leading to γ

values going form *1.0* to *4.0* having a wider agreement with the experimental observations on different kinds of infilled frames.

5.2. Experimental validation of the procedure

5.2.1 Identification of infilled-frame force displacement curve

The reliability of the updated procedure before described was tested by means of a comparison with the results of the experimental campaign discussed in §.2 on the cyclic behavior of infilled frames arranged with 3 different kinds of masonry: calcarenite masonry, clay hollow masonry, lightweight concrete masonry.

The steps defining the identification procedure were subsequently applied. The geometrical and mechanical features of the considered specimens and the identification parameters (adopted and calculated) are reported in **Tab. 5.1**, while the final values identifying the simplified force-displacement curve of the infilled frames are in **Tab. 5.2**.

Specimen	P_v *[kN]*	E_c *[MPa]*	E_w *[MPa]*	G_w *[MPa]*	A_w *[mm²]*	AR_w	c_0 *[MPa]*	ψ	μ	κ	n
S1B (Clay)	400	25000	6401	2547	240000	1.0	0.15	0.5	0.5	0.43	0.256
S1C (LW Conc.)	400	25000	4565	2042	480000	1.0	0.15	0.5	0.55	0.33	0.183
S1A (Calc.)	400	25000	3933	1348	320000	1.0	0.15	0.5	0.6	0.39	0.157

Specimen	P_w *[kN]*	K_I *[kN/mm]*	K_{Isec} *[kN/mm]*	α	ΔS	γ
S1B (Clay)	173.8	276.84	138.42	0.5	1.58	3.01
S1C(LW Conc.)	131.0	475.91	237.95	0.5	1.11	3.39
S1A (Calc.)	154.5	211.19	105.60	0.5	1.80	2.82

Table 5.1. Mechanical features and parameters defining the infill-frame curves.

Specimen	Force			Drift			Displacement		
	Q_y [kN]	Q_{max} [kN]	Q_{res} [kN]	δ_{Qy} [%]	δ_{Qmax} [%]	δ_{Qres} [%]	d_{Qy} [mm]	d_{Qmax} [mm]	d_{Qres} [mm]
S1B (Clay)	133.9	200.9	150.7	0.054	0.53	1.58	1.0	9.5	28.5
S1C (LW Conc.)	182.7	274.0	205.5	0.043	0.53	1.79	0.8	9.5	32.2
S1A (Calc.)	145.8	218.7	164.0	0.077	0.53	1.49	1.4	9.5	26.7

Table 5.2. Force-displacement values identifying the infill-frame curves

The validation of the predictive capacity of the above described procedure was performed comparing the resulting simplified force-displacement curves with the monotonic strength envelopes of the experimental cyclic tests. The comparisons are reported in **Fig. 5.3**, where it can be recognized an average good agreement with the experimental responses. Even if the simplified curve shows an extremely linearized behavior with respect to the experimental envelopes, the latter has the sole function to guide the equivalent strut fiber model calibration as described in the subsequent section.

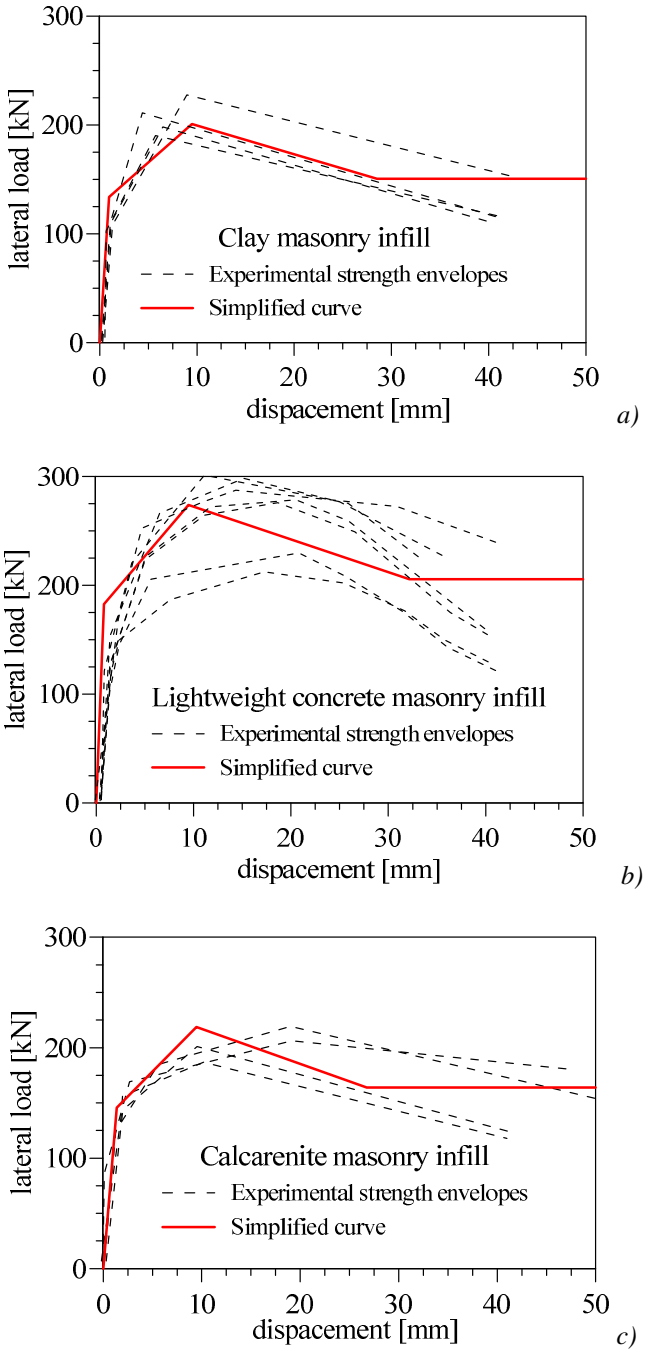

Fig. 5.3. Simplified force-displacement infilled-frame curves

5.2.2 Calibration of the equivalent strut fiber model.

A fiber model of each specimen was realized by OpenSees code. The members constituting the frame were modeled by means of force based beam column elements. A built-in Concrete-02 (Yassin) uniaxial material model (**Fig. 5.4a**) was used to model concrete while rebars were modeled using a Steel-02 model (Menegotto-Pinto). In each cross section, confined and unconfined concrete laws were assigned to core and cover fibers respectively (**Fig. 5.4b**). The mechanical parameters defining the core, cover and steel fibers constitutive laws are reported in **Tab. 5.3**.

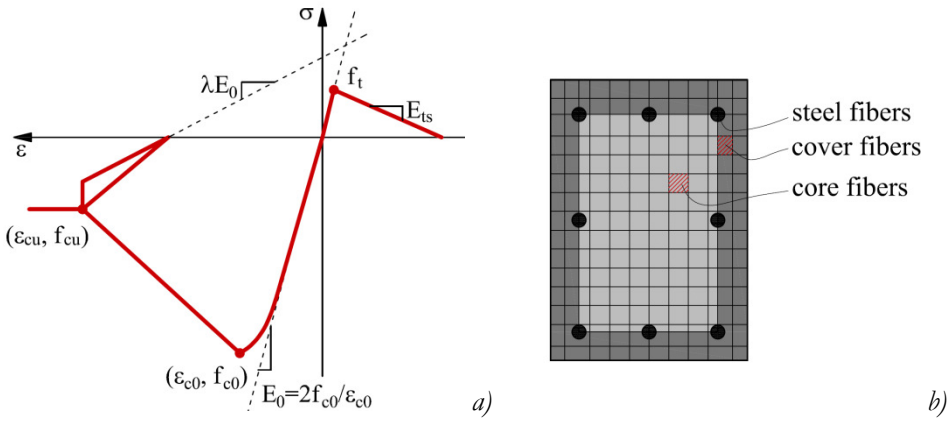

Fig. 5.4. *a)* OpenSees Concrete 02 constitutive law; *b)* Fiber discretization of the cross section.

Concrete	f_c [MPa]	f_{cu} [MPa]	f_t [MPa]	ε_{c0}	ε_{cu}	**Steel**	f_y [MPa]	E_s [MPa]
Cover	25.0	13.0	0.0	0.002	0.010	Rebars	450.0	210000
Core	25.0	11.0	0.0	0.002	0.008			

Table 5.3. Concrete and steel parameters for RC elements.

Two diagonal truss elements were used to model the infill. The attribution of the cross section dimensions was carried out simply assigning a thickness equal to the actual thickness of the infill and width equal to 1/3 of the diagonal strut length. For in plane loading only a more accurate identification of the equivalent strut cross section is not necessary since the calibration of the equivalent strut properties is carried out at the level of the

material constitutive law. The attribution of this stress-strain relationship for the equivalent strut was determined for each infilled frame iteratively calibrating a fictitious masonry law in order to achieve the best correspondence with the force-displacement simplified curve by means of a static pushover analysis of the model.

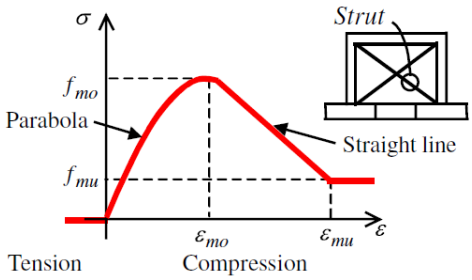

Fig. 5.4. Constitutive law model for fibers constituting equivalent struts.

Also for the diagonals a Concrete-02 uniaxial material model was attributed to fibers of the cross sections. The parameters calibrated for the struts which allowed obtaining the best agreement of the OpenSees model pushover curves with the simplified ones are reported in **Tab. 5.4**.

Specimen	w [mm]	t [mm]	f_{m0} [MPa]	f_{mu} [MPa]	ε_{m0}	ε_{mu}
S1B (Clay)	750	150	2.2	1.3	0.0015	0.008
S1C (LW Conc.)	750	300	1.2	0.7	0.0015	0.008
S1A (Calc.)	750	200	1.8	1.1	0.0020	0.008

Table 5.4. Concrete and steel parameters for RC elements.

It can be observed that despite the wide differences of the considered masonry infill typologies, a small variability of the characteristic stress and strain values identifying the constitutive law was recognized. Among those the peak strain ε_{m0}, which varied in the range *0.0015-0.0020,* the ultimate strain ε_{mu} which could be fixed at the value of *0.008* and the ultimate strength f_{mu}, considered as $0.6f_{m0}$.

The calibration has shown that the most sensitive parameter involved in the identification process of the equivalent strut constitutive law was the peak strength f_{m0} which depended not only on the mechanical

characteristics of masonry infills but also on the failure mechanism actually activated in experiments.

The good agreement between the proposed model pushover curves and simplified curves of the infilled frames is shown in **Fig. 5.5**. A final comparison of the model pushover curves with the experimental strength envelopes is furthermore shown in **Fig. 5.6** demonstrating a quite good reliability of the proposed to capture the average in plane monotonic response of the infilled frame.

In order to test the reliability of the model as instrument to perform dynamic analyses, the cyclic behavior was also investigated. The experimental cyclic tests made on the specimens were simulated on the OpenSees models of the infilled frames. The latter were subjected to the same history of displacements of the specimens actually tested. The comparison has permitted to evaluate the reliability of the concrete law model assigned to the equivalent strut to capture the cyclic-hysteretic behavior of the infill-frame system in order to extend the use for nonlinear time history analyses.

The hysteretic behavior of the Concrete-02 model is ruled by the parameter λ defining each time the ratio between unloading slope at and initial slope. The best results were obtained by setting the masonry law with $\lambda=0.085$ for the calcarenite and clay hollow masonry infilled specimens and $\lambda=0.070$ for lightweight concrete masonry infilled specimens. A $\lambda=0.1$ value was attributed to the concrete elements constituting the frames.

In **Figs. 5.7-5.9** the model cyclic response is compared with the experimental one of three specimens (one for each typology of masonry infill). The comparison demonstrates the suitability of the proposed model to predict also the cyclic response of masonry infilled frames that is as more precise as accurate is the estimation of the monotonic curve.

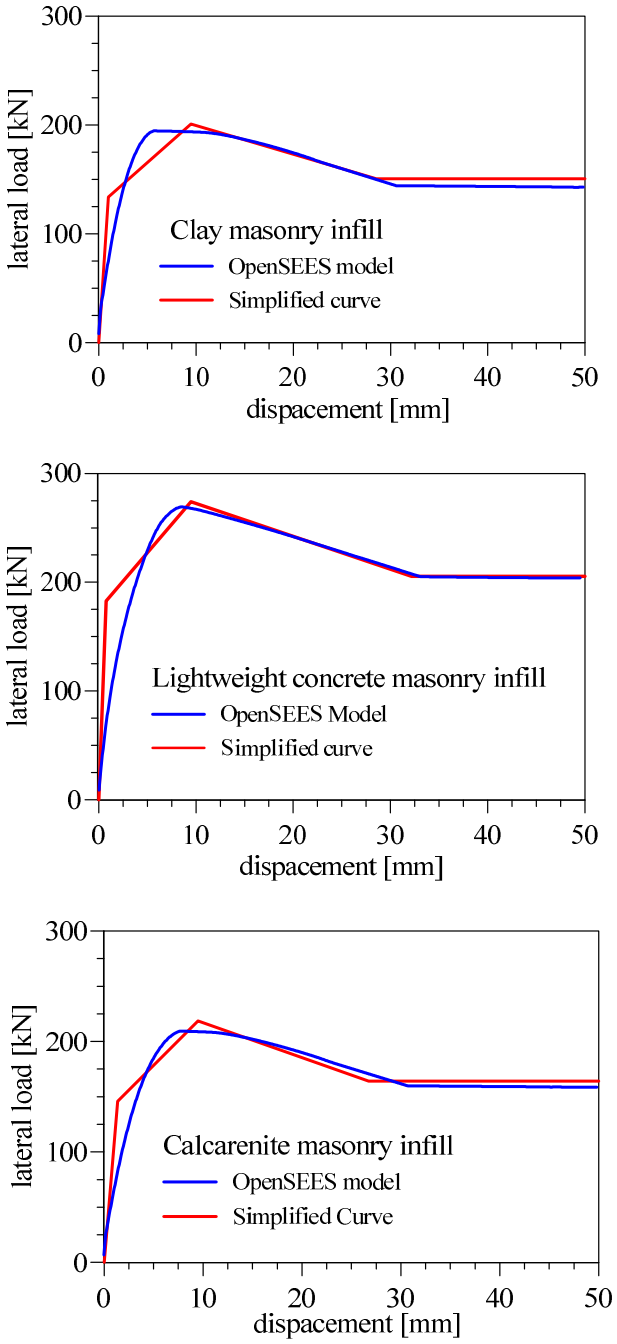

Fig. 5.5. Comparison between OpenSees model pushover curves and simplified curves.

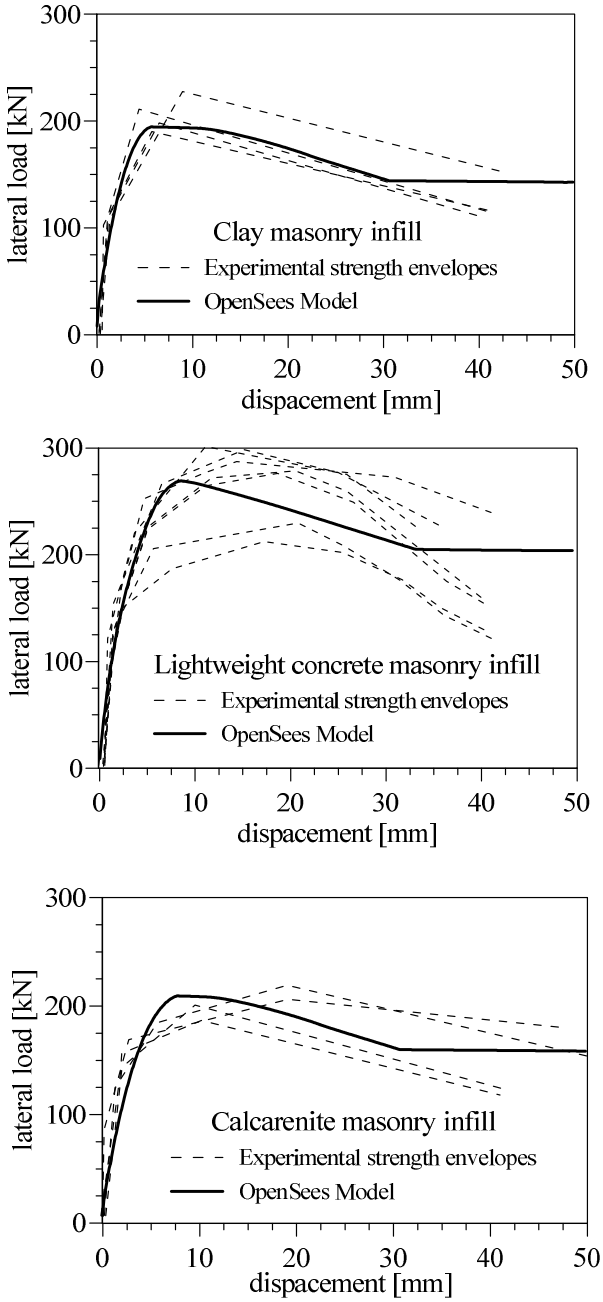

Fig. 5.6. Comparison between OpenSees model pushover curves and experimental strength envelopes.

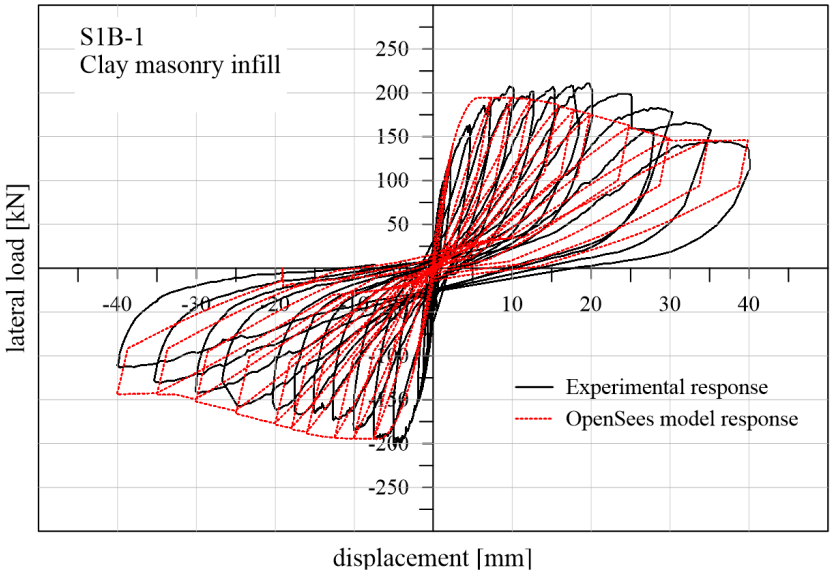

Fig. 5.7. Comparison between experimental test and OpenSees model for a clay hollow masonry infilled frame specimen.

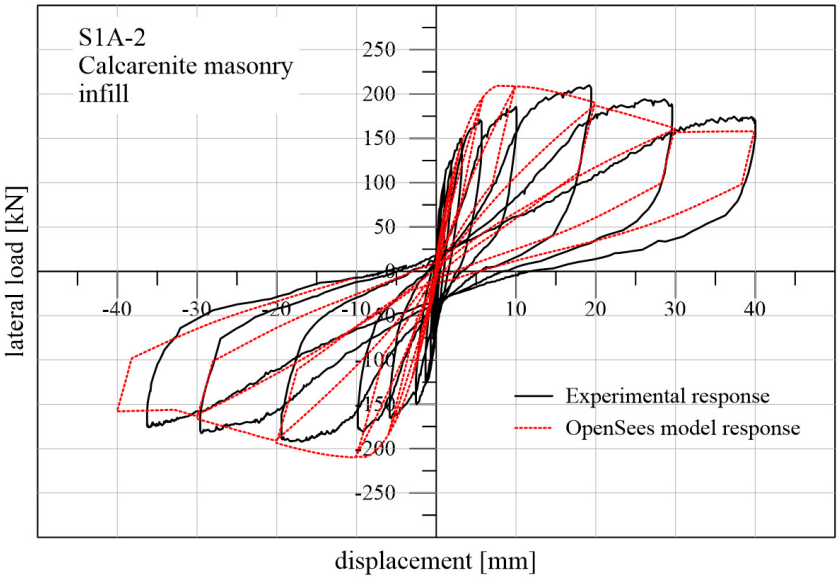

Fig. 5.8. Comparison between experimental test and OpenSees model for a calcarenite masonry infilled frame specimen.

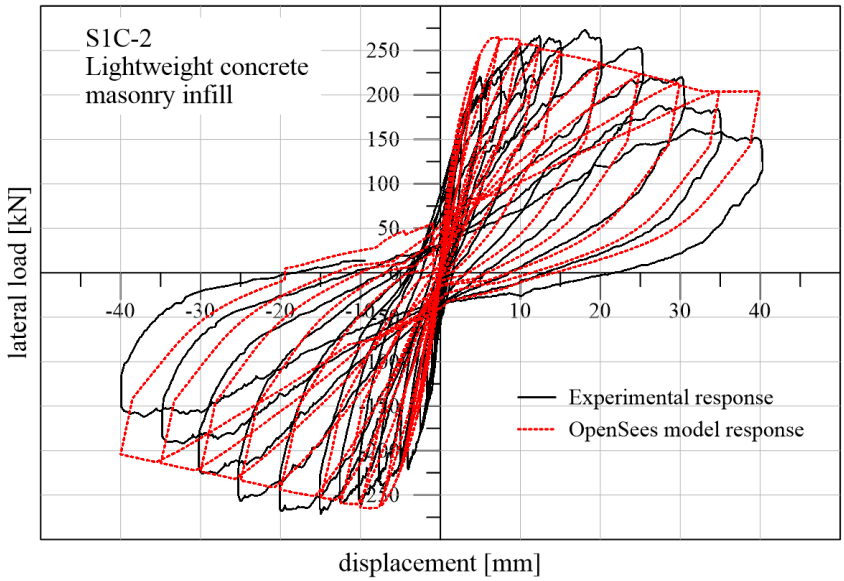

Fig. 5.9. Comparison between experimental test and OpenSees model for a lightweight concrete masonry infilled frame specimen.

5.3 Extension of the model to account in plane-out of plane behavior of masonry infills.

5.3.1 In plane-out of plane response of masonry infills and interaction issues.

In the last decades the most of the research works on infilled frame interaction have been addressed to prediction and modeling of in plane response. However the assessment of out of plane (OOP) capacity and reciprocal interaction with in plane (IP) capacity appears to be a quite relevant issue, since the final response depends on the damage history both in plane and out of plane. Masonry infills are stiff but brittle elements that often attract large lateral story shears when loaded parallel to their plane. Following moderate or strong earthquakes, it is common to observe an x pattern of cracks from each corner of an infill panel which is a result of large in-plane stiffness, but small in-plane diagonal tensile strength. The probability of occurrence for a second earthquake with equal intensity is small. However, it is probable that a lighter earthquake may occur and shake a cracked infill panel from its surrounding frame with inertial forces applied

normal to its plane. The x pattern of cracks resulting from in-plane forces is similar to the crack pattern for a square panel subjected to out-of-plane forces. This implies that the out-of-plane strength may be related to the in-plane damage. The out-of-plane strength may be substantially weakened by in-plane cracking of the panels.

Furthermore the evaluation IP-OOP combined response has to be also assessed during the same ground motion in order to evaluate the respective damage evolution and the consequences on the overall safety of structures and of people that could be involved in falling down of masonry infills.

The studies carried out on this topic have demonstrated that masonry infills can develop a significant out of plain strength due to the arching effects that originates when a masonry panel, confined by a RC frame, is subjected to out plane actions (**Fig. 5.10-a**). Moreover observing the crack patterns of infills after OOP experimental tests it results evident that infill panel, restrained by the surrounding frame behaves as plate, therefore the arching effect has a 2-way generation (**Fig. 5.10-b**).

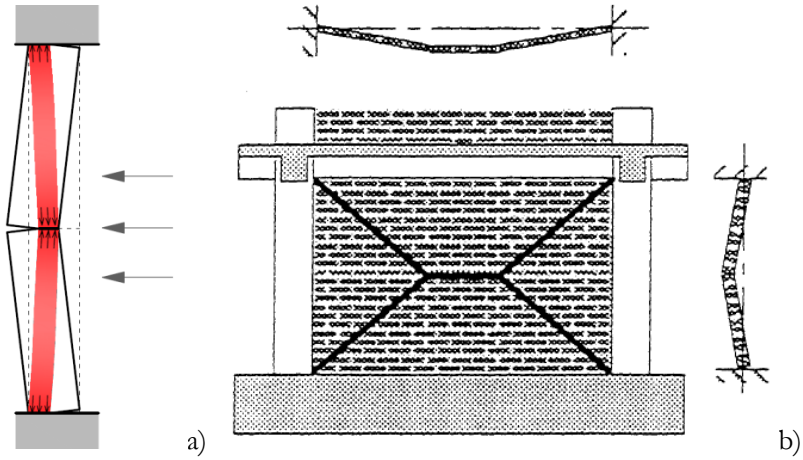

Fig. 5.10. *a)* Scheme of development of the arching effect of OOP actions in masonry infills; *b)* Cracking pattern scheme of a masonry infill after an OOP test (Angel *et. al* (1994).

A number of theories and analytical models (MacDowell et al (1956a-b), Monk (1958), Angel *et al.* (1994), Abrams *et al.* (1996), etc.) have been developed to predict the out-of-plane behavior of masonry infills. The latter included elastic and inelastic plate theory as well as one and two way arching action. Analytical models varied from simple expressions and coefficients,

to elaborate computer programs. Moreover experimental investigations have been carried out (Abrams *et al.* (1996), Griffith and Vaculik (2007)) demonstrating a significant OOP strength of infills due to arching action an overall ductile behaviour for undamaged and low damaged panels.

The main conclusion which comes from the main research studies on the out-of-plane mechanical behaviour of infill panels are here summarized:

- Out-of-plane strength depends on compressive strength of the masonry and not on the tensile strength;
- Out-of-plane strength decreases with the square of the slenderness ratio of panels;
- Infills develop a 2-way arching action if are well confined by the frame;
- For slenderness ratios larger than 30, the arching action is small.

Consistently with these determinations most of the analytical expressions proposed for the evaluation of OOP strength of the infill panels (Timoshenko (1959), Haseltine (1976, 1977), Hendry (1973, 1976), McDowell et al. (1956), refer to a proportionality between the OOP maximum load q_a (defined as a pressure) and the ratio between compressive strength of masonry f_m and square of the slenderness ratio *h/t* (Eq. 5.11).

$$q_a \propto k \frac{f_m}{\left(\frac{h}{t}\right)^2} \tag{5.11}$$

The different expressions differ by the choice of a coefficient *k* which can account different aspects according to the hypothesis of each theory.

A similar relationship is proposed also be FEMA 356 where is stated that if arching action is considered, the lower bound OOP strength of an infill panel (in psf), shall be determined using the following equation

$$q_a = \frac{0.7 f_m \lambda_2}{\left(\frac{h}{t}\right)} \times 144 \tag{5.12}$$

The major influence of the slenderness ratio is here taken into account by the parameter λ_2 whose values for different *h/t* ratios are reported in **Tab. 5.5**. A plot of λ_2 values is represented in **Fig. 5.11** where a possible best fitting equation is also provided.

h/t	5	10	15	25
λ_2	0.129	0.060	0.034	0.013

Table 5.5. Values of λ_2 for Use in Eq. (5.12)

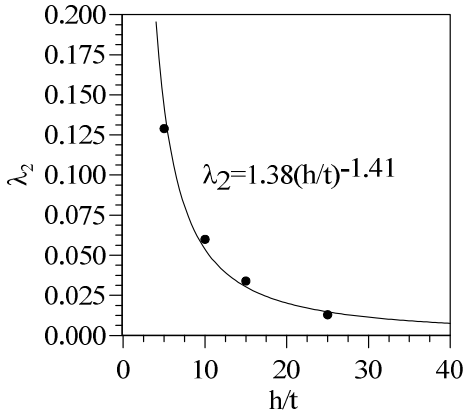

Fig. 5.11. FEMA 356 λ_2 – (h/t) points and suggested best fitting curve.

It is also stated that arching action shall be considered only if all of the following conditions exist

- the panel is in full contact with the surrounding frame components;
- the frame members have a sufficient stiffness;
- the frame components have sufficient strength to resist thrusts from arching of an infill panel;
- the *h/t* ratio is less than or equal to 25.

Moreover if arching action is considered the code provides an expression (Eq. 5.13) for the evaluation of the out of plane drift ratio Δ/h of panels which is associated to the maximum load

$$\frac{\Delta}{h} = \frac{0.002\left(\frac{h}{t}\right)}{1+\sqrt{1-0.002\left(\frac{h}{t}\right)^2}} \tag{5.13}$$

Eq. 5.13 can be however applied only if the above reported conditions are satisfied.

Although a conspicuous number of expressions for the prediction of out of plane strength of infill walls have been provided, the latter can be only

employed prescriptively for the verification of OOP infill capacity that is without the introduction in the structural model.

The issue of the definition of a macromodel able to capture both in plane and out of plane behaviour of infilled frames has been dealt with only recently. The major question regarded how to update the current macromodels (based on the definition of an equivalent strut) to simultaneously predict IP and OOP response and their mutual influence in terms of damage. The classical configuration, based on equivalent bracing struts, is not suitable to be updated in a simple way. First of all because the equivalent strut is an abstraction of the actual physics that well approximates the in plane response but cannot account for the 2-way arching effect. Moreover the majority of existing macro-models makes use of classic Eulero-Benoulli beam elements for which axial force and bending moment are uncoupled quantities. This second aspect is quite important since the arching effect is due to an axial load that is generated along the element by a flexural regime. For this reason modelling of arching action can only be performed by mean of beam elements with distributed plasticity (force based or displacement based beam-column elements) which include axial force-bending moment coupling in their formulation.

Among the most recently developed IP-OOP macromodels, Hashemi and Mosalam (2007) proposed a 8 strut 3D strut-and-tie (SAT) model (Fig. 5.12) in which the arching action is accounted by shifting out of plane the midspan joint of each strut of a specified distance. The diagonal elements are compression only resistant fiber elements with a specified compressive law. A tension only link element connects the midspan joints. Using monotonic pushover analyses the authors have calibrated the properties of the model so that its IP, OOP, and interaction behavior matches those of a nonlinear finite element model of a prototype infill panel.

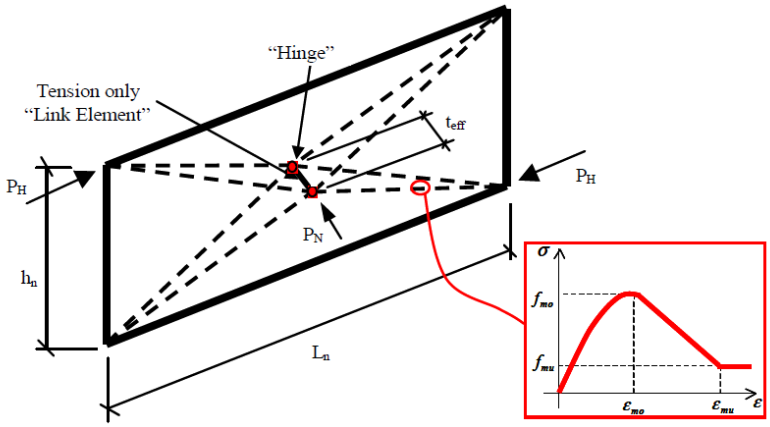

Fig. 5.12. Hashemi and Mosalam (2007) SAT macromodel.

In a further work Mosalam and Günai (2014) developed a single strut fiber macromodel (**Fig. 5.13**) able to account for both in plane and out of plane response.

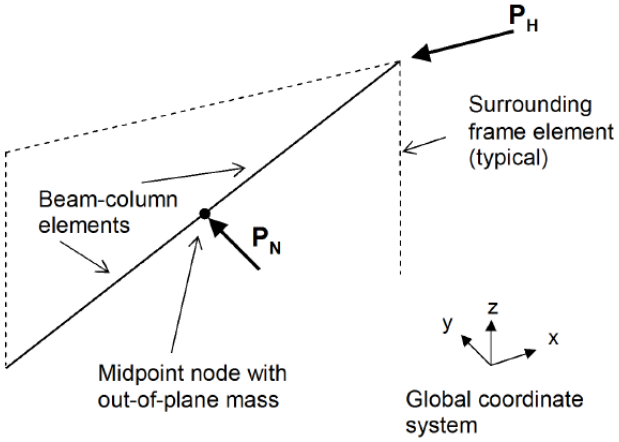

Fig. 5.13. Mosalam and Günai (2014) IP-OOP macromodel.

The diagonal strut was resisting in tension and compression. An elastic perfectly plastic constitutive law is adopted. The calibration of the IP-OOP response of the strut was performed at the fiber level. The fibers were defined with a different weight inside the cross section in terms of area, strength and strain in order to match an ideal IP-OOP failure surface whose analytical law were previously determined by authors by means of a FE analysis.

Although these 2 models permit to perform analyses of infilled frames considering IP-OOP interaction they don't take the advantage of the fiber elements with distributed plasticity to reproduce the arching action but account for it in a fictitious manner. The second one, due to the presence of single strut reacting in tension and compression, affects the real distribution of the internal forces in RC members. Moreover the choice of a elastic perfectly plastic law for the fibers constituting the diagonal's cross section makes the model unable to predict loss of bearing capacity both in plane and out of plane response.

5.3.2 Coupling between axial force and bending moment in displacement based formulation of distributed plasticity beam column elements

It is considered a generic beam-column element (Fig. 5.14) having the nodal end forces and displacements described by the vectors $\boldsymbol{U}^e$ and $\boldsymbol{P}^e$ (Eq. 5.14), and the displacements field described by the vector $\boldsymbol{u}(x)$ (Eq. 5.15) containing the displacement functions $u(x)$ and $v(x)$.

$$\boldsymbol{U}^e = [U_1,...,U_6]^T \; ; \; \boldsymbol{P}^e = [P_1,...,P_6]^T \tag{5.14}$$

$$\boldsymbol{u}(x) = [u(x), v(x)]^T \tag{5.15}$$

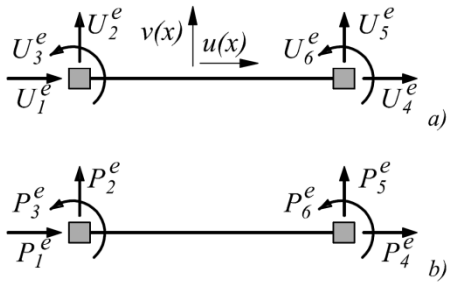

Fig. 5.14. End forces and displacements in a generic beam-column element.

The displacement field is approximated by choosing the shape functions in order to provide a linear and cubic expression of $u(x)$ and $v(x)$ respectively. The displacement field vector $\boldsymbol{u}(x)$ is therefore connected to the nodal displacements through the shape function matrix $\boldsymbol{N}_U(x)$ as

$$\boldsymbol{u}(x)=\begin{bmatrix}u(x)\\ v(x)\end{bmatrix}\cong \boldsymbol{N}_U(x)\boldsymbol{U}^e \tag{5.16}$$

The generic section deformation $\boldsymbol{e}^e(x)$ vector along the element is therefore defined as

$$\begin{aligned}\boldsymbol{e}^s(x)=\begin{bmatrix}\varepsilon_0\\ \kappa\end{bmatrix}=\begin{bmatrix}u'(x)\\ v''(x)\end{bmatrix}=\begin{bmatrix}\frac{d}{dx} & 0\\ 0 & \frac{d^2}{dx^2}\end{bmatrix}\begin{bmatrix}u(x)\\ v(x)\end{bmatrix}\cong\\ \cong\begin{bmatrix}\frac{d}{dx} & 0\\ 0 & \frac{d^2}{dx^2}\end{bmatrix}\boldsymbol{N}_U(x)\boldsymbol{U}^e\end{aligned} \tag{5.17}$$

If one defines the matrix of the shape functions for the sections deformations $\boldsymbol{B}(x)$ as follow

$$\boldsymbol{B}(x)=\begin{bmatrix}\frac{d}{dx} & 0\\ 0 & \frac{d^2}{dx^2}\end{bmatrix}\boldsymbol{N}_U(x) \tag{5.18}$$

the generic section deformation vector assumes the expression

$$\boldsymbol{e}^s(x)=\begin{bmatrix}\varepsilon_0\\ \kappa\end{bmatrix}\cong\boldsymbol{B}(x)\boldsymbol{U}^e \tag{5.19}$$

which expresses the approximation that, along the element, the axial deformation and the curvature are constant and linear respectively.

The section forces $\boldsymbol{s}^s(x)$ are related to the section deformation through the section stiffness matrix that in the linear elastic case is a diagonal matrix which uncouples axial force and bending moment (Eq. 5.20).

$$\boldsymbol{s}^s(x)=\begin{bmatrix}N(x)\\ M(x)\end{bmatrix}=\boldsymbol{k}^s(x)\boldsymbol{e}^s(x)=\begin{bmatrix}EA(x) & 0\\ 0 & EI(x)\end{bmatrix}\begin{bmatrix}\varepsilon_0\\ \kappa\end{bmatrix} \tag{5.20}$$

The same constitutive relationship can be rewritten for the nonlinear case at a generic load step by substituting the section elastic stiffness matrix with the fiber section tangent stiffness matrix $\boldsymbol{k}_T^s(x)$ (Eq. 5.21).

$$\boldsymbol{s}^s(x) = \begin{bmatrix} N(x) \\ M(x) \end{bmatrix} = \boldsymbol{k}_T^s(x) \begin{bmatrix} \varepsilon_0 \\ \kappa \end{bmatrix} = \boldsymbol{k}_T^s(x)\boldsymbol{e}^s(x) \tag{5.21}$$

In this case the tangent stiffness matrix is a full matrix coupling the section forces *N(x)* and *M(x)* (Eq.5.22)

$$\begin{aligned} N(x) &= k_{T,11}^s \varepsilon_0 + k_{T,12}^s \kappa \\ M(x) &= k_{T,21}^s \varepsilon_0 + k_{T,22}^s \kappa \end{aligned} \tag{5.22}$$

This is reflected also in nodal forces of the element that can be calculated by the application of the principle of virtual displacements

$$\delta \boldsymbol{U}^{e^T} \boldsymbol{P}^e = \int_0^L \delta \boldsymbol{e}^{s^T}(x) \boldsymbol{s}^s(x) dx \tag{5.23}$$

and accounting Eq. (5.19) in Eq. (5.23) the nodal forces can be expressed as

$$\boldsymbol{P}^e = \int_0^L \boldsymbol{B}^T(x) \boldsymbol{k}_T^s(x) \boldsymbol{B}(x) \boldsymbol{U}^e dx \tag{5.24}$$

In Eq. (5.24) the tangent stiffness matrix of the beam-column element can be recognized as

$$\boldsymbol{K}_T^e = \int_0^L \boldsymbol{B}^T(x) \boldsymbol{k}_T^s(x) \boldsymbol{B}(x) dx \tag{5.25}$$

therefore the element end forces are

$$\boldsymbol{P}^e = \boldsymbol{K}_T^e \boldsymbol{U}^e \tag{5.26}$$

resulting also coupled by the full matrix $\boldsymbol{K}_T^e$.

5.3.3 Proposed in plane-out of plane interacting macro-model.

A new macro-model able to represent the in plane-out of plane response of an infilled frame is here presented. In the definition of the proposed model two main aspects have been pointed out, in order to better

reproduce the real physics of the problem. The first one is that the model has to account directly for the arching action without the definition of fictitious configurations of mechanical properties. The second is that the model shall be able to represent the mutual damaging for in plane and out of plane actions. In other words, if in plane damage occurs, the out of plane capacity have to be sensitive in order to account this damage and vice versa.

For this reason the model provides the use of fiber elements with distributed plasticity which, besides accounting the arching action in their formulation as specified in the previous section, are also suitable to well reproduce the damage by the definition of proper constitutive relationships for the material.

Similarly to what done in the previous section regarding the in plane modelling, the beam and columns elements, belonging to the RC frame are modelled by means of force based fiber elements with distributed plasticity. The infill panel is here instead replaced by 4 pinned struts, each one divided in two members in correspondence of the midspan node. A geometrical scheme of the model is represented in **Fig. 5.15**. It is important to underline all the equivalent struts representing the infill are beam-column displacement based fiber elements, differently to what done for in plane calibration in which truss elements can be simply used to model the diagonals.

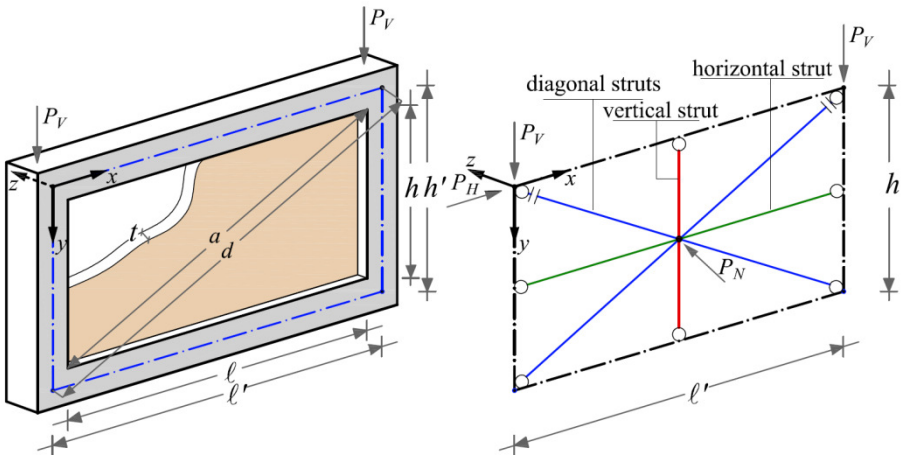

Fig. 5.15. Geometrical features of proposed 4 strut macro-model.

The model is constituted by 2 diagonals having only compressive strength. The diagonals have 3D pinned ends and a unilateral (only compression) axial constrain for the axial displacement at the upper joints. This special device is introduced to reproduce the detachment by the frame when the diagonal is not loaded. The 2 diagonals provide the whole in plane response of the infill when in plane action occurs. Moreover the latter offer their strength also for out of plane actions.

The horizontal and vertical struts are compression only resisting elements not influencing the in plane behavior of the infill but give their contribution only for in case of OOP loads.

It is important to point out that the 4 structures do not share the midspan node, therefore 4 independent nodes, belonging one to each strut are defined. However, although the in plane (*x, y*) relative displacements of the midspan nodes are free, the latter are constrained to have the same displacement along *z* direction. In this way each strut provides his strength contribution to the OOP response.

The geometrical and mechanical identification of the struts is performed starting from the definition of the diagonals. The initial dimensions of the diagonal struts are defined similarly to what done for the in plane case as well as the definition of the constitute law. The only difference regards the definition of the width of the diagonal (w_d) that is in this case preferable to fix as 1/3 of the internal diagonal length (*a*) instead of (*d*). The thickness is initially fixed as the actual thickness *t* of the infill. Subsequently a constitutive law is assigned in order to fit the prediction of the in plane monotonic response obtained by simplified curve as previously exposed. When performing this operation the actual peak strength of masonry f_{m0} is replaced by a significantly lower fictitious strength f_{md0} due to the fact that the failure of the panel is dominated by the sliding of the mortar joints rather than the crushing of masonry. Even if this assumption is correct for the reproduction of the in plane response, the out of plane behavior of the diagonal cannot be simultaneously predicted by using this fictitious strength. The OOP capacity of the diagonal in terms of maximum load, shall be in fact proportional to f_{m0} and its dimensions w_d , *t* and *a* (Eq. 5.27).

$$q_{a,d} \propto \frac{f_{m0} w_d}{\left(\frac{a}{t}\right)^2} \tag{5.27}$$

However, the same OOP capacity for the diagonal strut can be obtained by using the fictitious strength f_{md0} and modifying the dimensions of the cross section w_d and t into $\tilde{w}_d$ and $\tilde{t}$, in order to satisfy the equivalence in Eq. 5.28.

$$\frac{f_{m0} w_d}{\left(\frac{d}{t}\right)^2} = \frac{f_{md0} \tilde{w}_d}{\left(\frac{d}{\tilde{t}}\right)^2} \tag{5.28}$$

with the condition given in Eq. 5.29, that expresses that the resultant cross sectional area shall remain constant to maintain an equivalent in plane behavior of the diagonal strut.

$$w_d \, t = \tilde{w}_d \, \tilde{t} \tag{5.29}$$

Substituting Eq. 5.29 into Eq. 5.28 one obtains

$$\frac{f_{m0} w_d}{\left(\frac{d}{t}\right)^2} = \frac{f_{md0} w_d t}{\tilde{t}\left(\frac{d}{\tilde{t}}\right)^2} \tag{5.30}$$

that can be rewritten more simply as

$$\frac{f_{m0}}{f_{md0}} = \frac{\tilde{t}}{t} \tag{5.31}$$

Equations 5.29 and 5.31 allow one to maintain the identification made for the in plane behavior of the diagonal in terms of constitutive law by only operating a simple modification of the cross section dimensions as function of the ratio between the actual strength of masonry f_{m0} and the fictitious one f_{md0}. The final dimensions of the diagonal strut generalized to account for the in plane behavior can be therefore directly expressed as follows

$$\tilde{t} = \frac{f_{m0}}{f_{md0}} t; \quad \tilde{w}_d = \frac{w_d t}{\tilde{t}} \tag{5.32}$$

A graphical exemplification of the geometrical modification of the diagonal strut is provide in **Fig. 5.16**.

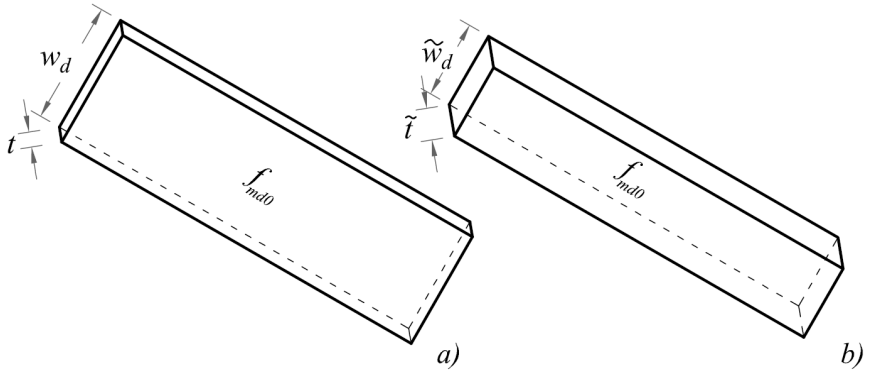

Fig. 5.16. Identification of the equivalent dimensions for the cross section of diagonal strut. *a)* IP identification; *b)* IP-OOP identification.

As before mentioned this final configuration for the diagonal struts does not modify the in plane capacity. Moreover the increase of the thickness confers them the majority of the OOP capacity of the infill. In this way if an in plane damage occurs, this will significantly influence the out of plane capacity.

The residual OOP strength is provided by the horizontal and vertical struts which are defined maintaining the actual thickness t of the infill and the actual strength f_{m0}. The widths of the struts result as difference between the height and length of the panel and the horizontal and vertical projections of the diagonal initial width w_d on the infill perimeter. With reference to **Fig. 5.17a-b** the widths of the horizontal (w_h) and vertical (w_v) struts can be thus determined as

$$w_h = h - \frac{w_d}{\cos\theta}\,; \quad w_v = \ell - \frac{w_d}{\sin\theta} \tag{5.33}$$

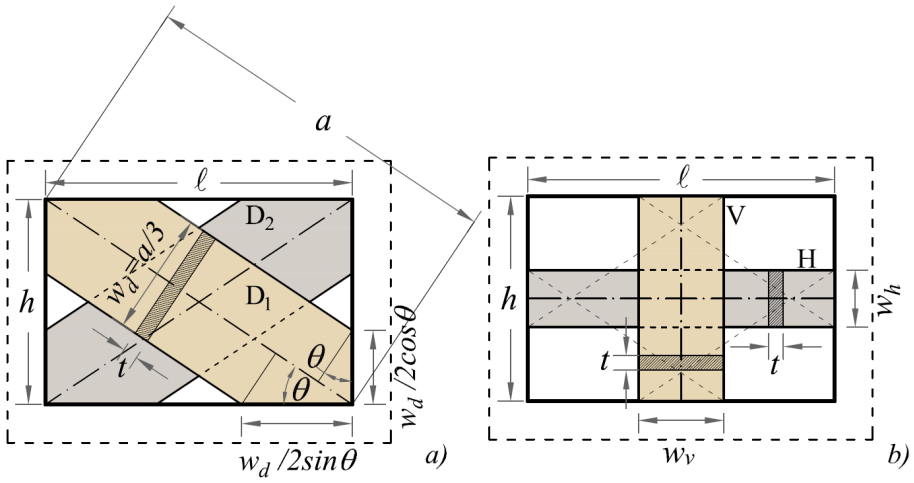

Fig. 5.17. Identification of the equivalent dimensions for the cross section of horizontal and vertical strut. *a)* definition of the geometrical projections of the diagonal width on the frame; *b)* dimensions of the horizontal and vertical strut.

The four strut model in this way generated is a generalization of the 2 strut in plane model initially presented. The big attractiveness consists in the possibility to predict simultaneously both IP and OOP response and reciprocal damage evolution when nonlinear time history analyses are performed.

5.3.4 Experimental validation of the model

The model has been validated on the basis of the experimental results provided by Angel *et al.* (1994). In their research work the author exanimated losses in out-of-plane strength resulting from a previous in - plane damage for unreinforced masonry infills. Test were carried out on a full-scale, single-story, single-bay reinforced concrete frame infilled with different kinds of masonry. The specimens were first subjected to in plane cyclic lateral history displacement until the masonry infills reached the first cracking Δ_{cr} (phase a). Then, the same panels were subjected to normal monotonic pressure using an air bag (phase b). A simplified scheme of the test is reported in **Fig. 5.18**.

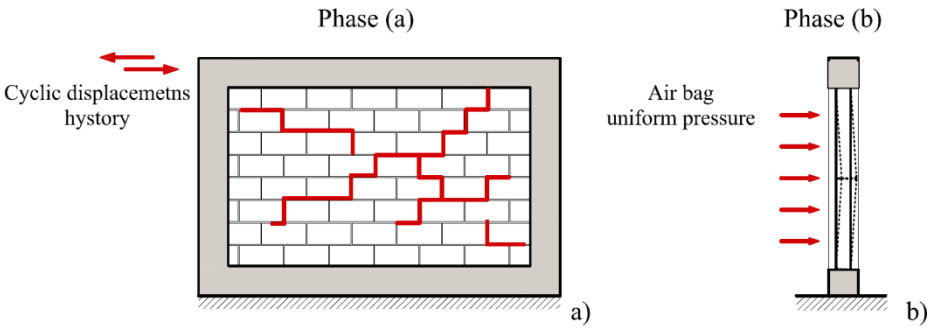

Fig. 5.18. Scheme of the tests by Angel *et al.* (1994). *a)* Phase a. Cyclic in plane loading until first cracking Δ_{cr}; *b)* Phase b. Out of plan monotonic loading.

The validation is carried out modelling by OpenSees the specimens by means of the proposed approach. For each specimen's model the same displacement history is applied at the upper joints. At the end of the in plane loading an out of plane pushover of the midspan node is started. The OOP pushover curve is finally compared with the experimental one. Since in the experimental OOP the load is given as a pressure, the latter is converted in a force multiplying pressure itself by the area of the infill.

The original experimental program consisted of testing eight full-scale specimens of unreinforced clay bricks or concrete masonry infills placed within a single-story, single-bay reinforced concrete frame. Clay brick masonry infills were arranged in three different thicknesses corresponding to 0.5, 1.0 and 2.0 wythes while 2 thicknesses were used for concrete masonry infills. The details of the specimens are reported in **Figs. 5.19-5.20**. In the current validation 5 of them were selected for the comparison. Geometrical and mechanical features of masonry infills belonging to the selected specimens are reported in **Tab. 5.6** where the original notation is used indicating each specimen with a number followed by a letter (*a* or *b*) indicating the testing phases *a* and *b* which the specimens were subjected. The RC frame was a heavily reinforced strong and ductile frame. The latter was designed in accordance to technical codes used in USA after 1989. Details of geometrical and mechanical features of the frame are reported in **Tab. 5.7**.

Spec.	Infill type	Mortar type	E_m Mpa ksi	G_m Mpa ksi	f_m Mpa psi	h/t	t (mm)
2a-b	Brick	N	8040 1167	3162 459	11.5 1575	34.2	47.6
3a-b	Brick	lime	5208 756	1743 253	10.13 1470	34.2	47.6
4a-b	Block	N	12429 1804	1033 152	22.90 3321	17.7	92.0
5a-b	Block	N	11616 1686	4306 625	22.82 3313	11.4	143.0
6a-b	Brick	lime	2136 310	861 125	4.60 665	16.6	98.4

Tab. 5.6. Geometrical and mechanical features of the infills selected for validation.

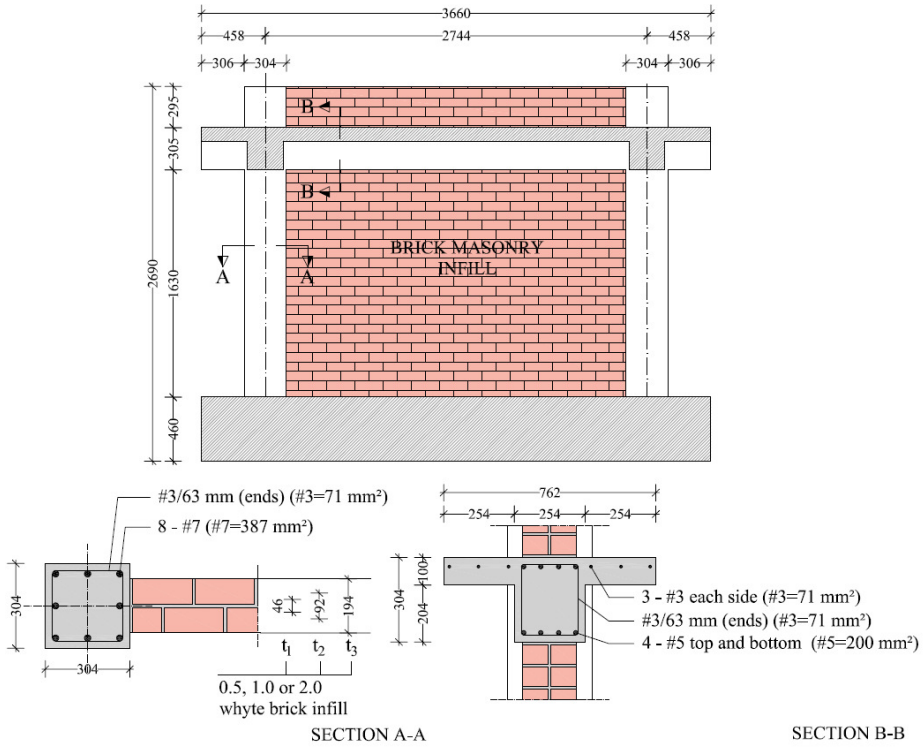

Fig. 5.19. Detail of the brick masonry infilled frame specimens (Angel *et al.* (1994)).

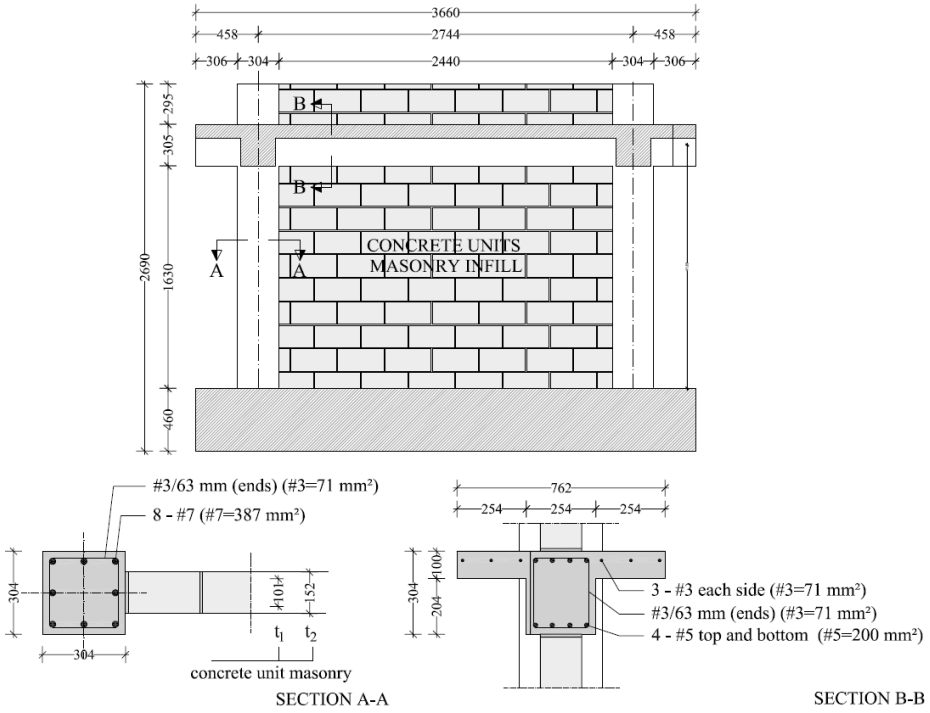

Fig. 5.20. Detail of the concrete unit masonry infilled frame specimens (Angel *et al.* (1994)).

Reinforced concrete frame	
Lateral Strength (kN)	302.4
Concrete Compressive Strength (MPa)	55.12
Axial Force on columns (kN)	222.4
Column Area (mm^2)	92903
Column Moment of Inertia (cm^4)	71924.8
Column reinforcement ratio (%)	3.33
Beam Area (mm^2)	129032
Beam Moment of Inertia (cm^4)	96315.9

Tab. 5.7. Geometrical and mechanical features of the RC frames.

According to the procedure exposed in the previous sections, the identification of equivalent strut IP-OOP model provides first the definition of the fictitious constitutive law (parameters f_{md0}, f_{mdu}, ε_{co}, ε_{cu}) for the diagonals in order to match the IP behavior that is predicted by the

construction simplified IP curve. However since in this case the experimental data of the in plane cyclic test of each specimen (phase a) were available, the calibration of the constitutive law has been carried out more properly by the comparison of the in plane pushover of the model with the 2 backbone curves (positive and negative loading) of each cyclic test. The results of the IP pushover curves after the calibration are reported in **Fig. 5.21** where are also represented the backbone curves of the cyclic tests.

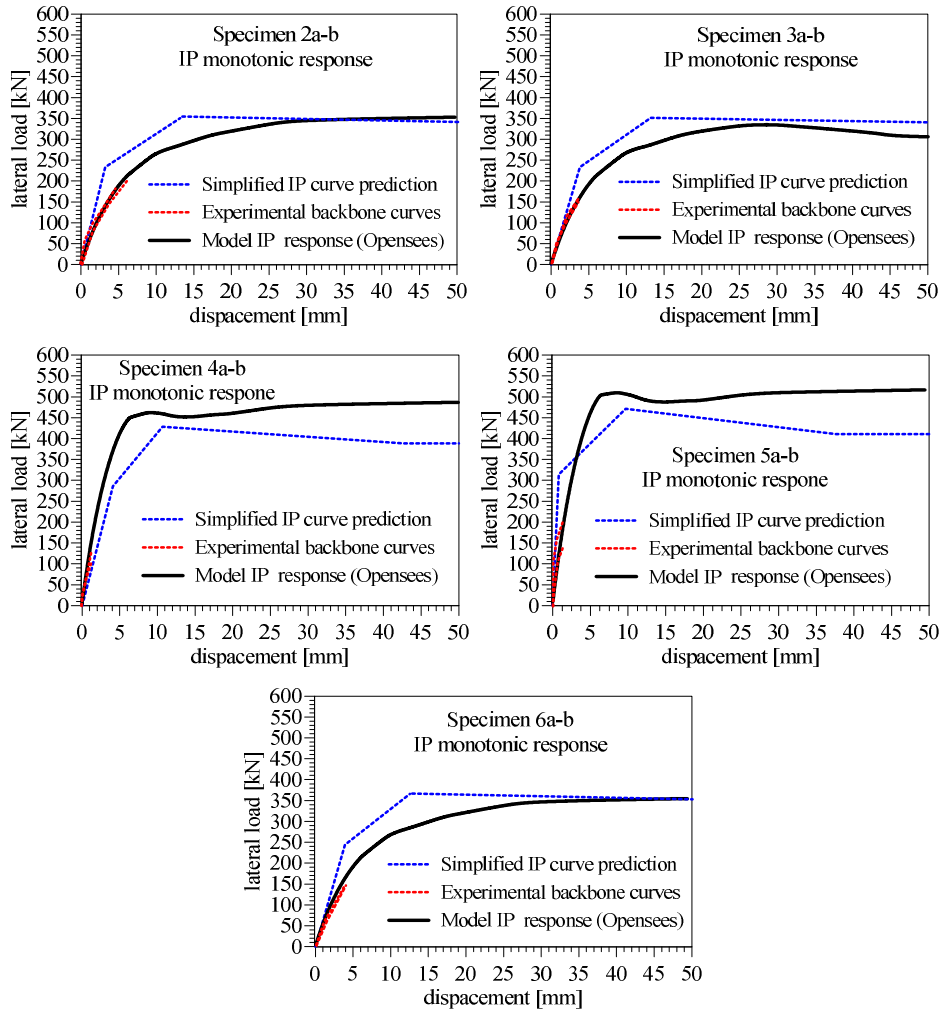

Fig. 5.21. Calibration of the IP response of the model.

However since the in plane cyclic tests were carried out on a limited force-displacement excursion, a necessary comparison with the overall IP

behavior, predicted by means of the simplified IP curves (estimating the complete force displacements curves of the infilled frames according to the procedure presented in §5.1) has been also provided in the diagrams. The latter also show a good agreement of the experimentally calibrated IP response with the simplified force displacement curve.

The cross section dimensions of the diagonal struts (initially w_d and t) were subsequently converted in $\tilde{w}_d$ and $\tilde{t}$ to account also for OOP behavior by means of Eq. 5.32. The horizontal and vertical strut widths were finally determined by Eq. 5.33. For the different specimens the final geometrical and mechanical features of the struts are reported in Tabs. 5.8-5.10.

The models were subjected to the same loading condition (phase *a* and *b*) originally applied to the actual specimens. The IP loading pattern of displacement followed the scheme reported in **Fig. 5.22** that is normalized with respect to the cracking displacement Δ_{cr} (deflection at which initial cracking of infill occurs). In **Figs. 5.23-5.27** the displacement history pattern, specialized for each specimens, and the associated responses are reported.

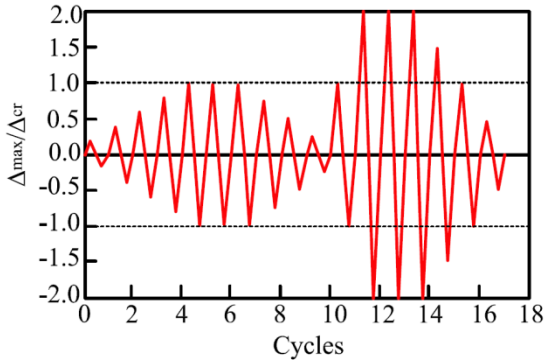

Fig. 5.22. In plane normalized displacement pattern.

Once the in plane loading finished, the phase *b* is started. The midspan node is pushed in out-of-plane direction by means of a concentrated load. Since the two phases are run in the same analysis, in the phase *b* the diagonals account for the in plane damage previously accumulated in the phase *a*. The response of the models during the phase (*b*) is reported in **Figs. 5.28-5.32** in terms of OOP force, OOP displacement of the midspan node and is compared with the experimental one. To be comparable with

the model response force-displacement format, the original experimental diagram, provided in pressure-displacement format, is converted multiplying pressures for the infill area.

In Figs. 5.23-5.27 the individual force displacement diagram of the diagonal struts and the horizontal and vertical strut is also reported in order to appreciate the different contribution in the overall response.

Diagonal struts											
Spec.	a (mm)	$w_d=a/3$ (mm)	ℓ (mm)	h (mm)	t (mm)	$\tilde{w}_d$ (mm)	$\tilde{t}$ (mm)	f_{md0} (Mpa)	f_{mdu} (Mpa)	ε_{co}	ε_{cu}
2a-b	2934.4	978.1	2440	1630	47.60	202.84	229.54	2.25	1.35	0.0015	0.008
3a-b	2934.4	978.1	2440	1630	47.60	217.25	214.31	2.25	1.35	0.0015	0.008
4a-b	2934.4	978.1	2440	1630	92.00	192.21	468.18	4.50	2.70	0.0010	0.008
5a-b	2934.4	978.1	2440	1630	143.00	145.73	959.78	3.40	2.04	0.0010	0.008
6a-b	2934.4	978.1	2440	1630	98.40	239.21	402.35	1.13	0.68	0.0015	0.008

Tab. 5.8. Geometrical and mechanical features of the RC frames.

Vertical strut								
Spec.	w_v (mm)	ℓ (mm)	h (mm)	t (mm)	f_{m0} (Mpa)	f_{mu} (Mpa)	ε_{co}	ε_{cu}
2a-b	679.2	2440.0	1630.0	47.6	10.85	6.51	0.0015	0.008
3a-b	679.2	2440.0	1630.0	47.6	10.13	6.08	0.0015	0.008
4a-b	679.2	2440.0	1630.0	92.0	22.90	13.74	0.0015	0.008
5a-b	679.2	2440.0	1630.0	143.0	22.82	13.69	0.0015	0.008
6a-b	679.2	2440.0	1630.0	98.4	4.60	2.76	0.0015	0.008

Tab. 5.9. Geometrical and mechanical features of the RC frames.

Horizontal strut								
Spec.	w_h (mm)	ℓ (mm)	h (mm)	t (mm)	f_{m0} (Mpa)	f_{mu} (Mpa)	ε_{co}	ε_{cu}
2a-b	453.70	2440.0	1630.0	47.6	10.85	6.51	0.0015	0.008
3a-b	453.70	2440.0	1630.0	47.6	10.13	6.08	0.0015	0.008
4a-b	453.70	2440.0	1630.0	92.0	22.90	13.74	0.0015	0.008
5a-b	453.70	2440.0	1630.0	143.0	22.82	13.69	0.0015	0.008
6a-b	453.70	2440.0	1630.0	98.4	4.60	2.76	0.0015	0.008

Tab. 5.10. Geometrical and mechanical features of the RC frames.

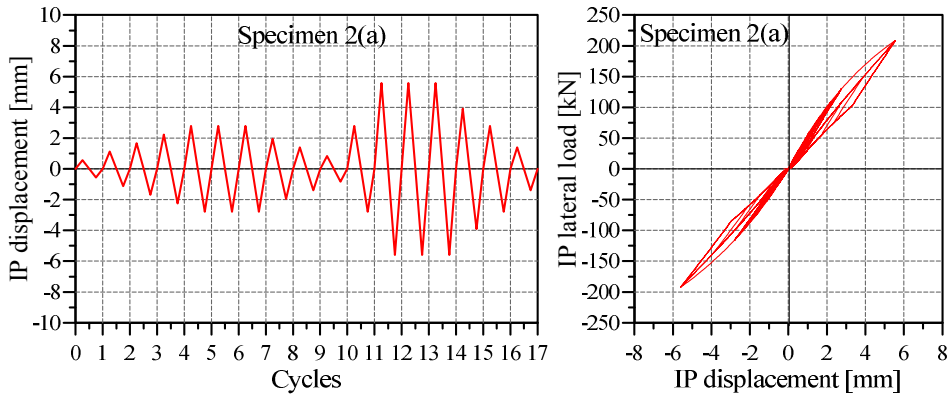

Fig. 5.23. Phase (a). In plane damaging for specimen 2(a): *a)* IP displacement pattern; *b)* IP response of the model.

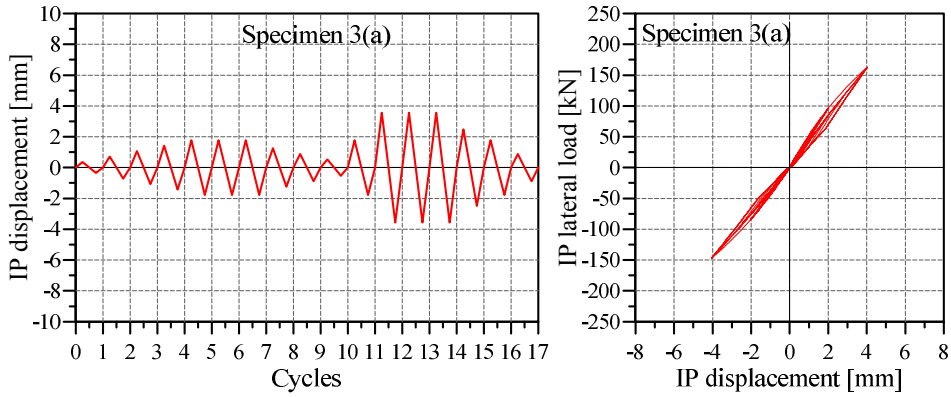

Fig. 5.24. Phase (a). In plane damaging for specimen 3(a): *a)* IP displacement pattern; *b)* IP response of the model.

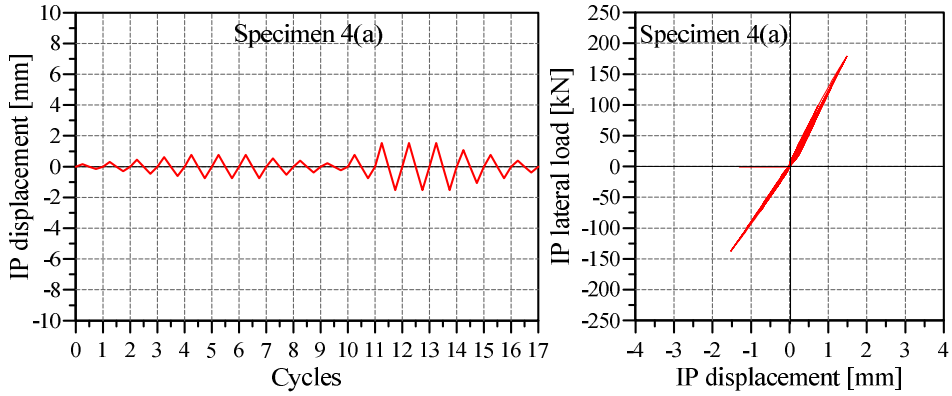

Fig. 5.25. Phase (a). In plane damaging for specimen 4(a): *a)* IP displacement pattern; *b)* IP response of the model.

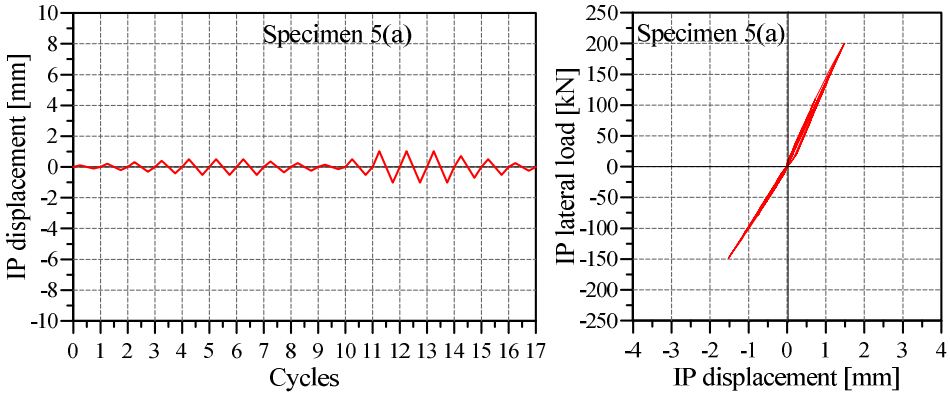

Fig. 5.26. Phase (a). In plane damaging for specimen 5(a): *a)* IP displacement pattern; *b)* IP response of the model.

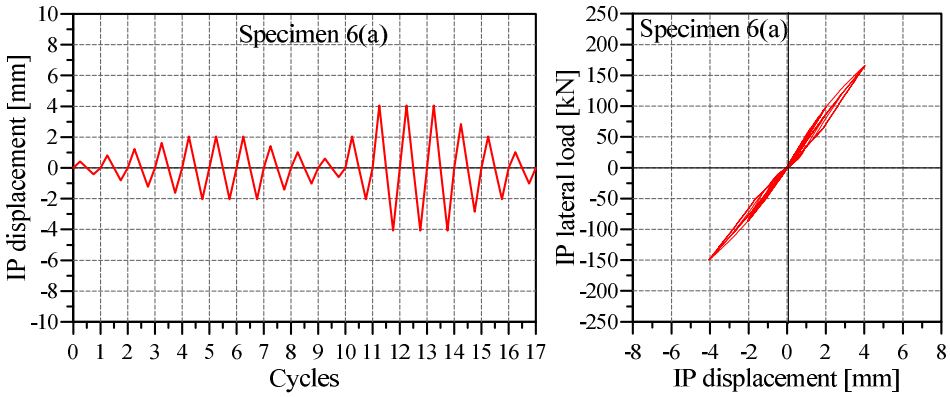

Fig. 5.27. Phase (a). In plane damaging for specimen 6(a): *a)* IP displacement pattern; *b)* IP response of the model.

It appears evident the dominant role exerted by the diagonals also in OOP response especially in terms of strength and stiffness. This fact respects the expectations originally stated for the model to be sensitive to IP damaging in OOP response. If the diagonals are in fact the only struts damaged during IP loading, and provide also the main contribution to the OOP response, they grant that they effectively are able to transfer the IP damage effects in the overall OOP response.

However, since their cross section is fictitiously increased according to the identification procedure, their ductility is lower than the one provided by the horizontal and vertical struts. The latter are in fact less strong and less stiffen but show a noticeable ductile behavior which balances the post peak loss of strength affecting the diagonals.

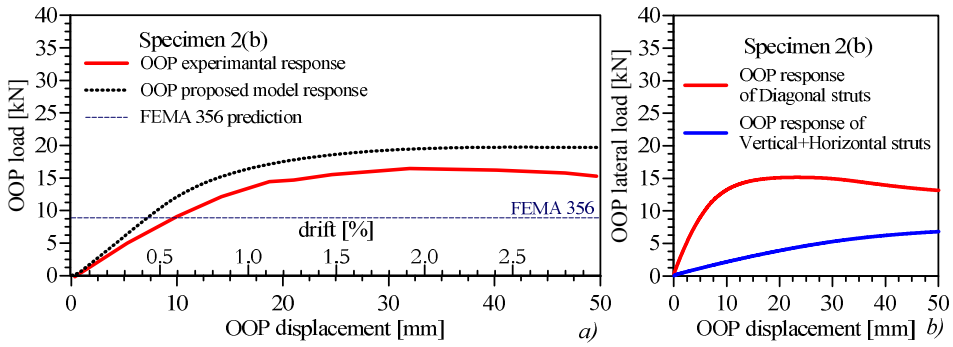

Fig. 5.28. Phase (b), Specimen 2(b): *a)* OOP experimental/proposed model comparison; *b)* Model OOP response of diagonal and vertical struts.

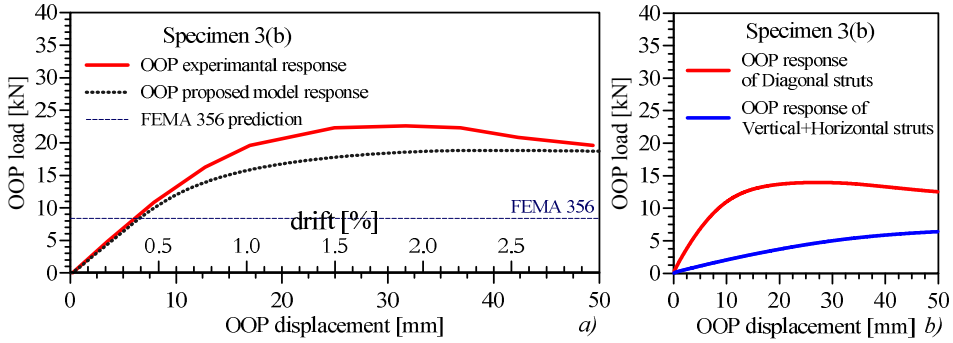

Fig. 5.29. Phase (b), Specimen 3(b): *a)* OOP experimental/proposed model comparison; *b)* Model OOP response of diagonal and vertical struts.

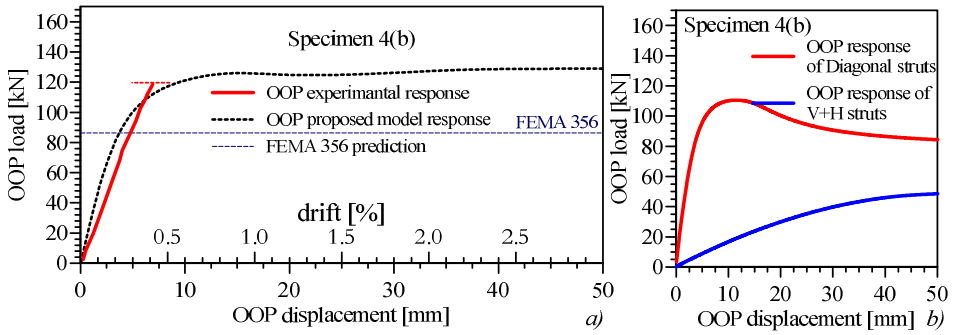

Fig. 5.30. Phase (b), Specimen 6(b): *a)* OOP experimental/proposed model comparison; *b)* Model OOP response of diagonal and vertical struts.

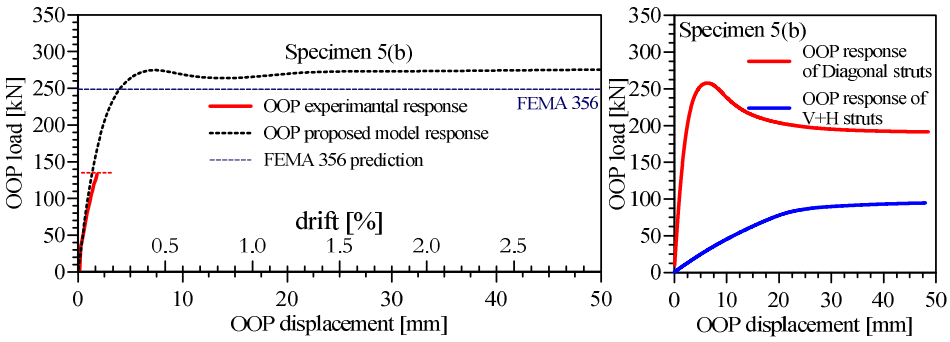

Fig. 5.31. Phase (b), Specimen 5(b): *a)* OOP experimental/proposed model comparison; *b)* Model OOP response of diagonal and vertical struts.

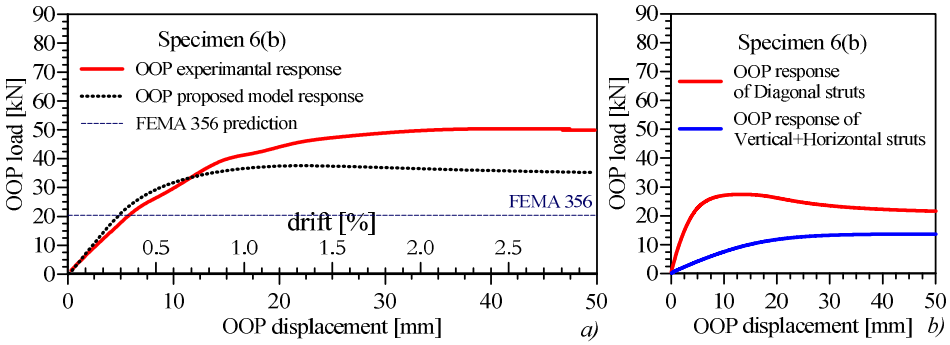

Fig. 5.32. Phase (b), Specimen 6(b): *a)* OOP experimental/proposed model comparison; *b)* Model OOP response of diagonal and vertical struts.

The comparison between the proposed model and the OOP experimental response of the tested specimens showed a good predictive capability to estimate the OOP behavior accounting also in plane damaging.

Especially the prediction of the initial stiffness was particularly accurate, suggesting the suitability of the model to be used to for dynamic applications.

Except from the cases in which the experimental tests were stopped for reaching of the maximum load capacity of the instrumentation, the model also showed a good reliability in prediction of maximum OOP load. The prediction error, in the order of 15-20%, is however acceptable if one considers the simplicity of the model as first. Moreover it should be also noticed that only one specimen for each typology of infill was available for comparisons therefore it was not possible to define an average experimental curve. The magnitude of the predictive error for OOP maximum load was

however lower than the experimental dispersion generally expected by masonry specimens.

In Figs. 5.28-5.32 the OOP maximum load capacity, predictable by FEMA 356 (Eq. 5.12), is also reported as reference value. It appears evident that the expression proposed by FEMA 356 provides a more conservative estimation with respect to experimental results and model prediction. However FEMA 356 prediction of maximum OOP load seems to be much more conservative (-50%) for infills presenting an high slenderness ratio while in the case of thick infills the underestimation is in the order of (10-25%).

The post peak behavior exhibited by the specimens is ductile in general. This is due to the 2 way arching action that allows significant stress redistributions. Also this aspect is well captured by the model thanks to the contribution offered by the horizontal and vertical struts. As before mentioned the latter compensates the post peak loss of strength of the diagonals guarantying an overall ductile behavior.

5.3.5 Conclusions on the IP-OOP interacting macromodel.

A simplified macro-model for the assessment of both in plane – out of plane behaviour of the infilled frame was developed and validated. The model provides the use of distributed plasticity fiber elements with a proper calibration of the constitutive law of the equivalents struts.

For the assessment of the response to in plane action only the model can be defined by using two diagonal struts resisting only to compression while the combined IP-OOP interaction provided the introduction of two further struts properly defined. In this case the adaption of the diagonal cross section dimensions is necessary in order to account for both IP and OOP response by means of a procedure here developed.

The calibration of the constitutive law for the diagonals has been based on the technique proposed by Shing and Stavridis (2014) which starts from the definition of a simplified in plane monotonic curve for the infilled frame. The latter, originally calibrated for strong infills, have been updated to account also the behaviour of RC frame with weak infills.

The validation of the in-plane (monotonic and cyclic) predictive capacity of the model have been carried out by means of a comparison with the

results of the experimental campaign presented in §.2 for different kinds of masonry infilled frames. The model has shown a good accuracy in reproduction of both monotonic and cyclic behavior with a simple definition of the cross section width and of the parameters defining the constitutive law of the diagonals.

The extension for the accounting of interacting IP-OOP behaviour was performed adding to the model a horizontal and a vertical strut and providing a redefinition of the cross section dimensions for the diagonals.

Also in this case the validation was performed by means of a comparison with results of experimental tests (Angel et al. (1994)). The latter, performed on specimens of infilled frames arranged with different kinds of masonries and different thickness, provided an initial in plane damaging by means of the application of a prescribed displacement history. In a second phase the infills were pushed out applying a transversal pressure with and airbag.

The model proved also in this case a good accuracy in simulating the OOP response being sensitive to the in plane damage previously assigned, thanks to the capability offered by distributed plasticity fiber elements to simulate the arching action that actually occurs.

A test of reliability of the progressive loss of OOP capacity of the model due to cyclic IP actions of increasing magnitude was also performed. The model showed a noticeable capacity to strongly reflect the IP damaging effect in the OOP capacity.

Despite its simplicity the model has proved to be sufficiently accurate in the prediction of a complex behavior. Moreover it takes the advantage to be light from a computational point of view and flexible in its application to more complex nonlinear static and dynamic analyses. An example of the Opensees code used for the generation of IP-OOP model is reported in Appendix A.

CONCLUSIONS

In this work the issue of the interaction between masonry infill and RC frame is dealt with from an experimental and numerical point of view.

The aim was to fill some lacks belonging to the macromodeling approaches which produce a loss of information when performing the analyses. In this sense some new techniques updating the classical macromodel approach in order to extend its flexibility are developed and proposed maintaining its advantages.

As base reference a large experimental campaign has been carried out and presented in Chapter 2.

The experimental investigation dealt with the cyclic behaviour of RC frames specimens infilled with different kinds of masonry among the most employed in the worldwide building traditions (calcarenite masonry, clay hollow masonry, lightweight concrete unit masonry).

The experimental campaign has shown a large interaction between infills and RC fames that radically modifies the structural response.

In terms of maximum average lateral strength an increment of strength from 2 to 4 times with respect to bare frames was recognized in the experiments accompanied by a low strength degrading after peak reaching that was the consequence of an efficient confinement effect exercised by the frames on the infill panels.

Regarding to stiffening effects, it was recognized a substantial dependence on the stiffness ratio between infill and frame varying from 2 to 10 time with respect to bare frames.

For the tested specimens the cracking propagation affected initially both frames and infills with diagonal cracks on frames at the upper joints and corresponding diagonal cracks mainly following mortar joints of infills. Clay and lightweight concrete masonry infills were affected by partial crushing of corner units along the two diagonal directions while more diffused cracking patterns were recognized on calcarenite masonry infills. This observation suggested that the collapse mechanism may be quite different when changing ratios between strength and stiffness of infill and frame. Cyclic experimental curves showed for all tested specimens a significant pinching effect at load reversal, justified by the fact that the entire plastic excursion, previously accumulated, had to be recovered to regain stiffness and bearing capacity. By enveloping the cycles of the responses a global ductile behaviour could be observed, though the collapse of the whole system was governed by failures of RC column mechanisms not clearly recognizable as ductile.

The results of the experiments allowed developing a predictive strategy for the assessment of cyclic response of infilled frames systems in structural analysis bases on a macromodel approach. The model was based on a hysteretic "pivot" law needing few mechanical parameters for the identification and based on geometric rules rather than analytical. The study has shown that despite the simplicity of the model, it was able to provide an adequate accuracy to represent the cyclic hysteretic response of infilled frames. The modelling of cyclic behaviour was radically simplified; being this governed by only one parameter (α_2). Also the computational effort was strongly reduced. The optimal values of the α_2 parameter were also calibrated for the investigated typologies of masonry infills.

Experimental/numerical comparisons of the responses showed a good reliability in the prediction effectiveness of the pivot model. Limited differences of strength and stiffness with respect to the experimental tests were recorded; further, dissipation energy comparisons revealed good matching with very low errors. The application of the model resulted particularly suitable when an assessment of the global response in terms of displacements, ductility and energy dissipation is necessary and nonlinear time history analyses have to be performed.

A further study provided in this research work, regarded the assessment of the local shear effects produced at the ends of beams and columns of RC infilled frames in the presence of lateral loads when macromodels are used. Infill panels are in fact able to attract a large portion of the lateral actions during earthquakes that can be however supported by the frame members if the latter have an adequate transversal reinforcing. The equivalent strut approach is unable to provide information about the additional shear demand arising on beams and column ends, therefore the study was addressed to fill this predictive lack.

In the study, a strategy for the prediction of the actual shear demand in RC member ends is provided. A comparison has been carried out between the force arising in the frame members in the case of an infill modelled as an equivalent concentric strut and in the case of an infill "exactly" modelled by finite shell elements, at different drift levels, for a single infilled frame. The comparison was repeated in a parametric study varying the geometrical and mechanical characteristics of the frame-infill system and a correlation law between a parameter synthesizing the characteristics of frame and infill and the actual shear distribution in the critical sections was derived. The latter allows one to express the local shear forces acting on beam and column ends as a fraction of the axial load experienced by the equivalent strut and for this reason it can be considered a basis for a predictive tool to be used for the assessment of shear demand on RC member critical sections that is otherwise undetectable by simple macromodels. The predictive capacity of the correlation proposed was finally tested on two numerical case studies having two different aspect ratios. A good accuracy is vivificated for all investigated drifts. A further comparison was made with the shear demand assessment proposed by FEMA 356 code, confirming on one hand the reliability of the approach proposed and on the other one the possibility of an overestimation of the FEMA approach for lower drifts than those for which the equivalent strut is affected by force equal to its resistance.

The last study presented in this thesis regarded the calibration of a simplified macro-model for the assessment of both in plane – out of plane behaviour of the infilled frame which was here developed and validated.

The model provided the use of distributed plasticity fiber elements with a proper calibration of the constitutive law of the equivalents struts.

If in plane prediction is only needed the model can be simply configured with 2 diagonal truss elements properly calibrated. If instead the combined IP-OOP interaction should be assessed, the introduction of two further struts, 1 horizontal, one vertical is necessary. In this case an adaption of the diagonal cross section dimensions is provided in order to account for both IP and OOP response.

The validation of the in-plane (monotonic and cyclic) predictive capacity of the model has been performed by means of a comparison with the results of the experimental campaign presented in §.2. The model has shown a good accuracy in reproduction of both monotonic and cyclic behavior with an easy definition of the cross section width and of the parameters defining the constitutive law of the diagonals.

The extension for the accounting of interacting IP-OOP was also experimentally validated by means of a comparison with results of experimental tests by Angel et al. (1994). The latter, performed on specimens of infilled frames arranged with different kinds of masonries and different thickness, provided an initial in plane damaging by means of the application of a prescribed displacement history. In a second phase the infills were pushed out applying a transversal pressure with and airbag.

The model proved also in this case a good accuracy in simulating the OOP response being sensitive to the in plane damage previously assigned, thanks to the capability offered by distributed plasticity fiber elements to simulate the arching action that actually occurs.

Despite its simplicity the model has demonstrated to be sufficiently reliable in the prediction of this complex interacting behavior. Moreover it takes the advantage to be light from a computational point of view and flexible in its application to more complex cases and when nonlinear static and dynamic analyses are needed to perform.

APPENDIX A

Opensees code for the IP-OOP model generation

An example of the Opensees code provided for the definition of the IP-OOP model is here reported. The code is referred to Specimen 3(a-b) as sample.

```
# Create ModelBuilder (with two-dimensions and 3 DOF/node)
wipe

model basic -ndm 3 -ndf 6

# Create nodes
# ------------

# Set parameters for overall model geometry
set width    2740.0
set height   1930.0

# Create nodes
#    tag        X       Y   Z
node  1     0.0     0.0   0.0
node  2    $width     0.0   0.0
node  3    0.0 $height   0.0
node  4    $width $height   0.0
node  61   [expr  $width/2] [expr $height/2] 0.0
node  62   [expr  $width/2] [expr $height/2] 0.0
node  63   [expr  $width/2] [expr $height/2] 0.0
node  64   [expr  $width/2] [expr $height/2] 0.0
node  5    [expr  $width/2] 0.0 0.0
node  7    [expr  $width/2] 0.0 0.0
node  8    [expr  $width/2] $height 0.0
node  9    [expr  $width/2] $height 0.0
node  12   0.0 [expr $height/2] 0.0
node  13   0.0 [expr $height/2] 0.0
node  14   [expr  $width] [expr $height/2] 0.0
node  15   [expr  $width] [expr $height/2] 0.0
node  33   0.0 $height   0.0
node  44   $width $height   0.0

# Fixupports at base of columns
#    tag   DX   DY  DZ   RX RY RZ
fix   1     1    1   1   1   1  0
fix   2     1    1   1   1   1  0
fix   3     0    0   0   1   1  0
fix   4     0    0   0   1   1  0
fix   5     0    1   0   1   1  0
fix   9     0    0   0   1   1  0

equalDOF 63 62   3
equalDOF 63 61   3
equalDOF 63 64   3

# Define materials for nonlinear RC elements
# -------------------------------------------
# CONCRETE (confined)

                            Tag   fpc   epsc0   fpcu    epscu  lambda  ft     Et
uniaxialMaterial Concrete02   1   -55.2 -0.002  -38.7  -0.01    0.10   0.00   0.00
# Cover concrete (unconfined)
uniaxialMaterial Concrete02  2    -55.  -0.002  -23.28 -0.008   0.10   0.00  0.0
```

```
# STEEL
# Reinforcing steel
set fy 400.0;      # Yield stress
set E 210000.0;    # Young's modulus

#                         tag   fy  E0    b       R0   cR1   CR1
uniaxialMaterial Steel02  3   $fy  $E  0.005     15  0.925  0.15


# Masonry                  Tag    fpc    epsc0     fpcu    epscu   lambda  ft    Et
# (DIAGONALS)
uniaxialMaterial Concrete02  4    -2.25 -0.0015    -1.35  -0.0080   0.07  0.0   0.0
# (Horizontal and Vertical)
uniaxialMaterial Concrete02  5   -10.13 -0.0015    -6.08  -0.008    0.1   0.0   0.0

# Define cross-sections
# ------------------------------------------
#
# set some paramaters for COLUMNS sections
set colWidth 304.0
set colDepth 304.0

set cover  35.0
set As    387.0;     # area of 1 bar

set y1 [expr $colDepth/2.0]
set z1 [expr $colWidth/2.0]

section Fiber 1 {

    # Create the concrete core fibers
patch rect 1 30 30 [expr $cover-$y1] [expr $cover-$z1] [expr $y1-$cover][expr $z1-
$cover]

    # Create the concrete cover fibers (top, bottom, left, right)
patch rect 2 20 20  [expr -$y1] [expr $z1-$cover] $y1 $z1
patch rect 2 20 20  [expr -$y1] [expr -$z1] $y1 [expr $cover-$z1]
patch rect 2 20 20   [expr -$y1] [expr $cover-$z1] [expr $cover-$y1] [expr $z1-
$cover]
patch rect 2 20 20  [expr $y1-$cover] [expr $cover-$z1] $y1 [expr $z1-$cover]

    # Create the reinforcing fibers (left, middle, right)
layer straight 3 3 $As [expr -$y1+$cover] [expr $z1-$cover] [expr $y1-$cover] [expr
$z1-$cover]
layer straight 3 2 $As [expr -$y1+$cover] 0.0 [expr $y1-$cover] 0.0
layer straight 3 3 $As [expr -$y1+$cover] [expr -$z1+$cover] [expr $y1-$cover] [expr
-$z1+$cover]
}
#SHEAR AND TORSION FOR 3D ANALYSIS
set Gc 25000000
set C250 10
#_________________________
# column torsional stiffness
# Linear elastic torsion for the column

set GJcol [expr $Gc*$C250*$colDepth*pow($colWidth,3)]
set GAcol [expr $Gc*$colWidth*$colDepth*5/6]

uniaxialMaterial Elastic 50 $GJcol
uniaxialMaterial Elastic 51 $GAcol

# Attach torsion to the RC beam section
#                tag uniTag uniCode secTag
#section Aggregator $secTag $matTag1 $string1 $matTag2 $string2 ....... <-section
$sectionTag>
section Aggregator     10    51 Vy      51 Vz    50 T      -section 1


# set some paramaters for EQUIVALENT DIAGONAL STRUT section
set strWidth 217.25
set strDepth 214.31
set coverstr 10.0
```

```
set Asp   1.0;     # area of 1 bar
# some variables derived from the parameters
set ys1 [expr $strDepth/2.0]
set zs1 [expr $strWidth/2.0]

section Fiber 3 {

    # Create the concrete core fibers
    patch rect 4 30 30 -$ys1 -$zs1 $ys1 $zs1

# Create the reinforcing fibers (left, middle, right)
layer straight 3 2 $Asp [expr -$ys1+$coverstr] [expr $zs1-$coverstr] [expr $ys1-
$coverstr] [expr $zs1-$coverstr]
layer straight 3 2 $Asp [expr -$ys1+$coverstr] 0.0 [expr $ys1-$coverstr] 0.0
layer straight 3 2 $Asp [expr -$ys1+$coverstr] [expr -$zs1+$coverstr] [expr $ys1-
$coverstr] [expr -$zs1+$coverstr]
}
# EQSTRUT torsional stiffness
# Linear elastic torsion for the column

set GJstr [expr $Gc*$C250*$strDepth*pow($strWidth,3)]
set GAstr [expr $Gc*$strWidth*$strDepth*5/6]

uniaxialMaterial Elastic 60 $GJstr
uniaxialMaterial Elastic 61 $GAstr

# Attach torsion to the RC beam section
#                tag uniTag uniCode secTag
#section Aggregator $secTag $matTag1 $string1 $matTag2 $string2 ....... <-section
$sectionTag>
section Aggregator     30    61 Vy      61 Vz    60 T      -section 3

# set some paramaters for EQUIVALENT VERTICAL STRUT section
set vWidth 680.0
set vDepth 47.6
set coverv 10.0

set Asv    1.0;     # area of 1 bar
# some variables derived from the parameters
set yv [expr $vDepth/2.0]
set zv [expr $vWidth/2.0]

section Fiber 5 {

# Create the concrete core fibers
patch rect 5 30 30 -$yv -$zv $yv $zv

# Create the reinforcing fibers (left, middle, right)
layer straight 3 3 $Asv [expr -$yv+$coverv] [expr $zv-$coverv] [expr $yv-$coverv]
[expr $zv-$coverv]
layer straight 3 2 $Asv [expr -$yv+$coverv] 0.0 [expr $yv-$coverv] 0.0
layer straight 3 3 $Asv [expr -$yv+$coverv] [expr -$zv+$coverv] [expr $yv-$coverv]
[expr -$zv+$coverv]
 }
# EQSTRUT torsional stiffness
# Linear elastic torsion for the column

 set GJv [expr $Gc*$C250*$vDepth*pow($vWidth,3)]
 set GAv [expr $Gc*$vWidth*$vDepth*5/6]

 uniaxialMaterial Elastic 70 $GJv
 uniaxialMaterial Elastic 71 $GAv

# Attach torsion to the RC beam section
#                tag uniTag uniCode secTag
#  section Aggregator $secTag $matTag1 $string1 $matTag2 $string2 ....... <-section
$sectionTag>
 section Aggregator     50    71 Vy      71 Vz    70 T      -section 5


# set some paramaters for EQUIVALENT HORIZONTAL STRUT section
set hWidth 454.0
```

```
set hDepth 47.6
set coverstrh 10.0

set Ash    1.0;     # area of 1 bar
# some variables derived from the parameters
set yh [expr $hDepth/2.0]
set zh [expr $hWidth/2.0]

section Fiber 8 {

# Create the concrete core fibers
patch rect 5 30 30 -$yh -$zh $yh $zh

Create the reinforcing fibers (left, middle, right)
layer straight 3 3 $Ash [expr -$yh+$coverstrh] [expr $zh-$coverstrh] [expr $yh-
$coverstrh] [expr $zh-$coverstrh]
layer straight 3 2 $Ash [expr -$yh+$coverstrh] 0.0 [expr $yh-$coverstrh] 0.0
layer straight 3 3 $Ash [expr -$yh+$coverstrh] [expr -$zh+$coverstrh] [expr $yh-
$coverstrh] [expr -$zh+$coverstrh]
 }
# EQSTRUT torsional stiffness
# Linear elastic torsion for the column

set GJh [expr $Gc*$C250*$hDepth*pow($hWidth,3)]
set GAh [expr $Gc*$hWidth*$hDepth*5/6]

uniaxialMaterial Elastic 80 $GJh
uniaxialMaterial Elastic 81 $GAh

# Attach torsion to the RC beam section(QUESTO COMANDO ATTACCA TAGLIO E TORSIONE
ALLE SEZIONI DELLE TRAVI)
#                 tag uniTag uniCode secTag
# section Aggregator $secTag $matTag1 $string1 $matTag2 $string2 ..... <-section
$sectionTag>
 section Aggregator     80    81 Vy      81 Vz    80 T      -section 8

# ###############################################
# set some paramaters for BEAM sections
set beaWidth 304.0
set beaDepth 254.0

set cover  30.0
set Ast    200.0;     # area of 1 bar

# some variables derived from the parameters
set yb1 [expr $beaDepth/2.0]
set zb1 [expr $beaWidth/2.0]

section Fiber 4 {

# Create the concrete core fibers
patch rect 1 40 40 [expr $cover-$yb1] [expr $cover-$zb1] [expr $yb1-$cover] [expr
$zb1-$cover]

# Create the concrete cover fibers (top, bottom, left, right)
patch rect 2 20 10  [expr -$yb1] [expr $zb1-$cover] $yb1 $zb1
patch rect 2 20 10  [expr -$yb1] [expr -$zb1] $yb1 [expr $cover-$zb1]
patch rect 2 20 10   [expr -$yb1] [expr $cover-$zb1] [expr $cover-$yb1] [expr $zb1-
$cover]
patch rect 2 20 10  [expr $yb1-$cover] [expr $cover-$zb1] $yb1 [expr $zb1-$cover]

# Create the reinforcing fibers (left, middle, right)
layer straight 3 4 $Ast [expr -$yb1+$cover] [expr $zb1-$cover] [expr $yb1-$cover]
[expr $zb1-$cover]
layer straight 3 4 $Ast [expr -$yb1+$cover] [expr -$zb1+$cover] [expr $yb1-$cover]
[expr -$zb1+$cover]
}
#_____________________________________
# BEAM torsional stiffness
# Linear elastic torsion for the equivalent strut

set GJbea [expr $Gc*$C250*$beaDepth*pow($beaWidth,3)]
```

```
set GAbea [expr $Gc*$beaWidth*$beaDepth*5/6]

uniaxialMaterial Elastic 54 $GJbea
uniaxialMaterial Elastic 55 $GAbea

# Attach torsion to the RC beam section
#                 tag uniTag uniCode secTag
#section  Aggregator  $secTag  $matTag1  $string1  $matTag2  $string2  ....... <-section
$sectionTag>
section Aggregator     40    55 Vy      55 Vz    54 T      -section 4

#COLUMNS#
# Geometry of column elements
#               tag

geomTransf Linear 1  -1 0 0

# Number of integration points along length of element
set np 5
set nps 10
# Create the columns using Beam-column elements
#               e             tag ndI ndJ nsecs secID transfTag
set eleType forceBeamColumn
element $eleType                          1    1   12   $np    10      1
element $eleType                          101  12   3   $np    10      1
element $eleType                          2    2   15   $np    10      1
element $eleType                          202  15   4   $np    10      1
#
################################################################################
#########
#BEAMS#
# Define beam element
# -----------------------------

# Geometry of beam elements
#                tag
geomTransf Linear 2  0 1 0

set tranfeloriz 2
set tranfelvert 1
# Create the NONLINEAR BEAM  using Beam-column elements
#               e              tag ndI ndJ nsecs secID transfTag
set eleType2 dispBeamColumn
# TRAVI
element $eleType         3    3   9   $np    40   $tranfeloriz
element $eleType         4    9   4   $np    40   $tranfeloriz
element $eleType         11   1   5   $np    40   $tranfeloriz
element $eleType         12   5   2   $np    40   $tranfeloriz
#VERTICAL
element $eleType2        9    7   63  $nps   50  $tranfelvert
element $eleType2        10   63  8   $nps   50  $tranfelvert
#HORIZONTAL
element $eleType2        13   13  64  $nps   80  $tranfeloriz
element $eleType2        14   64  14  $nps   80  $tranfeloriz

#DIAGONAL
element $eleType2        5    33  61  $nps  30   $tranfeloriz
element $eleType2        6    61  2   $nps  30   $tranfeloriz
element $eleType2        7    1   62  $nps  30   $tranfeloriz
element $eleType2        8    62  44  $nps  30  $tranfeloriz

#element zeroLength $eleID $Node1ID $Node2ID -mat $matID $matID -dir 1 2
#uniaxialMaterial Elastic $matTag $E

uniaxialMaterial Elastic 20 500000000;
uniaxialMaterial Elastic 10 100;
uniaxialMaterial Elastic 15 100;
uniaxialMaterial ENT 91 50000000;
```

```
#VERTICAL
 element zeroLength 90 5 7 -mat 20 20 20 15 10 10 -dir 1 2 3 4 5 6  -orient 0 1 0 -1
0 0
 element zeroLength 91 8 9 -mat 20 20 20 15 10 10 -dir  1 2 3 4 5 6  -orient 0 1 0 -
1 0 0
#HORIZONTAL
 element zeroLength 88 12 13 -mat 20 20 20 15 10 10 -dir 1 2 3 4 5 6 -orient 1 0 0 0
1 0
 element zeroLength 89 14 15 -mat 20 20 20 15 10 10 -dir  1 2 3 4 5 6  -orient 1 0 0
0 1 0
#DIAGONAL
element zeroLength 93 44 4 -mat 91 20 20 15 10 10 -dir  1 2 3 4 5 6 -orient 1 1 0 -1
1 0
element zeroLength 94 3 33 -mat 91 20 20 15 10 10 -dir 1 2 3 4 5 6 -orient 1 -1 0 1
1 0

# Define gravity loads
# --------------------

# Set a parameter for the axial load
set P 222400.0;               # 10% of axial capacity of columns

# Create a Plain load pattern with a Linear TimeSeries
pattern Plain 1 "Linear" {

        # Create nodal loads at nodes 3 & 4
        #    nd    FX          FY  FZ      MX   MY    MZ
        load  3   0.0   [expr -$P]   0.0   0.0  0.0   0.0
        load  4   0.0   [expr -$P]   0.0   0.0  0.0   0.0

# ------------------------------
# End of model generation
# ------------------------------

# ------------------------------
# Start of analysis generation
# ------------------------------

# Create the system of equation, a sparse solver with partial pivoting
system BandGeneral

# Create the constraint handler, the transformation method
constraints Transformation

# Create the DOF numberer, the reverse Cuthill-McKee algorithm
numberer RCM

# Create the convergence test, the norm of the residual with a tolerance of
# 1e-12 and a max number of iterations of 10
test NormDispIncr 1.0e-12  1000 3

# Create the solution algorithm, a Newton-Raphson algorithm
algorithm Newton

# Create the integration scheme, the LoadControl scheme using steps of 0.1
integrator LoadControl 0.1

# Create the analysis object
analysis Static

# ------------------------------
# End of analysis generation
# ------------------------------


# ------------------------------
# Finally perform the analysis
# ------------------------------

# perform the gravity load analysis, requires 10 steps to reach the load level
analyze 10
```

REFERENCES

Abrams DP, Angel R, Uzarski J, "Out-of-Plane Strength of Unreinforced Masonry Infill Panels", *Earthquake Spectra* 1996;12(4):825-844.

Amato G, Cavaleri L, Fossetti M, Papia M, "Infilled frames: Influence of vertical loads on the equivalent diagonal strut model". *XIV WCEE*, Beijing;2008.

Amato G, Fossetti M, Cavaleri L, Papia M, "An updated model of equivalent diagonal strut for infill panels". Workshop: Quali Prospettive per l'Eurocodice 8 alla Luce delle Esperienze Italiane, Napoli;2009.

Angel R, "Behavior of reinforced concrete frames with masonry infill walls". University Illinois at Urbana-Champaingn, Illinois, 1994.

Asteris PG, Antoniou ST, Sphianopulos DS, Chrysostomou CZ, "Mathematical macromodeling of infilled frames": State of the art. *J Struct Eng (ASCE)* 2011;137(12):1508-1517.

Asteris PG, "Finite Element Micro-Modeling of Infilled Frames", *Electronic J. of Structural Engineering*, vol. 8, pp.1-11, 2008.

Asteris PG, "Lateral Stiffness of Brick Masonry Infilled Plane Frames", *J. Struct. Eng. (ASCE)* 2003;129(8):1071-1079.

Bertoldi SH, Decanini LD, Gavarini C, "Telai tamponati soggetti ad azioni sismiche, un modello semplificato: confronto sperimentale e numerico". *Atti del 6 Convegno Nazionale ANIDIS*, Vol.2:815–24, Perugia;1993.

Cavaleri L, Di Trapani F, Macaluso G, Papia M, "Reliability of code-proposed models for assessment of masonry elastic moduli". *Ingegneria Sismica* 2012;29(1):38-59.

Cavaleri L, Fossetti M, Papia M, "Infilled frames: developments in the evaluation of cyclic behaviour under lateral loads". *Structural Engineering and Mechanics* 2005;21(4):469-94.

Cavaleri L, Papia M, "A new dynamic identification technique: Application to the evaluation of the equivalent strut for infilled frames". *Engineering Structures* 2003;25(7):889-901.

Cavaleri L, Di Trapani F, Papia M, "Strutture intelaiate e tamponate in c.a.: sperimentazione e sviluppi nella modellazione analitica e numerica", Proceedings in *19° Congresso CTE*, Bologna, Italy, November, 2012, pp. 8-10.

Cavaleri L, Di Trapani F, Macaluso G, Colajanni P, "Definition of diagonal Poisson's ratio and elastic modulus for infill masonry walls". *Mat. and Struct.* DOI 10.1617/s11527-013-0058-9, 2013.

Crisafulli FJ, "Seismic behaviour of reinforced concrete structures with masonry infills". PhD Thesis, University of Canterbury, New Zealand;1997.

Crisafulli FJ, Carr AJ, "Proposed macro-model for the analysis of infilled frame structures". *Bull New Zealand Soc Earthquake Eng* 2007;40(2):69–77.

Crisafulli FJ, Carr AJ, Park R, "Analytical modelling of infilled frames structures –a general review", *Bull. NZ Soc. Earth. Eng.*, vol. 33(1), pp. 30–47, 2000.

Chrysostomou CZ, **Asteris PG**, "On the in-plane properties and capacities of infilled frames". *Engineering Structures* 2012;41: 385–402.

Chrysostomou CZ, Gergely P, Abel JF."A six-strut model for nonlinear dynamic analysis of steel infilled frames." *Int. J. Struct. Stab. Dyn.,* 2002;Vol. 2(3), pp. 35–353.

Dawe JL, Seah CK, "Analysis of concrete masonry infilled steel frames subjected to in-plane loads". *Proceeding of the 5th Canadian Masonry Symposium*, Vancouver; 329–40;1989.

D.M. LL. PP. 14 Gennaio 2008, Nuove norme tecniche per le costruzioni.

Dolšek M, Fajfar P, "The effect of masonry infills on the seismic response of four storey reinforced concrete frame - a deterministic assessment". *Engineering Structures* 2008; 30(7):1991-2001.

Doudoumis IN, "Finite element modelling and investigation of the behaviour of elastic infilled frames under monotonic loading", *Eng. Struct.* 2007;Vol. 29(6), pp. 1004–24.

Doudoumis IN, Mitsopoulou EN, "Non-linear analysis of multi-storey infilled frames for unilateral contact condition". *Proceedings 8th European Conference on Earthquake Engineering*, Vol.3:63-70, Lisbon;1986.

Dowell RK, Seible F, Wilson EL, "Pivot Hysteresis model for reinforced concrete members". *Struct J (ACI)* 1998;95(5):607-17.

El-Dakhakhni W, Elgaaly M, Hamid, A. "Three-Strut Model for Concrete Masonry-Infilled Steel Frames." *J. Struct. Eng. (ASCE)* 2003;129(2), 177–185.

Durrani AJ, Luo YH, "Seismic retrofit of flat-slab buildings with masonry infill". *Proc of the NCEER Workshop on Seismic Response of Masonry Infills*, Report NCEER-94-0004; 1994.

Eurocode 8, "Design of structures for earthquake resistance - Part 1: General rules, seismic actions and rules for buildings", 2004.

FEMA 356, "Prestandard and commentary for the seismic rehabilitation of buildings", 2000.

FEMA 273, "NEHRP Guidelines for the seismic rehabilitation of buildings". Whashington DC;1997.

Fiore A, Netti A, Monaco P, "The influence of masonry infill on the seismic behaviour of RC frame buildings". *Engineering Structures* 2012;44:133-145.

Ghosh AK, Made AM, "Finite element analysis of infilled frames", *J. Struct. Eng.*, 2002;Vol 128(7), pp. 881–89.

Griffith MC, Vaculik J, "Out-of-Plane Flexural Strength of Unreinforced Clay Brick Masonry Walls", *TMS Journal* 2007.

Haseltine BA, "Design of Laterally Loaded Wall Panels", Proceedings of the British Ceramic Society. *Load Bearing Brickwork* 1976. Stoke-on-Trent, U.K., Vol. 5(24):pp. 115-126.

Haseltine BA, West HWH, Tutt JN, "Design of Walls to Resist Lateral Loads", *The Structural Engineers* 1977; Pr. 2, Vol. 55(10):pp 422-430.

Hashemi A, Mosalam KM, "Seismic Evaluation of Reinforced Concrete Buildings Including Effects of Masonry Infill Walls", *PEER Report*, 2007/100.

Hashemi A, Mosalam KM, "Shake-table experiment on reinforced concrete structure containing masonry infill wall", *Earthquake Engng Struct. Dyn.* 2006; 35:1827–1852

Hendry AW, "The Lateral Strength of Unreinforced Brickwork", *The Structural Engineers* 1973;Vol. 51(2): pp. 43-50.

Hendry AW , Kheir AMA, "The Lateral Strength of Certain Brickwork Panels", Proceedings of the *Fourth International Brick Masonry Conference* 1976; Brugge, Belgium, pp. 4.a.3.1-4.a.3.4.

Holmes M, "Steel frames with brickwork and concrete infilling". *Proc. of Institution of Civil Engineers*, Paper No.6501:473-478;1961.

Jones RM, "Mechanics of composite materials", 2nd Edition (1998), Taylor and Francis.

Kakaletsis DJ, Karayannis CG, "Experimental investigation of infilled reinforced concrete frames with openings". *Struct J (ACI)* 2009;106(2):132-141.

Kappos AJ, Stylianidis KC, Michaildis CN, "Analytical models for brick masonry infilled R/C frames under lateral loading". *J Earthquake Engrg* 1998;2(1):59-87.

Klingner RE, Bertero VV, "Earthquake resistance of infilled frames". *J Struct Eng (ASCE)*, 1978;104(6):973-89.

Koutromanos I, Stavridis A, Shing PB, Willam K, "Numerical modeling of masonry-infilled RC frames subjected to seismic loads". *Computers and Structures* 2011;89(11-12):1026-1037.

Lofti HR, Shing PB, "An appraisal on smeared crack models for masonry shear walll analysis". *J Computers and Structures* (ASCE) 1991;41(1):413-425.

Lofti HR, Shing PB, "Interface model applied to fracture of masonry structures". *J Struct Eng* (ASCE) 1994;120(1):63-80.

Madan A, Reinhorn AM, Mander JB, Valles RE, "Modeling of masonry infill panels for structural analysis". *J Struct Eng* (ASCE) 1997;123(10):1295-302.

Mainstone RJ, "Supplementary note on the stiffness and strength of infilled frames". Current Paper CP 13/74, Building Research Station, UK;1974.

Mallick DV, Severn RT, "The behaviour of infilled frames under static loading", *Proc. Inst. Civ. Eng.*, 1967;Vol. 38, pp. 639-56,.

Mander JB, Nair B, "Seismic resistance of brick infilled steel frames with and without retrofit". *The masonry J* 1994;12(2):24-37.

Mander JB, Nair B, Wojtkowski K, Ma J, "Experimental study on the seismic performance of brick infilled steel frames with and without retrofit". *NCEER*, Tech Rep 93-0001, Buffalo; 1993.

McDowell EL, McKee KE, Sevin E, "Action Theory of Masonry Walls", Proceedings of the American Society of Civil Engineers, *Journal of the Structural Division* (1956), Vol.82, No. ST2, pp. 915-1 to 915-18.

McDowell EL, McKee KE, Sevin E, "Discussion of Arching Action Theory of Masonry Walls", Proceedings of the American Society of Civil Engineers, *Joumal of the Structural Division* September 1956, pp. 1067-27 to 1067-40.

Mehrabi AB, Shing PB, "Finite element modelling of masonry-infilled RC frames", *J. Struct. Eng.* 1997;Vol. 123(5), pp. 604-13.

Mehrabi AB, Shing PB, Schuler MP, Noland JL, Experimental evaluation of masonry-infilled RC frames. *J Struct Eng (ASCE)* 1996;122(3):228-37.

Monk CB, "Resistance of Structural Clay Masonry to Dynamic Forces", Research Report No.7, Structural Gay Products Research Foundation, Geneva, Illinois, November 1958.

Mosalam KM, Günay S, "Progressive Collapse Analysis of RC Frames with URM Infill Walls Considering In-Plane/Out-of-Plane Interaction", *Earthquake Spectra* 2014. In Press.

Panagiotakos TB, Fardis MN, "Seismic response of infilled RC frames structures". *XXI WCEE*, Acapulco, Mexico;1996.

Papia M, "Analysis of infilled frames using A coupled finite element and boundary element solution scheme". *Int J Numerical Methods in Engineering* 1988; Vol 26(3), pp. 731–742.

Papia M, Cavaleri L, Fossetti M, "Infilled frames: developments in the evaluation of the stiffening effect of infills". *Structural engineering and mechanics* 2003;16(6):675-93.

Saneinejad A, Hobbs B, "Inelastic design of infilled frames". *J Struct Eng (ASCE)* 1995;121(4):634-50.

Shing PB, Mehrabi AB, "Behaviour and analysis of masonry-infilled frames", *Prog. Struct. Eng. Mater.* 2002;Vol. 4(3), pp. 320–31.

Shing PB, Stavridis A, "Analysis of Seismic Response of Masonry-Infilled RC Frames through Collapse", *ACI Structural Journal* 2014; Special Paper 297-7.

Stafford Smith B, "Behaviour of the square infilled frames". *Struct Div (ASCE)* 1966;92(1):381-403.

Stafford Smith B, Carter C, "A method for analysis for infilled frames". *Proc. of Institution of Civil Engineers*, Paper No.7218:31-48;1969.

Stavridis A, Koutromanos I, Shing PB, "Shake-table tests of a three-story reinforced concrete frame with masonry infill walls". *Earthquake Engrg Struct Dyn 2012*;41(6):1089-1108.

Takeda T, Sozen MA, Nielsen NN, "Reinforced concrete response to simulated earthquakes". *J Struct Div (ASCE)* 1970;Vol.96, No.ST12:2557-73.

Timoshenko S, Woinowsh -Krieger S, "Theory of Plates and Shells", McGraw-Hill, 1959.

Uva G, Porco F, Fiore A, "Appraisal of masonry infill walls effect in the seismic response of RC framed buildings: a case study". *Engineering Structures* 2012;34:514–26.

Žarnić R, Gostič S, "Masonry infilled frames as an effective structural subassemblage". *Seismic design methodologies for the next generation of codes* (Fajfar, Krawinkler, editors)1997;335–46.Rotterdam: Balkema.